

**INVESTIGATION OF EMISSIONS AND COMBUSTION KINETICS OF
WASTE WOOD SAMPLES WITH THERMAL AND SPECTRAL
METHODS**

**A THESIS SUBMITTED TO
THE GRADUATE SCHOOL OF NATURAL AND APPLIED SCIENCES
OF
MIDDLE EAST TECHNICAL UNIVERSITY**

BY

SEMA (YURDAKUL) YORULMAZ

**IN PARTIAL FULFILLMENT OF THE REQUIREMENTS
FOR
THE DEGREE OF MASTER OF SCIENCE
IN
ENVIRONMENTAL ENGINEERING**

SEPTEMBER 2006

Approval of the Graduate School of Natural and Applied Sciences

Prof. Dr. Canan Özgen
Director

I certify that this thesis satisfies all the requirements as a thesis for the degree of Master of Science.

Prof. Dr. Filiz B. Dilek
Head of Department

This is to certify that we have read this thesis and that in our opinion it is fully adequate, in scope and quality, as a thesis for the degree of Master of Science.

Prof. Dr. Aysel Atımtay
Supervisor

Examining Committee Members

Prof. Dr. Göksel Demirer (METU, ENVE)

Prof. Dr. Aysel Atımtay (METU, ENVE)

Prof. Dr. Hayrettin Yücel (METU, CHE)

Prof. Dr. Şahinde Demirci (METU, CHEM)

Asst. Prof. Dr. İpek İmamoğlu (METU, ENVE)

I hereby declare that all information in this document has been obtained and presented in accordance with academic rules and ethical conduct. I also declare that, as required by these rules and conduct, I have fully cited and referenced all material and results that are not original to this work.

Name, Last name: Sema (Yurdakul) Yorulmaz

Signature

ABSTRACT

INVESTIGATION OF EMISSIONS AND COMBUSTION KINETICS OF WASTE WOOD SAMPLES WITH THERMAL AND SPECTRAL METHODS

(Yurdakul) Yorulmaz, Sema

M.Sc., Department of Environmental Engineering

Supervisor: Prof. Dr. Aysel T. Atımtay

September 2006, 173 pages

The mechanisms and kinetics of combustion of waste wood as well as the phases during combustion processes are important to eliminate these wastes without any possible damage to environment. In the present study, combustion mechanisms, activation energy and pre-exponential constants, and phases of combustion were investigated for untreated natural pine and treated Medium Density Fiberboard (MDF), plywood and particleboard samples that involve some chemicals and additives. Waste wood samples were heated in air at 10, 20 and 30°C/min heating rates in a Thermo Gravimetric Analyzer (TGA) from room temperature to 900°C. Thermogravimetry (TG) and Derivative Thermogravimetry (DTG) curves for all samples were obtained. The gases formed during combustion reactions were directly fed to a Fourier Transform Infrared Spectroscopy (FTIR) instrument coupled to TGA. Emission characteristics of the samples were determined in-situ by using the FTIR spectrums.

As a result of TG analysis, thermal decomposition of treated samples was observed at lower temperatures as compared to the untreated pine sample because of the catalyzing effects of the chemicals in the treated samples.

Therefore, there were less flammable products, lower weight losses in the main oxidation region, decrease in the max. weight loss temperatures and formation of more char for treated samples as compared to untreated pine sample. In other words, chemicals used during production of these samples lead to decrease in the combustibility of the treated samples.

Thermal kinetic constants for the samples were calculated by using Coats Redfern and Broido Methods. In order to find out the mechanisms responsible for the oxidation of the waste wood samples in different regions, six solid state mechanisms of Coats Redfern Method were tested.

As a result of FTIR analysis of the emitted gases from TG analysis, several chemical groups were detected from pine and treated samples. Combustion of all samples revealed some gases containing aromatics, C-H groups, CO₂ and CO. However, there were some toxic and carcinogenic gases like formaldehyde, isocyanate group, ammonia, phenyl group and benzoylbromide among the emissions of treated samples which need utmost attention when recovering energy from treated waste woods.

Key words: Waste Wood, MDF, Plywood, Particleboard, TGA, FTIR analysis, Activation energy, Pre-exponential constant, Emissions, Chemical groups.

ÖZ

ATIK ODUN ÖRNEKLERİNDE EMİSYONLARIN VE YANMA KİNETİKLERİNİN TERMAL VE SPEKTRAL YÖNTEMLERLE İNCELENMESİ

(Yurdakul) Yorulmaz, Sema

Yüksek Lisans, Çevre Mühendisliği Bölümü

Tez Danışmanı: Prof. Dr. Aysel T. Atımtay

Eylül 2006, 173 sayfa

Atık odunların yanma mekanizması, kinetiği ve yanma süreçlerindeki aşamalar, bu atıkların çevreye zarar vermeden imhası açısından önem arz etmektedir. Bu çalışmada, kimyasal işlem görmemiş çam örneği ve işlem görmüş, yani bazı kimyasallar ve katkı maddeleri içeren MDF, kontraplak ve sunta gibi maddelerin yanma mekanizmaları, aktivasyon enerjileri, üssel sabitleri ve yanma aşamaları incelenmiştir. Atık odun örnekleri hava ortamında 10°, 20° and 30°C/dak ısıtma hızlarında Thermo Gravimetrik Analiz (TGA) cihazında, oda sıcaklığından 900 °C'a kadar ısıtılmıştır. Tüm incelenen örnekler için TG ve DTG eğrileri elde edilmiştir. TG cihazındaki yanma reaksiyonları sonunda oluşan gazlar, hemen TGA'ya bağlı olan FTIR Spektrofotometresine yönlendirilmiş ve yanma sonunda oluşan gazların in-situ olarak emisyon karakteristikleri tayin edilmiştir.

TG analizleri sonunda, işlem görmüş örneklerde ısıl bozulmanın, işlem görmemişlere göre daha düşük sıcaklıklarda oluştuğu gözlenmiştir. Bunun, içeriğindeki kimyasallara bağlı olduğu düşünülmüştür. Dolayısıyla, işlem görmüş örneklerde çam gibi işlem görmemiş örneğe göre daha az yanabilir ürünler, ana oksidasyon bölgesinde daha az ağırlık kayıpları ve daha fazla kok (char) oluşumu meydana gelmiştir. Başka bir deyişle, bu örneklerin üretimi esnasında kullanılan kimyasallar, işlem görmüş örneklerin yanabilirliğinde azalmaya neden olmaktadır.

İncelenen örneklerin yanma kinetik sabitleri Coats Redfern ve Broido Yöntemleri kullanılarak hesaplanmıştır. Atık odun örneklerinin değişik bölgelerdeki oksitlenme mekanizmalarını incelemek üzere Coats Redfern metodundaki 6 değişik mekanizma denenmiştir.

TG analizleri sonunda çıkan gazların FTIR analizleri yapıldığında, işlem görmemiş çam ve işlem görmüş atık odun örneklerinden çıkan gazların çeşitli kimyasal gruplar içerdiği bulunmuştur. Tüm örneklerin yanma gazlarında aromatikler, C-H grupları, CO₂ ve CO bulunduğu görülmüştür. Ancak, işlem görmüş örneklerde formaldehit, izosiyanat grubu, amonyak, fenil grubu ve benzoilbromür gibi bazı toksik ve kanserojen maddelerin de bulunduğu ortaya konmuştur. Bu konu, atık odunlardan enerji geri kazanımı yapılırken dikkat edilmesi gereken en önemli noktalardan biri olarak belirlenmiştir.

Anahtar Kelimeler: Atık odun, MDF, Kontraplak, Sunta, TGA, FTIR analizi, Aktivasyon enerjisi, Üssel sabit (A), Emisyonlar, Kimyasal gruplar.

ACKNOWLEDGEMENTS

I would like to express my sincere appreciation to my supervisor Prof. Dr. Aysel Atımtay for her guidance, advice, criticism throughout the research.

I also thank to my dear husband, Orçun Yorulmaz, for his valuable and unconditional support and faith in me throughout the thesis. I wish to thank to all my friends, especially my roommates for their support.

Finally, I would like to express my deepest appreciation to my family for their endless support, understanding and patience not only during this study but also throughout my life.

TABLE OF CONTENTS

PLAGIARISM.....	iii
ABSTRACT	iv
ÖZ	vi
ACKNOWLEDGEMENTS	viii
TABLE OF CONTENTS	ix
LIST OF TABLES	xii
LIST OF FIGURES	xvi
ABBREVIATIONS	xxi

CHAPTER

1. INTRODUCTION	1
1.1. Energy Situation of Turkey	1
1.2. Why Biomass should be used?.....	5
1.3. Biomass Potential of Turkey	10
1.3.1. Virgin Biomass (Forest Resources) Potential of Turkey	12
1.3.2. Waste Biomass Sources of Turkey	13
1.3.2.1. Agricultural Residue Potential of Turkey	13
1.3.2.2. Animal Waste Potential of Turkey	13
1.3.2.3. Woody Waste Potential of Turkey	13
1.3.2.4. Municipal Solid Waste (MSW) Amount	18
1.3.2.5. Pulp and Paper Sludge	19
1.4. Objective of This Study	20
2. LITERATURE SURVEY	22
2.1. Waste Wood.....	22
2.2. Sources of Waste Wood.....	23
2.2.1. Forestry residues	23

2.2.2. Primary Processing	24
2.2.3. Secondary Processing	24
2.2.4. Waste Streams	25
2.3. Categories of Waste Wood	26
2.4. Properties of Waste Wood	31
2.4.1. Physical Properties of Waste Wood.....	32
2.4.2. Chemical Properties of Waste Wood.....	33
2.4.2.1. Summative Analysis.....	33
2.4.2.2. Proximate and Ultimate Analysis.....	33
2.4.2.3. Heating Value	35
2.5. Energy Production from Waste Wood.....	37
2.6. Thermal Analysis of Waste Wood	40
2.7. General Information about IR Spectroscopy	45
2.8. Functional Groups of Wood with FTIR.....	49
3. MATERIALS AND METHODS.....	55
3.1. Physical and Chemical Characteristics of Waste Wood Samples.....	55
3.2. Thermal Analysis	57
3.2.1. Thermogravimetric Analysis of Waste Wood Samples.....	58
3.2.2. FTIR Analysis of Evolved Gases.....	59
3.3. Methods Used for the Calculation of Thermal Kinetics.....	60
4. RESULTS AND DISCUSSION.....	69
4.1. Thermogravimetric Analysis (TGA) Results.....	69
4.1.1. Pine Samples.....	71
4.1.2. MDF Samples	87
4.1.3. Particleboard Samples.....	99
4.1.4. Plywood Samples.....	111
4.2. Comparison of the TGA Results of the Samples	123
4.3. FTIR Results of the Waste Wood Samples.....	134
4.3.1. 3-D/FTIR Results of the P Samples.....	138
4.3.2. 3-D/FTIR Results of the M Samples	143
4.3.3. 3-D/FTIR Results of the PB-30 Sample.....	147

4.3.4. 3-D/FTIR Results of the PL-30 Sample.....	149
4.3.5. Comparison of the FTIR Results for all Samples.....	151
5. CONCLUSIONS.....	154
REFERENCES	157
APPENDIX A.....	167
REPEATED TG ANALYSIS OF P-10 AND M-10 SAMPLES	167

LIST OF TABLES

TABLES

Table 1.1. Amount of primary energy sources in Turkey (WEC/TNC, 1996).....	2
Table 1.2. General energy demand projections for Turkey, (KTOE) (Energy and Natural Sources Panel, 2003).....	3
Table 1.3. Primary energy production and consumption (in parenthesis) targets of Turkey between 2005 and 2025 (KTOE) (Kaygusuz et al., 2002).....	4
Table 1.4. GHG emissions of Turkey, with respect to years (thousand tons) (Kaygusuz et al., 2002).....	10
Table 1.5. Present and planned biomass production of Turkey (KTOE) (Balat, 2005)	11
Table 1.6. Industrial round wood production and consumption by years, 2000-2004 (1000 m ³) (Ballı, 2005).....	15
Table 1.7. Production, apparent consumption and trade amounts of sawn wood by years, 1995-2004 (1000 m ³) (Ballı, 2005)	15
Table 1.8. Wood based panel production amounts in Turkey with respect to years (FAO, 2006).....	16
Table 1.9. Telephone and mining poles production amounts between, 2000 and 2004 (GDF, 2006).....	18
Table 1.10. Total energy potential of Turkey from waste biomass sources in 2004.....	20
Table 2.1. Proportion of wastes generated in selected forest products industries FAO Corporate Document Repository, 2006).....	24
Table 2.2. General classification of waste wood arising from regular assortments and samples (Peek, 2004).....	27

Table 2.3. Types and usage purpose and places of the oil borne preservatives (Ibach, 1999).....	31
Table 2.4. Wood fuels, wood composites and their moisture contents and densities (Sims, 2002; Youngquist, 1999).....	32
Table 2.5. Ultimate analysis of some selected untreated wood species (on dry basis) (Cheremisinoff et al., 1976; Tillman, 1981).....	33
Table 2.6. Proximate analysis of some untreated wood species (on dry basis) (Cheremisinoff et al., 1976; Tillman, 1981).....	34
Table 2.7. Ultimate analysis of some waste wood samples (dry, wt%) (Skodras et al., 2002)	34
Table 2.8. Proximate analysis of some waste wood samples (on dry basis) (Skodras et al., 2002)	35
Table 2.9. Heating values of different treated waste woods, (kJ/kg) (Phyllis, 2006).....	37
Table 2.10. FTIR band assignments (Drobniak et al., 2006).....	51
Table 3.1. List of waste wood samples.....	55
Table 3.2. Elemental composition of all samples (on dry, ash free basis)	56
Table 3.3. Proximate analysis and calorific values of all samples (on dry basis).....	57
Table 3.4. Properties of the Perkin Elmer TG Analyzer (Model Pyris-1).....	59
Table 3.5. Properties of the Perkin Elmer Spectrum-1 FTIR Spectrometer analyzer	60
Table 3.6. Coats and Redfern Mechanisms used for the calculation of thermal kinetics in this study (Sun et al., 2006)	65
Table 4.1. Test runs conducted during the experiments.....	69
Table 4.2. Temperature intervals belonging to the regions	71
Table 4.3. Activation energies and pre-exponential constants of P -10 sample for three regions	74
Table 4.4. Activation energies and pre-exponential constants of P -10 sample for three regions	75

Table 4.5. Temperature intervals and weight losses belonging to the regions	76
Table 4.6. Activation energies and pre-exponential constants of P-20 sample for three regions	77
Table 4.7. Activation energies and pre-exponential constant values of P - 20 sample for three regions	79
Table 4.8. Temperature intervals and weight losses belonging to the regions	79
Table 4.9. Activation energies and pre-exponential constant values of P-30 sample with respect to the three regions.....	81
Table 4.10. Activation energies and pre-exponential constants of P-30 sample by using the Broido Method for three regions.....	82
Table 4.11. Activation energies and pre-exponential constants of all pine samples with respect for three regions	85
Table 4.12. Temperature intervals and weight losses belonging to the regions	88
Table 4.13. Temperature intervals and weight losses belonging to the regions	90
Table 4.14. Temperature intervals and weight losses belonging to the regions	92
Table 4.15. Activation energies and pre-exponential constants of all MDF samples with respect of the three regions.....	96
Table 4.16. Temperature intervals and weight losses belong to the regions.....	99
Table 4.17. Temperature intervals and weight losses belonging to the regions	102
Table 4.18. Temperature intervals and weight losses belonging to the regions	104
Table 4.19. Activation energies and pre-exponential constant values of all particleboard samples with respect of the three regions	108
Table 4.20. Temperature intervals and weight losses belonging to the regions	111

Table 4.21. Temperature intervals and weight losses belonging to the regions	113
Table 4.22. Temperature intervals and weight losses belonging to the regions	116
Table 4.23. Activation energies and pre-exponential constant values of all plywood samples with respect of the three regions	120
Table 4.24. Weight loss of all samples for different regions	124
Table 4.25. Peak and burnout temperatures of the samples	126
Table 4.26. Maximum weight loss rates for all samples	127
Table 4.27. Comparison of the activation energies found in the present study with that of literature for the main oxidation region.....	132
Table 4.28. Comparison of the results of the present study and literature for the second and fourth regions.....	134
Table 4.29. Functional groups: observed wave numbers and their literature values (Poljansek et al., 2005; Schanzer et al., 2002)	138
Table 4.30. Releasing temperatures of the main groups of P and M samples in the FTIR spectrums as a result of heating rate	151
Table 4.31. Releasing temperatures of the main groups of all samples in the FTIR spectrums at 30 °C/min heating rate	152
Table 4.32. Temperatures which was the highest amount emissions were released as compared to sample type	153
Table A.1. Temperature intervals and weight losses belonging to the regions	167
Table A.2. Activation energies and pre-exponential constant values of RP -10 sample with respect to the three regions	169
Table A.3. Temperature intervals and weight losses belonging to the regions	170

LIST OF FIGURES

FIGURES

Figure 1.1. Percentages of energy production and import in Turkey with respect to years (WEC/TNC, 2006).....	1
Figure 1.2. Projections of renewable energy percentages in Turkey, (KTOE) (Energy and Natural Sources Panel, 2003).....	5
Figure 1.3. Emission coefficient characteristics of fuel (kgsCO ₂ /GJ) (IPCC, 1996).....	6
Figure 1.4. Raising of CO ₂ concentrations in the atmosphere (Demirbaş, 2004).....	8
Figure 1.5. Fuel wood production in Turkey with respect to years (GDF, 2006).....	12
Figure 2.1. Sources of wood wastes (Scotland, 2003)	23
Figure 2.2. Change in net calorific value of the waste wood as a function of moisture content (Sims, 2002).....	36
Figure 2.3. Competing reactions in the pyrolysis and combustion of cellulose (Schiewind, 1989)	39
Figure 2.4. Summary of the IR absorptions (Blackburn, 2003)	46
Figure 3.1. Photograph of the TG-FTIR instrument	58
Figure 3.2. Schematic diagram of the TG-FTIR system	58
Figure 4.1. TG and DTG graph of the P-10 sample at 10 °C/min heating rate.....	71
Figure 4.2. Curves showing the solid state mechanisms for Coats Redfern method for three regions of P-10 sample	73
Figure 4.3. Curves showing the Broido method for three regions of P-10 sample.....	75
Figure 4.4. TG and DTG graph of the P-20 sample at 20 °C/min heating rate.....	76

Figure 4.5. Curves showing the solid state mechanisms for Coats Redfern method for three regions of P-20 sample	77
Figure 4.6. Curves obtained with the Broido method for three regions of P-20 sample	79
Figure 4.7. TG and DTG graph of the P-30 sample at 30 °C/min heating rate.....	80
Figure 4.8. Curves indicating the solid state mechanisms by using Coats Redfern Method for three regions of P-30 sample.....	81
Figure 4.9. Curves showing the Broido method for three regions of P-30 sample.....	82
Figure 4.10. Change of maximum peak temperatures of pine sample in the third region with respect to the heating rate	83
Figure 4.11. Change of maximum peak temperatures of pine samples in the fourth region according to the heating rate.....	84
Figure 4.12. TG and DTG graph of the M-10 sample at 10 °C/min heating rate.....	88
Figure 4.13. Curves showing the solid state mechanisms for Coats Redfern method for three regions of M-10 sample.....	89
Figure 4.14. Curves obtained with the Broido method for three regions of M-10 sample	89
Figure 4.15. TG and DTG graph of the M-20 sample at 20 °C/min heating rate.....	90
Figure 4.16. Curves showing the solid state mechanisms for Coats Redfern method for three regions of M-20 sample.....	91
Figure 4.17. Lines showing the Broido method for three regions of M-20 sample.....	91
Figure 4.18. TG and DTG graph of the M-30 sample at 30 °C/min heating rate.....	92
Figure 4.19. Curves indicating the solid state mechanisms for Coats Redfern method for three regions of M-30 sample.....	93

Figure 4.20. Curves showing the Broido method for three regions of M-30 sample.....	93
Figure 4.21. Change of maximum peak temperatures of MDF samples in the third region according to the heating rate	94
Figure 4.22. Change of maximum peak temperatures of MDF samples in the fourth region according to the heating rate	95
Figure 4.23. TG and DTG graph of the PB-10 sample at 10 °C/min heating rate	100
Figure 4.24. Curves showing the solid state mechanisms for Coats Redfern Method for three regions of PB-10 sample	101
Figure 4.25. Curves showing the Broido method for three regions of PB-10 sample.....	101
Figure 4.26. TG and DTG graph of the PB-20 sample at 20 °C/min heating rate	102
Figure 4.27. Curves indicating the solid state mechanisms for Coats Redfern method for three regions of PB-20 sample	103
Figure 4.28. Curves showing the Broido method for three regions of PB-20 sample.....	103
Figure 4.29. TG and DTG graph of the PB-30 sample at 30 °C/min heating rate	104
Figure 4.30. Curves which show the solid state mechanisms for three regions of PB-30 sample	105
Figure 4.31. Curves showing the Broido method for three regions of PB-30 sample.....	105
Figure 4.32. Change of maximum peak temperatures of PB samples in the third region according to the heating rate.....	106
Figure 4.33. Change of maximum peak temperatures of PB samples in the fourth region according to the heating rate.....	107
Figure 4.34. TG and DTG graph of the PL-10 sample at 10 °C/min heating rate	112

Figure 4.35. Curves indicating the solid state mechanisms for Coats Redfern method for three regions of PL-10 sample.....	112
Figure 4.36. Curves showing the Broido method for three regions of PL-10 sample.....	113
Figure 4.37. TG and DTG graph of the PL-20 sample at 20 °C/min heating rate	114
Figure 4.38. Curves showing the solid state mechanisms for Coats Redfern method for three regions of PL-20 sample.....	115
Figure 4.39. Curves indicating the Broido method for three regions of PL-20 sample.....	115
Figure 4.40. TG and DTG graph of the PL-30 sample at 30 °C/min heating rate	116
Figure 4.41. Curves which show the solid state mechanisms for three regions of PL-30 sample.....	117
Figure 4.42. Curves showing the Broido method for three regions of PL-30 sample.....	117
Figure 4.43. Change of maximum peak temperatures of plywood samples in the third region according to the heating rate	118
Figure 4.44. Change of maximum peak temperatures of PL samples in the fourth region according to the heating rate.....	119
Figure 4.45. Temperature vs. weight losses of all samples at different heating rates.....	125
Figure 4.46. 3-D presentation of the P-10 sample	139
Figure 4.47. 3-D presentation of the P-20 sample	139
Figure 4.48. 3-D presentation of the P-30 sample	140
Figure 4.49. Areas of the seven regions of P-10 sample.....	141
Figure 4.50. Areas of the seven regions of P-20 sample.....	142
Figure 4.51. Areas of the seven regions of P-30 sample.....	142
Figure 4.52. 3-D presentation of the M-10 sample.....	143
Figure 4.53. 3-D presentation of the M-20 sample.....	144
Figure 4.54. 3-D presentation of the M-30 sample.....	145

Figure 4.55. Areas of the nine regions of M-10 sample.....	146
Figure 4.56. Areas of the nine regions of M-20 sample.....	146
Figure 4.57. Areas of the nine regions of M-30 sample.....	147
Figure 4.58. 3-D presentation of the PB-30 sample.....	148
Figure 4.59. Areas of the nine regions of PB-30 sample	149
Figure 4.60. 3-D presentation of the PL-30 sample.....	149
Figure 4.61. Areas of the nine regions of PL-30 sample.....	150
Figure A.1. TG and DTG graph of the RP-10 sample at 10 °C/min heating rate.....	167
Figure A.2. Curves indicating the solid state mechanisms for Coats Redfern method for three regions of RP-10 sample	168
Figure A.3. Curves showing the Broido method for three regions of RP- 10 sample.....	169
Figure A.4. TG and DTG graph of the RM-10 sample at 10 °C/min heating rate	171
Figure A.5. Curves indicating the solid state mechanisms for Coats Redfern method for three regions of RM-10 sample	172
Figure A.6. Curves showing the Broido method for three regions of RM- 10 sample.....	172

ABBREVIATIONS

A	: Pre-exponential constant (min^{-1})
ACC	: Acid Copper Chromate
ACQ	: Ammoniacal Copper Quat
CCA	: Chromated Copper Arsenate
D1	: One-way transport
D2	: Two-way transport
D3	: Three-way transport
D4	: Ginstling-Brounshtein equation
DTG	: Derivative Thermogravimetry
E	: Activation energy (kJ/mole)
EM	: Electromagnetic
F1	: First order chemical reaction
FAO	: Food and Agriculture Organization
FTIR	: Fourier Transform Infrared
GCV	: Gross Calorific Value
GDF	: General Directory of Forestry
GDP	: Gross Domestic Product
GHG	: Green House Gases
GJ	: Giga Joule
Glulam	: Glued-laminated timber
Ha	: Hectare
HHV	: Higher Heating Value
IEA	: International Energy Agency
IPCC	: Intergovernmental Panel on Climate Change
IPPC	: Integrated Pollution Prevention Control
IR	: Infrared Radiation
KTOE	: Kilo Ton Oil Equivalent

LHV	: Lower Heating Value
LOI	: Limiting Oxygen Index
LSL	: Laminated Strand Lumber
LVL	: Laminated Veneer Lumber
M	: MDF
MDF	: Medium Density Fiberboard
MF	: Melamine Formaldehyde
MFP	: Melamine, Formaldehyde and Phosphoric acid
MJ	: Mega Joule
MSW	: Municipal Solid Waste
MTOE	: Million Tons Oil Equivalent.
MW	: Mega Watt
OECD	: Organization for Economic Co-operation and Development
OSB	: Oriented Strand Board
OSL	: Oriented Strand Lumber
P	: Pine
PB	: Particle Board
PF	: Phenol-formaldehyde
PJ	: Petajoules
PL	: Plywood
PSL	: Parallel Strand Lumber
R3	: Three dimensions
SCL	: Structural Composite Lumber
SIS	: State Institute of Statistics
TGA	: Thermo Gravimetric Analysis
UDFP	: Urea, Dicyandiamide, Formaldehyde and Phosphoric acid
UF	: Urea-Formaldehyde
WEC/TNC	: World Energy Council Turkish National Committee

CHAPTER 1

INTRODUCTION

1.1. Energy Situation of Turkey

Turkey has a dynamic economy and growing population (Kaya, 2006). Owing to the fast population growth, urbanization and economic expansion, energy consumption in Turkey has increased more than three times between 1980s and 1990s, and this growth will continue in the future. The economic crises between 1999 and 2001 have led to the total energy consumption to fall by 4% in 2001. However, the consumption bounced back with a growth of 4.6% in 2002. Turkey is an energy importing country. More than 70 % of the energy demand of Turkey is imported from other countries and this amount continues to increase each year. A percentage of energy production and imports out of the total energy demand in Turkey with respect to years is shown in Figure 1.1.

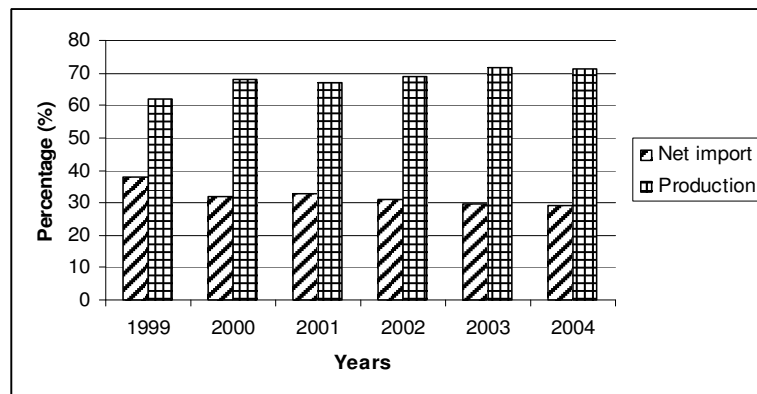


Figure 1.1. Percentages of energy production and import in Turkey with respect to years (WEC/TNC, 2006)

In 2004, total primary energy supply of Turkey reached 87.5 million tons oil equivalent (MTOE). About 72 % of the primary energy supply was met by imports and only 28 % was provided by domestic energy sources (WEC/TNC, 2006). The primary energy sources of Turkey are given in Table 1.1.

Table 1.1. Amount of primary energy sources in Turkey (WEC/TNC, 1996)

Sources	Apparent	Probable	Possible	Total
Hard coal (million tons)	428	449	249	1,126
Lignite (million tons)	7,339	626	110	8,075
Asphaltite (million tons)	45	29	8	82
Bituminous schist (million tons)	555	1,086	269	1,641
Hydropower (MW)	34,736	-	-	34,736
Oil (million tons)	36	-	-	36
Natural gas (million tons)	8	-	-	8
Nuclear (tons)				
Uranium (tons)	9,129	-	-	9,129
Thorium (tons)	380,000	-	-	380,000
Geothermal (MW)				
Electric (MW)	200	-		4,500
Thermal (MW)	1,000	-		31,100
Solar (Mtoe/year)				
Electric (Mtoe/year)	-	-	-	8.8
Heat (Mtoe/year)	-	-	-	26.4
Wood (Mtoe/year)	1,550	150	25	1,725
Dung (Mtoe/year)	175	30	13	218

As can be seen from Table 1.1, Turkey does not have enough oil and natural gas resources to supply its demand. Therefore, Turkey is heavily dependent on imported oil and gas. Imports account for about 90 % of the country's total annual oil consumption, over 95 % of its natural gas consumption and over 30 % of its coal consumption. Electricity generation plan of Turkey between 2005 and 2020 is to utilize 60 % indigenous resources and 40 % imported resources. By the year 2020, electricity has been planned to be produced from 15 million tones of imported coal, 31 billion cubic meters of natural gas, 4,500 MW of renewable

energy (wind, solar, biomass), 129 billion kWh of hydropower and 4,500 MW of nuclear energy (Kaya, 2006).

As the Ministry of Energy and Natural Resources announced in November 2004, the total energy demand is expected to reach 154 MTOE in 2010 and 282 MTOE in 2020 (Energy sector in Turkey, 2004). General energy demand projections for Turkey are given in Table 1.2. As can be seen from Table 1.2, in 2023 energy demand of Turkey will reach to 330 MTOE. Therefore, it is important to meet the energy demand of the country by using domestic nonrenewable resources (such as lignite, hard coal, oil and natural gas) and renewable resources (Kaya, 2006).

Table 1.2. General energy demand projections for Turkey, (KTOE) (Energy and Natural Sources Panel, 2003)

Sources	2010	Share%	2020	Share %	2023	Share %
Oil	51,16	33,3	71,89	25,5	79,99	24,2
Lignite	24,11	15,7	30,33	10,7	30,43	9,2
Coal	15,54	10,1	77,19	27,4	98,36	29,8
Natural gas	49,58	32,2	74,50	26,4	87,59	26,5
Hydro.	5,33	3,5	10,00	3,5	10,00	3,0
Noncommerical	4,41	2,9	3,92	1,4	3,89	1,2
Other	3,71	2,4	14,33	5,1	19,66	6,0
Total	153,86	100	282,19	100	329,93	100

Renewable energy sources which are biomass, wind, solar, geothermal energy and tidal energy have some advantages as compared to fossil fuels. Renewable energies are environmentally friendly, and they have no reserve problems: also each of them has its own special advantages. Nearly none of these sources release gaseous or liquids pollutants during the energy production process (Wereko et al., 1996). Turkey has considerable amounts of renewable energy resources due to its suitable geographical location and climate. These resources

are mainly hydro, biomass, wind, geothermal and solar energy (Kaya, 2006; Ediger et al, 1999). Primary energy production and consumption targets of Turkey are given in Table 1.3. As can be seen from Table 1.3, renewable energy production (hydropower, wood and waste, geothermal, solar, wind) has an important place as a primary energy source.

Table 1.3. Primary energy production and consumption (in parenthesis) targets of Turkey between 2005 and 2025 (KTOE) (Kaygusuz et al., 2002)

Energy sources	2005	2010	2015	2020	2023	2025
Coal (hard coal+lignite)	21259 (30,474)	28 522 (50,311)	31,820 (83,258)	3,985 (129,106)	42,732 (1,987,989)	45,944 (296,997)
Oil and natural gas	2127 (73,256)	1735 (92,637)	1,516 (112,993)	1,604 (136,365)	1,505 (158,467)	1,455 (179,765)
Hydropower	5845 (5,845)	7520 (7,520)	8,873 (8,873)	9,454 (9454)	10,002 (10002)	10,445 (10,445)
Wood and other waste	6760 (6,760)	6446 (6,446)	6,029 (6,029)	5,681 (5,681)	5,498 (5498)	5,393 (5,393)
Geothermal	1380 (1,380)	3760 (3,760)	4,860 (4,860)	4,860 (4,860)	5,400 (5,400)	5,400 (5,400)
Nuclear	0 (0)	3657 (3,657)	9143 (9,143)	18,286 (18,286)	26,988 (26,988)	29,200 (29,200)
Solar	259 (259)	907 (907)	1,508 (1,508)	2,294 (2,294)	2,845 (2,845)	3,248 (3,248)
Wind	250 (250)	620 (620)	980 (980)	1,440 (1,440)	1,786 (1,786)	2,134 (2,134)

Projections of renewable energy percentages in 2010 and 2020 are given in Figure 1.2. Wood, as the main biomass sources, is used as renewable energy source in our country. However, the use of solar, wind and geothermal energy is expected to increase in the future; but importance of the biomass will continue because of its huge amount as compared to the other renewable energy sources.

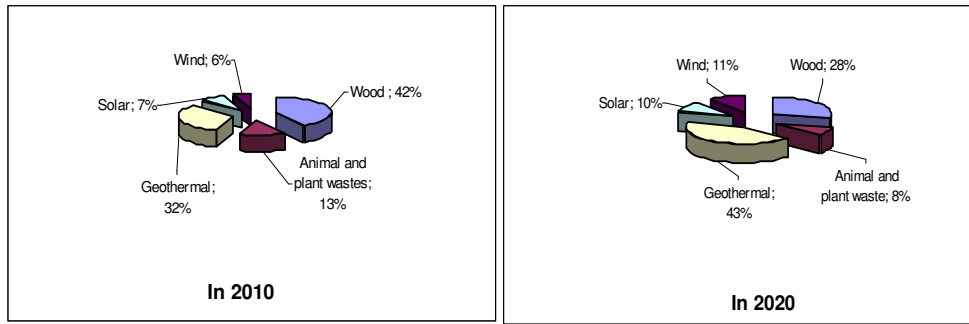


Figure 1.2. Projections of renewable energy percentages in Turkey, (KTOE) (Energy and Natural Sources Panel, 2003)

Biomass is important for Turkey among other renewable energy sources, since the share of biomass in the total energy consumption is as high as 10 % (its share in the total production is 26%) and techniques for the energy production from the biomass is also simple as compared to the other renewable energy sources. Therefore, implementation of biomass based energy programs will bring about great benefits to the energy policy of our country. Of course, it will not solve the problem completely, but it will provide new insight for efficient energy use in the household sector, especially in rural areas where 40% of the population lives (Kaygusuz et al., 2002).

1.2. Why Biomass should be used?

The term ‘Biomass’ is defined for all organic materials such as wood, wood processing residues, animal materials waste and plant waste. Wood waste and crops waste can be used for energy production (McKendry, 2002; Hepbaşlı et al., 2004). When bonds between carbon, hydrogen and oxygen molecules are broken in the biomass by different techniques such as digestion, combustion, pyrolysis or decomposition, the energy in the biomass is released. Biomass has always been a major source of energy of mankind, and it presently meets about 10-14% of world’s energy demand. Biomass is an important source of energy, and after

coal, oil and natural gas, it is the most important fuel worldwide (McKendry, 2002).

Biomass fuels are considered environmentally friendly for several reasons. Biomass does not emit carbon dioxide to the atmosphere, because it absorbs the same amount of carbon in growing, and CO₂ is released when biomass is consumed as a fuel. However, burning of these fossil fuels uses old biomass and it is converted into the new CO₂; this contributes to the greenhouse effect and decreases the nonrenewable sources. Burning new biomass contributes to no new CO₂ in the atmosphere, because replanted biomass ensures that CO₂ is absorbed and returned to a cycle of new growth. According to the IPCC, emission coefficient characteristics of the fuels are given in Figure 1.3. When biomass is used for the production of 1 GJ, 0 kg CO₂ is produced; however, when fossil fuels are used for the production of the same amount of energy, higher amounts (60-110 kg) of CO₂ will be released to the atmosphere (IPPC, 1996).

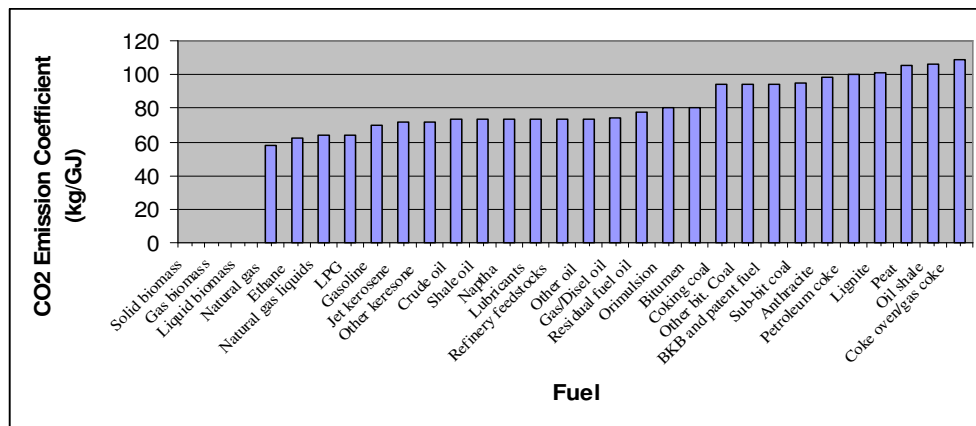


Figure 1.3. Emission coefficient characteristics of fuel (kgsCO₂/GJ) (IPCC, 1996)

CO₂ is one of the main greenhouse gases. It is estimated that CO₂ contributes almost 50 % to the anthropogenic greenhouse effect. After 1900 with the industrial revolution, CO₂ concentration in the atmosphere started to increase. The change of CO₂ concentration in the atmosphere with respect to years is shown in Figure 1.4. Due to increasing population and industrial activities, energy consumption of the countries increases every year. Therefore, more fossil fuels are consumed and more CO₂ emissions are released to the atmosphere.

As it can be seen from Figure 1.4, the concentration of the CO₂ in the atmosphere is still increasing, like other greenhouse gases. Increase of the concentration of greenhouse gases in the atmosphere can cause warmer temperatures on the earth. Rising of temperature 1.5- 4 °K in this century would have very important and complex effects on the world. All models about the global warming agree that an increase in the global average temperature will cause more evaporation and more precipitation. The precipitation would not increase everywhere, so there will be drought in the interior areas. Therefore, there will be water shortage in these areas; and humans, plants and animals will be adversely affected by this situation. In order to prevent a warming of more than a couple of degrees, current level of emissions must be reduced by about 60%. So, in order to reduce the potential warming, renewable energy sources should be used like biomass; energy efficiency for the energy productions should be increased and destruction of the tropical forests should be stopped (Demirbaş, 2004).

Accordingly, if biomass is produced on a renewable basis, usage of biomass energy does not result in a net carbon dioxide increase, because plants absorb it, when they grow. This will help to reduce the warming problem on the global scale. In addition to the CO₂ reduction, usage of biomass helps conservation of nonrenewable-fossil fuels. In the world, 80% of total primary energy supply was obtained from fossil fuels in 2001 (23.3% from coal, 35% from oil, 21.2% from natural gas) and 10.9% of total primary energy supply was obtained from

biomass (IEA, 2006). So, world mainly depends on the limited fossil fuels, and due to increasing energy demand, these sources are consumed increasingly every day.

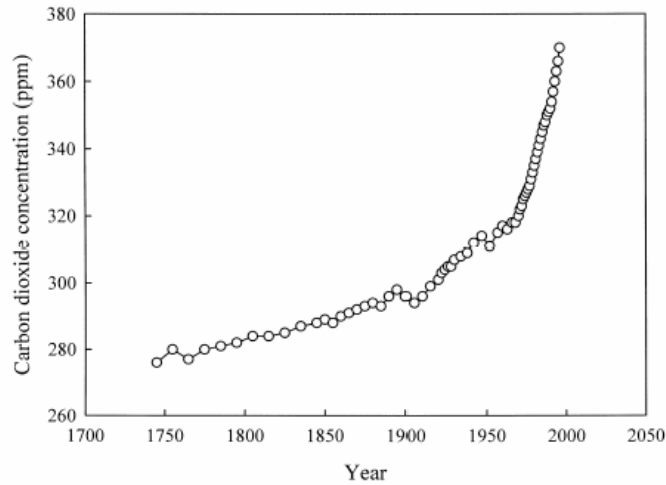


Figure 1.4. Raising of CO₂ concentrations in the atmosphere (Demirbaş, 2004)

In theory, it is assumed that if only proved reserves are used and there are no imports of fossil fuels and there is a constant rate of fuel consumption, coal will be supplied for 258 years. If proved reserves are used and annual growth rate of world economy is taken as constant (1.2%), oil will be supplied until 2027 (Klass, 1998). Therefore, one day fossil fuels would be finished because they are in limited supply; so, to solve this problem, renewable energy sources should be preferred, non-renewable energy sources should be used efficiently. In the meantime, new and cleaner energy sources should be searched. There are many advantages of biomass usage for the production of energy. These are:

- Biomass is very abundant. It can be found in every where
- It is easy to convert biomass to a high energy containing fuels such as alcohol or gas.
- It is cheap in contrast to the other energy sources.

- Biomass production can often mean re-saturation of waste land (e.g. deforested areas).
- It may also utilize areas of unused agricultural land and provide jobs in rural communities.
- If fossil fuels are used for the energy production, due to sulfur and nitrogen contents, SO₂ and NO_x will be released to atmosphere at high combustion temperatures. Therefore, replacement of fossil fuels with biomass which has lower sulfur content can reduce the acid rain problem.
- Biomass can be used to generate electricity with the same equipment or power plants that are now burning fossil fuels. Also among the biomass sources, some biomass types have high energy values; for example, 1 kilogram of dry plant tissue can produce as much as 16 MJ of heat which is equivalent to the heat available from 0.5 kg of a good quality coal. Therefore, biomass can be used effectively for the energy production processes.

Utilization of biomass is important for the production of clean energy in Turkey. In this way, the reduction of the green house gases, especially reduction of CO₂ can be managed. Although Turkey has a high population, due to its developing economy, CO₂ emissions of the country is low as compared to the other OECD countries such as USA, Japan, Canada, Denmark, Austria, Luxemburg, Italy, Hungary, Finland, Norway, and Germany. Also due to low GDP (Gross Domestic Product), carbon emissions per capita (3 ton CO₂ per year) are very low, when compared to the other OECD countries; for example for EU and USA, carbon emissions per capita are 2.4 ton and 20.5 CO₂ per year, respectively. However, Turkey is producing more pollutant, 0.95 kgCO₂ per unit GDP (\$) among the OECD and EU countries (e.g. Germany 0.33 kg CO₂, Japan 0.36 kg CO₂, USA 0.77 kg CO₂) in terms of carbon density of economy. Therefore, Turkey can not produce its energy by clean techniques; for this reason, Turkey is not being able to decrease its CO₂ emissions (Energy and Natural Sources Panel, 2003). GHG emissions of Turkey with respect to years are given in Table 1.4.

Table 1.4. GHG emissions of Turkey, with respect to years (thousand tons)
(Kaygusuz et al., 2002)

Emissions	1970	1975	1980	1985	1990	1995	2000	2005	2010
CO ₂	44,775	69,840	81,889	108,923	177,973	211,229	303,079	397,351	535,966
CH ₄	22,954	24,495	27,574	23,265	21,618	24,302	25,585	25,531	25,640
CO	2008	2665	2936	3115	3715	3961	8390	9552	11,433
N ₂ O	521	663	753	868	1128	6116	4656	4858	5394
NO _x	219	335	380	493	680	814	1154	1513	2073
VOC	241	332	360	380	524	599	1415	1638	1991
SO ₂	2	4	131	420	813	894	1038	1038	1038

However, according to the KYOTO protocol, Turkey will have to decrease its CO₂ emissions to 1990 level. Until now, Turkish energy policies to solve CO₂ problem have stressed only the energy efficiency and conservation as a part of the problem. However, renewable energy technologies have proven ability to offset increasing emissions of carbon dioxide and other GHGs. Therefore, biomass is one of the renewable energy sources that will be able to decrease the CO₂ emission problem of Turkey (Ocak et al., 2004).

1.3. Biomass Potential of Turkey

In 2001, contribution of the biomass to Total Primary Energy Supply was found as 258 Petajoules (PJ) including 204 PJ from wood and 55.7 PJ from animal-plant waste. In Turkey total 50-60 million tons of cereal products and fatty seed plants and 8-10 million tones of solid waste and animal waste are produced in a year; 70% of these biomass can be converted to energy (Kaya, 2006). Although the consumption of the biomass sources as compared to the total energy has decreased from 23% to 10% during the last decade, today biomass is still one of the most important energy sources on the national basis. Biomass is usually used in the commercial and rural areas for heating. Especially, fuel-wood is the primary fuel in poor regions of rural and urban areas. Present and projected

biomass energy production of Turkey between 2000 and 2030 is given in Table 1.5. Classical biomass such as animal and crops waste is obtained from conventional sources and methods, while modern biomass such as ethyl alcohol, biodiesel is obtained from renewable sources. As it can be seen from Table 1.7, modern biomass production will gain importance as compared to classical biomass production in the future (Balat, 2005).

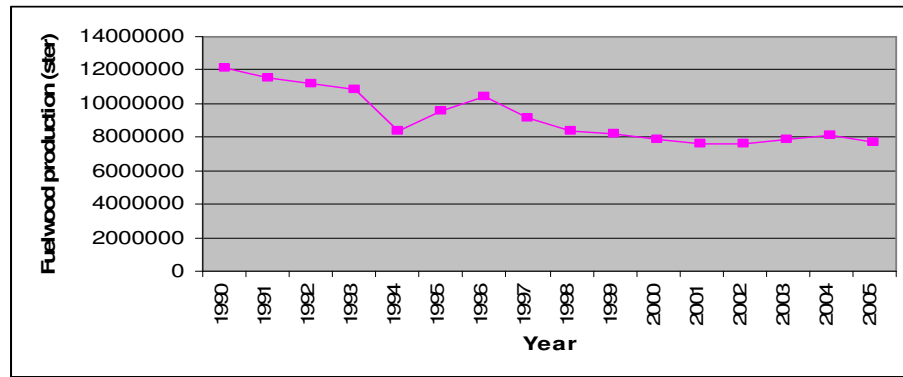
Table 1.5. Present and planned biomass production of Turkey (KTOE) (Balat, 2005)

Years	Classical biomass	Modern biomass	Total
2000	6965	17	6982
2005	6494	766	7260
2010	5754	1660	7414
2015	4790	2530	7320
2020	4000	3520	7520
2025	3345	4465	7810
2030	3310	4895	8205

The annual biomass potential of Turkey is about 32 MTOE and the total recoverable bioenergy potential is estimated to be approximately 17 MTOE. Important biomass sources of Turkey are forests as a virgin biomass, agricultural residues, animal wastes, and forest and wood industry residues as a waste biomass. When annual biomass potential of Turkey in 2001 was examined, forest residues and residues from wood industries were found as a second biggest biomass source of Turkey with 22.5% (7.2 MTOE) after annual and perennial crops with 70%. Therefore, Turkey has great potential for the production of the clean and renewable energy by using waste wood coming from forest and wood processing industries (Balat, 2005).

1.3.1. Virgin Biomass (Forest Resources) Potential of Turkey

The total forested area in Turkey occupies 27.22 % (21,188,746 Ha) of the land area, in 2004. The total forest potential of Turkey is around 935 million m³ with an annual growth of about 28 million m³ (GDF, 2006). According to the GDF (General Directory of Forestry) in 2005 about 7,000,000 Ster fuel wood and 8,000,000 m³ industrial wood were produced in Turkey. Fuel wood is the fifth largest source of energy in Turkey and it is the major source of energy in rural areas. In Turkey, energy supply from forest sector is about 3.5 MTOE per year (Forestry Special Impression Commission Report, 2001). Fuel wood production with respect to years in Turkey is given in Figure 1.5.



1 Ster=0.750 m³

Figure 1.5. Fuel wood production in Turkey with respect to years (GDF, 2006)

1.3.2. Waste Biomass Sources of Turkey

1.3.2.1. Agricultural Residue Potential of Turkey

Cereals, oily seeds and tube crops are most widespread crops in Turkey. The total annual amount of agricultural residues in the country is approximately 50-65 Mton and total calorific value for agricultural residues is 228 PJ. Among the total calorific value, maize has the biggest share with 33.4%, then wheat comes with 27.6%, and cotton comes with 18.1%. When total calorific value of the annual fruit residues of Turkey are calculated, total calorific value is found 75 PJ. As major crops, hazelnut with 55.8% and olive with 25.9% contribute a large percentage to the total calorific value.

1.3.2.2. Animal Waste Potential of Turkey

The number of cows, sheep and poultry in Turkey per year is about 13, 30 and 265 million, respectively. The capacities of the waste quantities of these animals are found as a 128, 25 and 8 million tons per year, respectively. The total calorific values for cow, sheep and poultry wastes in Turkey are calculated about 47.8, 3.6 and 8.7 million Gj/year, respectively (Exploitation of agricultural residues in Turkey, 2005).

1.3.2.3. Woody Waste Potential of Turkey

Forestry residues after harvesting and wood industry residues constitute the main woody waste potential of Turkey.

Logging Wastes

In Turkey, the annual apparent consumption of industrial wood is about 13-13.5 million m³, and that of the fuel wood is about 6-6.5 million m³. Annually about 7.5-8 million m³ of industrial round wood and 5.0 million m³ of fuel wood are produced from the state forests according to GDF. Fast-growing plantations of the private sector and agro forestry sites produce about 3.2 million m³ industrial round wood and 1.5 million m³ of fuel wood annually. Industrial wood production and consumption amounts are given in Table 1.6 (Ballı, 2005). The major tree species for round wood production in Turkey are Calabrian pine, Crimean pine, Scots pine, beech, fir, spruce, cedar, and oak. The major utilization areas of industrial wood are sawn wood manufacture industry, wood-based panel industry, wooden wrapping and packaging material production, and parquet production and other flooring, wood pulp production, mining, telecommunication and electrical transmission lines.

In 2004, 19,692,000 m³ industrial round wood were produced in Turkey. Therefore, 9,846,000 m³ (3,446,000 ton) logging residues (about 50% by volume) were produced in Turkey in 2004 (Sims, 2002). If the net calorific value is taken as 9 MJ/kg, a total of 3.1×10^{10} MJ energy is present in logging residues and chips. If collection and utilization efficiency is taken as 50% as an average value, the total energy from the logging residues for Turkey is found as 1.5×10^{10} MJ in 2004 (Todd, 2003).

Table 1.6. Industrial round wood production and consumption by years, 2000-2004 (1000 m³) (Ballı, 2005)

Years	2000	2001	2002	2003	2004
Production					
State	7328	6778	8005	7320	8196
Private	3262	3300	3300	3300	3300
Total	10590	10078	11305	10620	11496
Consumption					
State sales	7642	6778	8109	7420	7950
Private sector sales	3262	3300	3300	3300	3300
Net import	1880	930	1044	1398	1750
Total	12784	11008	12453	12118	13000

Sawmill Wastes

Sawn wood production and consumption amounts for Turkey between 2000 and 2004 are given in Table 1.7.

Table 1.7. Production, apparent consumption and trade amounts of sawn wood by years, 1995-2004 (1000 m³) (Ballı, 2005)

Years	Production		Import		Export		Consumption	
	Conifer	Non Con.	Conifer	Non Con.	Conifer	Non Con.	Conifer	Non Con.
2000	3118	2410	235	77	15	28	3338	2459
2001	2597	2337	140	38	132	36	2605	2339
2002	2764	2410	119	77	104	54	2779	2433
2003	2986	2629	130	106	59	41	3057	2694
2004	3625	2590	272	101	37	20	3860	2671

In 2004, 2,590,000 m³ of nonconifer, 3,625,000 m³ of conifer, and total OF 6,215,000 m³ of sawn wood were produced in Turkey, and these amounts were consumed. Therefore, in 2004 about 6,215,000 m³ (1,864,500 tons) sawmill residues were produced during the sawmill operations. If the net calorific value

of sawmill residues is taken as 8 MJ/kg, the total energy content of the sawmill residues is calculated as a 1.5×10^{10} MJ. If collection and utilization efficiency is taken as 50%, 0.75×10^{10} MJ is found in the sawmill residues of Turkey in 2004.

Wood Based Panel Wastes

Wood based panel production amounts in Turkey are given in Table 1.9. In 2004, 60,000 m³ plywood were produced in Turkey which makes about 15,000 tons plywood residue. If the average net calorific value is taken as 16 MJ/kg, the total energy content of the plywood residues is found as 2.4×10^8 MJ. If collection and utilization efficiency is taken as 50%, 1.2×10^8 MJ is found in plywood residues in 2004.

Table 1.8. Wood based panel production amounts in Turkey with respect to years (FAO, 2006)

Years	Plywood (m³)	Particle board (m³)	Total Fiber board (m³)	Hardboard (m³)	MDF (m³)	Insulating board (m³)
2000	47,000	1,884,000	422,000	-	388,000	34,000
2001	35,000	1,664,000	386,000	-	355,000	31,000
2002	55,000	1,999,000	600,000	-	570,000	30,000
2003	57,000	2,300,000	887,000	77,000	777,000	33,000
2004	60,000	2,700,000	1,003,000	120,000	850,000	33,000

From particle board and MDF production, lower amount of residues are produced with respect to the plywood residues. The residue amount from the particleboard industries can change between 5-10%. For Turkey if average 10% is used for the calculation of waste amount, it can be assumed that about 300,000 m³ particleboard and 100,000 m³ of MDF wastes are produced in 2004. If these volumes are converted to weight basis, 120,000 tons of particleboard wastes and 75,000 tons of MDF wastes makes about a total of 200,000 tons wastes (Dias et al., 2005). If net calorific value (as received) is taken as a 17 MJ/kg due to their

low moisture content of these wastes, the total energy content is found as 3.4×10^9 MJ.

Other Wood Industry, Furniture, Construction and Demolition Wastes

Industries of further processed sawn wood, parquet and other flooring, wooden wrapping and equipment packing, builder's joinery and carpentry wood are all important for Turkey; however, there is not enough information about production and consumption values of these industries. There is no net data about construction waste amounts in Turkey. However, after the 1999 Marmara earthquake, a significant (approximately 13 million tons) amount of debris was released. Esin and Cosgun (2006) examined the construction waste amounts from the modifications of buildings. According to their study, frequent modifications are made in Turkey and about 66% of wood was removed because of these interior modifications. Also, reuse or recovery ratio for modification wastes was found low for woody residues and this ratio was found to be about 34%. Therefore, important amounts of woody wastes are produced from the modification of buildings in Turkey and most of these woody wastes are not reused (Esin et al., 2006).

According to the waste statistics survey from manufacturing industry in Turkey, about 17.5 million tons of solid wastes were produced in 2004. 149,265 tons of this waste was produced from the furniture industry which makes about 1%. Out of this waste, 98,929 tons was reused, 43,516 tons of this amount was sold or donated, and 6,820 tons of this amount was disposed off (5728 tons were sent to the sanitary landfill site and 57 tons were incinerated) (SIS, 2006).

Telephone and Mining Poles Wastes

In Turkey, about 530,000 m³ of telephone and mining poles were produced in 2004. The production amounts of telephone and mining poles production amounts are given in Table 1.9 with respect to the years.

Table 1.9. Telephone and mining poles production amounts between, 2000 and 2004 (GDF, 2006)

Years	Telephone poles (m³)	Mining poles (m³)	Total (m³)
2000	155000	413000	568000
2001	85000	380000	465000
2002	28000	587000	615000
2003	39000	422000	461000
2004	45000	485000	530000

These poles, after their service life, will be considered as waste wood. There is no data about waste amounts of telephone and mining poles in Turkey. However, nowadays, most of the telephone poles in city centers can not be used since telephone cables are buried under ground; so, unused poles are collected from their places. Therefore, important amounts of telephone poles which are treated with chemicals are produced as a waste wood. If 3% of poles are assumed to be as waste, about 16,000 m³ of poles would be produced as a waste pole in 2004 in Turkey.

1.3.2.4. Municipal Solid Waste (MSW) Amount

In 2004, a total of 24.24 million tons of solid wastes was collected from municipalities that have solid waste services. Only 28.9% of this waste was sent to the sanitary landfills, and the rest was disposed in different ways. If anthropogenic methane emissions from MSW landfills in Turkey are calculated

according to the methodology recommended by IPCC (Kumar et al., 2004; Tsai, 2007), about 800,000 metric tones of CH₄ is calculated to be released as landfill gas in 2004. Pure heating value of methane is 33,810 kJ/m³. If the efficiency is assumed as 50% for CH₄, and 16.9 MJ/m³ value is taken as the heating value of CH₄, the total calorific value for municipal solid wastes of Turkey is found as 2x10¹⁰ MJ in 2004.

1.3.2.5. Pulp and Paper Sludge

According to the waste statistics survey of the manufacturing industry in Turkey, from 28 pulp and paper production industries, 55,687 tons of sludge was produced. 0.03% of this sludge was used for agriculture, 5.7% for production processes; 18.33% was sent to dumping sites of municipalities, 10.95% was dumped in ordinary way, 64.70% was sent to the sanitary landfills and only 0.29% of this sludge was burned (Waste inventory for the manufactured goods, 2004). However, if all sludge was burned (average effective heating value of sludge is taken as 5.5 MJ/kg at a moisture content of 60-65%, about 3x10⁸ MJ of energy would be produced in 2004 (Pulp and paper sludge to energy, 2006).

The summary of energy potential of Turkey from waste biomass sources is given in Table 1.10. It can be seen that the total energy potential of Turkey from waste biomass sources is found as 303 PJ which is equivalent to 7.3 MTOE. This makes about 9% of the total primary energy supply of Turkey in 2004.

Table 1.10. Total energy potential of Turkey from waste biomass sources in 2004

Waste Biomass Sources	Energy Amount
Agricultural and animal waste potential	
Agricultural residues	228 PJ*
Fruit residues	75 PJ*
Animal waste	60 GJ*
Woody waste potential	
Logging residues	31 GJ**
Sawmill residues	15 GJ**
Wood based panel residues	3.5 GJ**
MSW	20 GJ**
Pulp and paper sludge	0.3 GJ**
TOTAL	303 PJ

* Calculated according to the annual potential values of waste

** Calculated according to the 2004 data

1.4. Objective of This Study

As can be seen from the previous summary the waste wood potential of Turkey is good. Therefore, it is necessary to know the combustion kinetics of these materials containing high amount volatile organics in order to design the combustion equipments in the correct way for energy recovery.

The main goal of this study is to determine the combustion kinetics and emissions of the pine, MDF, plywood and particle board wastes selected as types of waste wood in this study. Analysis of the influence of the types of waste wood on the kinetic parameters and emissions as a result of the combustion phenomena are also among the goals of the study.

Two main objectives are established to achieve this main goal. In the first part of the study, the aim is to determine the thermal kinetics of the waste wood samples; pine, MDF, plywood and particle board in the air atmosphere aiming;

- To determine the weight losses of the different waste wood samples in the air atmosphere with respect to temperature (peak temperatures, oxidation regions, etc.).
- To determine the thermal kinetics (Activation energy and pre-exponential constant) using Broido Method and Coats-Redfern Method by using 6 unit solid state decomposition mechanisms for three oxidation regions and,
- To determine differences among the different types of wood waste for combustion mechanisms.

In the second part of the study, the aim is to examine the emissions as a result of combustion of waste wood samples. Emissions are examined specifically aiming:

- To determine main emission groups for each waste wood sample (OH groups, aliphatics, CO₂, CO, carbonyl groups, aromatics, cellulose, lignin, and other groups) with respect to time (temperature) and,
- To determine the emissions with respect to the oxidation regions of different types of waste wood samples.

CHAPTER 2

LITERATURE SURVEY

2.1. Waste Wood

Wood in many forms has played an important role in sustaining all forms of life on our planet. It has been used to cook food, to heat buildings and to power industries for many years. After the Industrial Revolution, importance of the fossil fuels such as coal, oil and gas has gained great importance, and they have been consumed increasingly as time passed.

Wood has a strategic role because of it is carbon-based renewable source of energy. Timber as a living plant absorbs atmospheric CO₂ and stores it. After it is combusted or thermally degraded to produce energy, wood emits the CO₂ to the environment. Therefore, wood is a carbon neutral renewable energy source. Moreover, replacing fossil fuels with the wood fuel to produce energy reduces net CO₂ atmospheric emission level by over 90% (De Jong, et al., 2003; Hagedorn, et al., 2003).

Wood is used in different fields such as in making electricity poles, telephone poles and in the production of wood based panels, furniture and construction material as well as fuel. During the production of wood based products or after the service life of these products, great amounts of waste wood are generated as by products. Therefore, “waste wood” term not only includes the residual wood from industry, but also used wood. Depending on the production processes or usage purpose, some types of these wastes can have different kinds of contaminants.

2.2. Sources of Waste Wood

An overview of the sources of wood waste is given in Figure 2.1. The principal sources of waste wood are (Scotland, 2003):

- Forestry residues,
- Primary processing: Sawmilling processes,
- Secondary processing: Furniture, panel, paperboard, joinery manufacture and construction,
- Waste streams: Industrial, commercial, demolition and domestic.

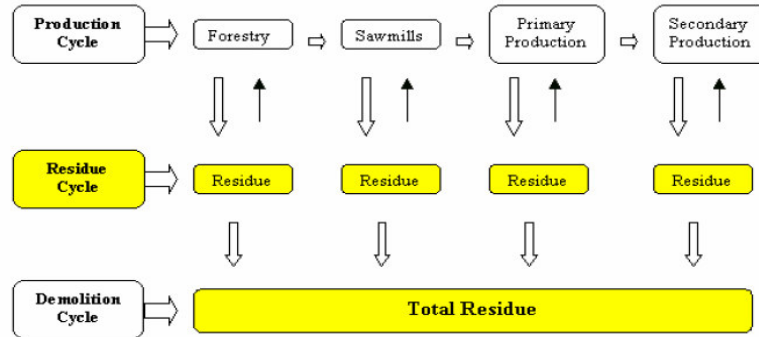


Figure 2.1. Sources of wood wastes (Scotland, 2003)

2.2.1. Forestry residues

Almost 60 percent of the total harvested tree is left in the forest and non-commercial species is subjected to slash and burn, or to make access easier for logging. Practices such as sawing and squaring logs in the forest, rather than at the sawmill, add wastes further 8-10 % and 30 to 50 %, respectively.

Proper training, appropriate tools and logging equipments can improve the methods of harvesting and reduce the excessive wastes; otherwise, a higher yield of wood waste will occur (FAO Corporate Document Repository, 2006).

2.2.2. Primary Processing

The primary processing of timber entails the removal of coarse material and natural contaminants that could reduce the quality and value of the timber in its identified market place. Typically, this comprises mechanical sawmilling to de-bark and cut the lumber into slabs and beams (Scotland, 2003). A breakdown of residues probably from sawmills are 70% solids (slabs, edgings and dockings), 19% sawdust and 11% bark. Additional wastes are produced from the sawn timber during subsequent machining (Fung et al., 2002). Mill residues can be utilized for energy production, secondary raw materials production such as MDF, particleboard, pallet manufacturing, pulp and paper industry and fertilizer (Enters, 2001). When available volume of residue is considered, primary processing residues are the most suitable residues for on-site and local markets, e.g. rural domestic heating.

2.2.3. Secondary Processing

The actual production of waste, generated from the manufacture of wood products, differs from plant to plant and depends on several factors. Proportion of the wastes generated in selected forest products industries are given in Table 2.1.

Table 2.1. Proportion of wastes generated in selected forest products industries
(FAO Corporate Document Repository, 2006)

	Sawmilling (air dried)	Plywood Manufacturing	Particleboard Manufacturing
Finished product (range) (%)	45-55	40-50	85-90
Finished product (average) (%)	50	47	90
Residues/Fuel (%)	43	45	5
Losses (%)	7	8	5
Total	100	100	100

All wood waste and bark, which are also commonly referred to as hog fuel due to the process of reducing the residues in size in a "hogger", has a fuel value. Although it is produced in a wide range of sizes with varying moisture contents, it is composed of mainly bark, coarse residues, cores, sawdust, planer shavings, sanderdust and particleboard residues. Bark which makes up some 10 to 22 percent of the total log volume depending on size and species; can itself represent a serious waste disposal problem unless it can be used as a fuel or removed prior to log preparation. Coarse residues, such as slabs, edgings, off-cuts, veneer clippings, sawmill and particleboard trim, when reduced in size, make ideal fuel, especially when dry. Cores come from plywood peeler logs. Sawdust is used for manufacturing of particleboard. Planer shavings result from dimensioning and smoothing lumber, plywood and particleboard with planers during the finishing stage. They are considered ideal for particleboard production and are particularly good for heating kilns and dryers. Sanderdust is produced during the abrasive sanding of lumber, plywood and particleboard during the finishing stage. Because of its size and very low moisture content, it is well suited for direct firing. Particleboard residues, being in the order of five percent, is negligible compared to that generated in other mechanical wood-based industries, as it is largely recycled within the production process (FAO Corporate Document Repository, 2006).

2.2.4. Waste Streams

Waste streams contain industrial, commercial, demolition and domestic waste streams. Demolition and construction wastes mainly consist of construction, formwork lumber, logs, plywood, laminates, coarse particles and residues, and they are generated in the construction and demolition of residential and commercial buildings, roads, tenant improvements and remodels, landscaping and site clearing activities. Share of the waste wood in the construction and demolition wastes can change, depending on the country. For example, in USA

about 20 % of the construction and demolition waste is wood-based, in Hong Kong it is 7.5 %, and in UK this ratio is 25% (Öztürk, 2006).

In European countries, most of the wood based demolition and construction wastes after cleaning are utilized for different purposes such as energy cogeneration, fence material, floor covering material, telephone poles. However, in undeveloped countries, these types of wastes are used for mainly heating. On the other hand, some of the wastes from the demolition and construction sites can contain some hazardous chemicals such as PCB, asbestos (Öztürk, 2006). Industrial and municipal wastes are two of the sources of waste wood. Furniture industry can produce important amounts of waste wood which contains different types of glue, paint or chemicals. Municipal wastes can also contain different amounts of waste wood.

2.3. Categories of Waste Wood

Waste wood can be categorized into four groups, depending on their pollution levels (Peek, 2004):

- **Waste wood category A1:** Waste wood in its natural state or only mechanically worked state which, during use, is the most insignificantly contaminated with substances harmful to wood.
- **Waste wood category A2:** Bonded, painted, coated, lacquered or otherwise treated waste wood with *no halogenated* organic compounds in the coating and no wood preservatives.
- **Waste wood category A3:** Waste wood *with halogenated* organic compounds in the coating with no wood preservatives.
- **Waste wood category A4:** Waste wood treated *with wood preservatives*, such as railway sleepers, telephone masts, hop holes, vine poles, as well as other waste wood which, due to contamination, can not be assigned to

waste wood categories 1, 2, 3 with the exception of waste wood containing PCBs.

General classing of waste wood arising from regular assortments and their samples are given in Table 2.2. As can be seen from Table 2.2, different kinds of waste wood are produced from the different types of sources. Depending on the production methods and usage purposes, some of the waste wood contains different types of pollutants. Especially production of the composite wood materials: plywood, oriented strand board, particleboard, hardboard, fiberboard and MDF, different chemicals are used. Commonly used resin–binder systems include phenol-formaldehyde, urea formaldehyde, melamine-formaldehyde, and isocyanate (Youngquist, 1999).

Table 2.2. General classification of waste wood arising from regular assortments and samples (Peek, 2004)

Common types of waste woods (examples)			Categories
Wood waste from woodworking and machining	Waste, cuttings, shavings from solid wood in its natural state		A-1
	Waste, cuttings, shavings, from derived timber products and other treated wood (with no harmful contaminant)		A-2
Packing	Pellets	Pellets made from solid wood	A-1
		Pellets made from derived timber products	A-2
		Other pellets with composite materials	A-3
	Transport cases		A-1
	Boxes for fruit, vegetables, ornaments		A-1
	Ammunition boxes		A-4
	Cable reeds from solid wood		A-1

Table 2.2. (Continued)

Waste wood from construction work	Waste wood from building sites	Solid wood in its natural state	A-1
		Derived timber products, barked wood, treated solid wood (with no harmful substances)	A-2
	Waste wood from demolition and restoration work	Boards, false ceilings, planks from interior works (with no harmful substances)	A-2
		Door leafes and frames (without harmful substances)	A-2
		Profile boards for the fitting out of rooms, ceiling panels, ornamental beams etc. (without harmful substances)	A-2
		Heat and sound insulation board treated with agents containing PCBs	Disposal
		Chipboard used in construction	A-2
		Timber framework and rafter	A-4
		Windows, window posts, outer doors	A-4
		Impregnated wood used in external structures	A-4
	Wood from construction and demolition work containing harmful contaminants		A-4
Impregnated waste wood used in external structures	Railway sleepers	A-4	
	Transmission poles	A-4	
	Various wood used in horticulture and landscaping, impregnated garden furniture	A-4	
	Various wood used in agriculture	A-4	
Furniture	Furniture, solid wood in its natural state	A-1	
	Furniture, with no halogenated organic compounds in the coating	A-2	
	Furniture, with halogenated organic compounds in the coating	A-3	
Waste wood from bulky refuse (mixed)		A-3	
Waste wood from industrial use		A-4	
Waste wood from hydraulic engineering			
Waste wood from dismantled vessels and goods wagons			
Waste wood from damaged structures			
Fine fraction from processing of waste wood to make derived timber			

For the production of composite wood materials, chemicals used are given below:

- **Phenol-formaldehyde (PF)** resins are typically used in the manufacture of products requiring some degree of exterior exposure durability, for example, OSB (Oriented Strand Board), softwood plywood, and siding.
- **Urea-formaldehyde (UF)** resins are typically used in the manufacture of products where dimensional uniformity and surface smoothness are of primary concern, for example, particleboard and MDF. Urea-formaldehyde resins (often referred to as urea resins) are more economical than PF resins and are the most widely used adhesive for composite wood products.
- **Melamine-formaldehyde (MF)** resins are used primarily for decorative laminates, paper treating, and paper coating. They are typically more expensive than PF resins. MF resins may be blended with UF resins for certain applications (melamine urea).
- **Isocyanate** as diphenylmethane di-isocyanate (MDI) is commonly used in the manufacture of composite wood products; MDI is used primarily in the manufacture of OSB. Facilities that use MDI are required to take special precautionary protective measures.

Also a number of additives are used in the production of conventional composite products. One of the most notable additives is wax, which is used to provide finished products with resistance to aqueous penetration. Other additives used for specialty products include preservatives, fire retardants, and impregnating resins.

For production of structural composite lumber (SCL) products; laminated veneer lumber (LVL), laminated strand lumber (LSL), parallel strand lumber (PSL), or oriented strand lumber (OSL) which consist of small pieces of wood glued together into sizes common for solid-sawn lumber, different chemicals are used. Production of the Glued-laminated timber (glulam) is also an engineered stress

rated product that consists of two or more layers of lumber, and chemicals are used (Ibach, 1999).

For production of the structural composites, glulam and wood based panels some wood preservatives such as oil borne, waterborne and creosote solutions are also used. Wood can be protected from the attack of decay fungi, harmful insects, or marine borers by applying chemical preservatives. The degree of protection achieved depends on the preservative used and the proper penetration and retention of the chemicals. Wood preservatives can be divided into two general classes; oil borne preservatives, such as creosote and petroleum solutions of pentachlorophenol and, waterborne preservatives that are applied as water solutions (Ibach, 1999).

1. Oil borne preservatives: Wood does not swell from treatment with preservative oils, but it may shrink if it loses moisture during the treating process. Creosote and solutions with heavy, less volatile petroleum oils often help protect wood from weathering, but may adversely influence its cleanliness, odor, color, printability, and fire performance (Ibach, 1999). Types of the oil borne preservatives and usage place and purposes are given in Table 2.3.
2. Waterborne Preservatives: Waterborne preservatives are often used, when cleanliness and printability of the treated wood are required. Several formulations involving combinations of copper, chromium, and arsenic have shown high resistance to leaching and very good performance in service. Waterborne preservatives are included in specifications for items such as lumber, timber, posts, building foundations, poles, and piling. Some of the water borne preservatives are Acid Copper Chromate (ACC): used for posts against to decay and termite attack, Chromated Copper Arsenate (CCA), Ammoniacal Copper Quat (ACQ) and Inorganic Boron (Borax/Boric Acid) against decay, termites, beetles, and carpenter

ants. Borates are widely used for log homes, natural wood finishes, and hardwood pallets (Ibach, 1999).

Table 2.3. Types and usage purpose and places of the oil borne preservatives (Ibach, 1999)

Type of the oil borne preservatives	Usage place and pupose
Coal-Tar Creosote	Timbers, poles, piles, and railroad ties.
Creosote Solution	Railroad ties and posts
Pentachlorophenol Solutions	Railroad ties and posts against fungi, molds, stains, and insects
Copper Naphthenate	Against fungi and insecticides
Chlorothalonil	Aboveground and ground contact applications
Chlorothalonil/Chlorpyrifos	Against fungi and insecticides
Oxine Copper (copper-8-quinolinolate)	Against fungi and insecticides
Zinc Naphthenate	Used against fungi and mildew
3-Iodo-2-Propynyl Butyl Carbamate	Nonstructural, aboveground use only (for example, millwork).
Alkyl Ammonium Compound	Against wood decay fungi and insects
Propiconazole	Aboveground and sapstain control application

2.4. Properties of Waste Wood

To understand the utility and performance of waste wood as an energy source, it is important to explain physical and chemical properties of waste wood which affects its behavior as a fuel, because these parameters determine the combustion and heat release characteristics of wood. Physical properties include moisture content and density. Chemical properties include proximate and ultimate analysis, holocellulose and lignin content and heating values.

Trees mainly can be grouped under the two section; conifers or softwood and nonconifers or hardwood. Both of them include cellulose, hemicellulose, and lignin in different amounts depending on the species. Commonly, hardwoods

contain more hemicellulose (for example carbohydrates) and less lignin than softwoods (Tillman et al., 1981).

2.4.1. Physical Properties of Waste Wood

The moisture content of the wood is especially important for the wet wood, because moisture content directly influences the net heating value of the wood, the pathways of the combustion and efficiency of the combustion.

The weight of wood and amount of energy obtained from the wood vary according to the moisture content and density of the wood. The moisture content on a dry basis expresses the quantity of the present water in a proportion of the weight of the oven dried wood (Wickens, 2001). Moisture contents and densities of the different types of waste wood are given in Table 2.4.

Table 2.4. Wood fuels, wood composites and their moisture contents and densities (Sims, 2002; Youngquist, 1999)

Waste wood types	Moisture content (% by wt)	Bulk density (kg/m ³)
Logging residue chips	50-60	250-400
Wood residue chips	10-50	150-300
Saw residue chips	45-60	250-350
Plywood residue	5-15	200-300
Uncoated wood	15-30	150-250
Softwood bark	50-65	250-300
Air dry wood chips	20-25	190-290
Kiln dry wood chips	10-15	160-250
Insulation board	Wet process	200-400
MDF	Wet process	600-800
MDF	Dry process	600-800
Particleboard	Dry process	600-800
Plywood	Dry process	400-800

2.4.2. Chemical Properties of Waste Wood

Woody biomass ($C_{3.3-4.9}H_{5.1-7.2}O_{2.0-3.1}$) is partially oxygenated materials. The chemical characteristics of these fuels are described by summative analysis, proximate analysis, and ultimate analysis (Tillman et al., 1981).

2.4.2.1. Summative Analysis

Wood is composed of mainly cellulose, hemicellulose ($C_5H_8O_4$), lignin ($C_9H_{10}(OCH_3)_{0.9-1.7}$) and certain extractives (aliphatics compounds, terpenes, terpenoids and phenolic compounds). Cellulose ($C_6H_{10}O_5$) and hemicellulose are grouped together as holocellulose, and they are primary components in the cell wall of wood fiber. Cellulose consists of repeating cellobiose units; however, hemicellulose consists of a variety of hexoses and pentoses. Lignin is a three dimensional cross-linked polymer (Tillman et al., 1981).

2.4.2.2. Proximate and Ultimate Analysis

Usually solid fuels are characterized by proximate and ultimate analysis. Ultimate analysis and proximate analysis of some selected untreated (natural) waste wood species are shown in Table 2.5 and Table 2.6.

Table 2.5. Ultimate analysis of some selected untreated wood species (on dry basis) (Cheremisinoff et al., 1976; Tillman, 1981)

Wood species	C (%)	H (%)	S (%)	O (%)	N (%)
Fir	52.3	6.3	-	40.5	0.1
Fir bark	54.1	6.1	-	38.8	0.17
Pine	59.00	7.10	-	32.68	-
Pine bark	53.4	5.6	0.1	37.9	0.1
Beech	51.64	6.26	-	41.45	-
Uncontaminated waste wood	39.58	5.17	0.08	54.13	0.19

Table 2.6. Proximate analysis of some untreated wood species (on dry basis)
(Cheremisinoff et al., 1976; Tillman, 1981)

Wood species	Volatile matter (%)	Fixed carbon (%)	Ash (%)
Black oak bark	81.0	16.9	2.1
Red alder bark	77.3	19.7	3.0
Tan oak bark	76.3	20.8	2.9
Fir	87.3	12.6	0.1

Proximate and ultimate and approximate analysis of treated waste wood can change depending on the chemical contents. Ultimate and proximate analyses of some treated waste wood samples are given in Table 2.7 and 2.8.

Table 2.7. Ultimate analysis of some waste wood samples (dry, wt%) (Skodras et al., 2002)

Waste wood type	C	H	S	O	N
Demolition wood	44.5	5.6	0.09	44.7	1.1
Wood, telephone poles	55.7	6.02	0.56	34.5	0.44
Power poles	45.34	5.38	-	48.20	0.18
Wood railroad sleepers	52	6.03	0.1	39.9	0.38
Railway sleepers	39.29	4.66	-	41.77	0.16
Wood plywood scarps	54.7	6.13	0.04	37.3	0.31
Wood, industrial wood waste	50.5	6	0	42.9	0.2
Furniture, wood waste	50.9	6.13	0.02	40.2	1.6
Wood waste	49.2	5.7	-	41.3	2.5
Wood residues containing adhesives	49.2	6.12	0.02	41.5	2.21
Sawdust from particleboard	48.9	6.22	0.1	38.5	5.03
Wood particleboard	51.8	5.81	0.03	38.8	2.96
Wood chipboard	47.8	6.09	0.08	40.2	3.91
Wood plywood	48.1	5.87	1.45	42.5	-
CCA treated wood	50.9	6.1	-	41.6	0.18
Wood salt impregnated	51	6.24	0.01	41.2	0.16
MDF	46.49	5.98	0.30	44.32	2.37

Table 2.8. Proximate analysis of some waste wood samples (on dry basis)
(Skodras et al., 2002)

Waste wood type	Volatile matter (%)	Fixed carbon (%)	Ash (%)
Railway sleepers	84.396	14.7	0.9
Demolition wood	88.799	9.398	1.803
Power poles	84.397	14.708	0.9
MDF	90.098	9.364	0.536
Plywood	82.1	15.8	2.1
Waste wood	89.8	7.8	2.4
Wood furniture waste	80.4	18.3	1.3
CCA treated wood	81.1	17.9	1

2.4.2.3. Heating Value

When energy is derived from the biomass fuels by combustion in air, the energy content equates the heat energy (calorific value) released. The higher heating value (HHV) or gross calorific value (GCV) of fuel is the amount of heat released from the fuel when it is combusted at the standard conditions (at 15 °C, 1 bar and 60% humidity). The lower heating value (LHV) or the net calorific value is related with the amount of useful energy as result of combustion. The difference between the HHV and LHV is due to moisture content of the fuel. The LHV is more meaningful for the comparison of the fuels (Sims, 2002). Energy yield is usually expressed on its net calorific value. Net calorific value increases when moisture content of a fuel decreases. Net calorific value of the waste wood (*Pinus radiata*) as a function of moisture content is given in Figure 2.2.

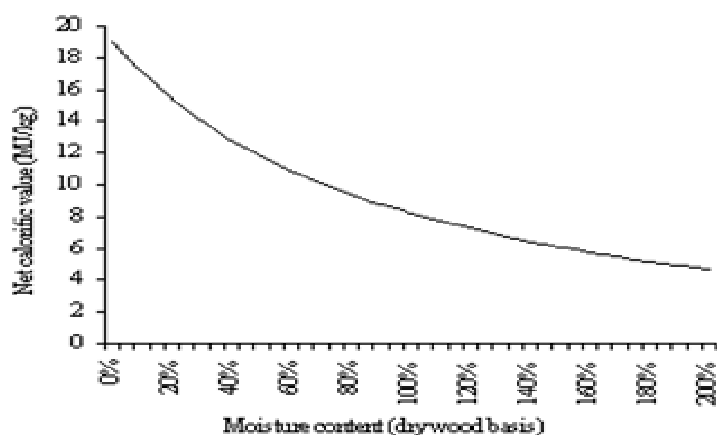


Figure 2.2. Change in net calorific value of the waste wood as a function of moisture content (Sims, 2002)

Untreated wood generally consists of 49-50% carbon, 6% hydrogen, 43-44% oxygen and 0.5-1% nitrogen, sulfur and ash. Because of this small variation, there is a slight difference for the heating values of the untreated woods (Wickens, 2001). The calorific value of the woody wastes is mainly affected by the lignin content of the substances, resins and used chemicals. The ash content of the non combustible inorganic minerals adversely affects the calorific value and decreases the heating value per unit weight of the fuel. Heating values of the different types of treated and untreated waste woods are given in Table 2.9.

As it can be seen from Table 2.9, according to the source of the waste wood and their usage purpose, calorific value of the waste wood can vary because different types of chemicals and resins will be used for different types of production processes.

Table 2.9. Heating values of different treated waste woods, (kJ/kg) (Phyllis, 2006)

Waste wood type	Heating value	Dry	Dry ash free	As received
Demolition wood	HHV	19600	20020	17914
	LHV	18378	18872	16587
Telephone poles	HHV	21922	22463	
	LHV	20608	21117	
Railroad sleepers	HHV	19000	19289	
	LHV	17400	17665	
Waste wood	HHV	18100	18402	11946
	LHV	16744	17024	10221
Urban waste wood	HHV	20143	20807	17194
	LHV	18762	19381	15658
Plywood	HHV	17500	17821	15050
	LHV	16155	16451	13552
Wood residues contain adhesives	HHV	18000	18163	
	LHV	16500	16650	
Furniture waste	HHV	19626	19840	
	LHV	18288	18488	
Industrial wood waste dust	HHV	19700	19779	17474
	LHV	18391	18465	16037
Plywood scarps	HHV	21370	21695	
	LHV	20032	20337	
Particleboard	HHV	19361	19408	
	LHV	18093	18137	
CCA treated wood	HHV	20600	20808	17922
	LHV	19269	19464	16446
Forest residues	HHV	18100	18320	12742
	LHV	16791	16995	11098
Pine dust	HHV	20768	21048	17929
	LHV	19450	19713	16458

2.5. Energy Production from Waste Wood

Wood is a form of biomass which is capable of different ways of generating more valuable and flexible forms of energy. There are 3 types of technologies for processing biomass (Scotland, 2003). These are biochemical conversion, thermochemical conversion and digestion.

The main process used is thermochemical conversion for waste wood in Turkey because producers of forest products use their wood waste in their boilers. The thermochemical conversion processes are:

- Direct combustion
- Pyrolysis
- Gasification

Lignocellulosic materials are not directly combustible; however, under sufficiently strong source of energy or pilot ignition, wood decomposes to volatile pyrolysis products which burn in the gas phase with flaming combustion. The charred residue burns at a relatively slower rate by surface oxidation or glowing combustion. Competing reactions in the pyrolysis and combustion of cellulose are given in Figure 2.3 (Anderson, 1977).

In the direct combustion process, wood is burned with adequate oxygen and energy is released. In the combustion of wood and bark, the following three processes occur, orderly at first but then simultaneously (Cheremisinoff et al., 1976):

1. First, heat must be supplied to evaporate the water in the wood fuel,
2. Secondly, volatile hydrocarbon gases are evolved and burn with oxygen giving off heat,
3. Lastly, more heat is released and combustion is completed with reaction of oxygen with the fixed carbon at high temperatures.

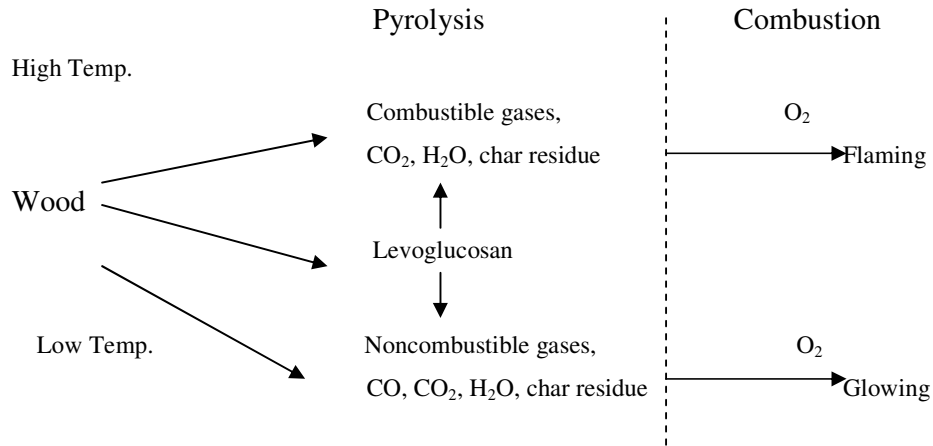


Figure 2.3. Competing reactions in the pyrolysis and combustion of cellulose (Schiewind, 1989)

For the combustion of the wood, shrinking core model can be used. Because, despite the different problems, on the basis of studies of numerous systems, the “**shrinking core**” model is the best simple representation for the majority of reacting gas-solid systems. According to the model, when no ash is formed, like in the burning of pure carbon, the reacting particle shrinks during the reaction and then finally disappears. This kind of model can be explained by using three phases. These phases are (Levenspiel, 1972);

- Diffusion of the reactant from the main body of gas through the gas film to the surface of the solid,
- Reaction at the surface between reactant and solid,
- Diffusion of reaction products from the surface of solid through the gas film back in to the main body of gas.

When wood is exposed to elevated temperatures, changes in the structure of the wood occur. The extents of these changes depend on the temperature level and the length of time under conditions the wood is exposed. At a temperature below 100 °C, permanent reductions in strength can occur. The magnitude of the

reduction depends on the moisture content, heating medium, exposure time and the materials. There is no carbohydrate degradation below 100 °C. If the wood is treated with a chemical to reduce the flammability, more reductions in strength can occur at lower temperatures, when compared to untreated wood, because chemicals in the treated wood can catalyze dehydration and depolymerization reactions.

At temperature above 100 °C, chemical bonds begin to break. The rate of the broken bonds increase as temperature increases. Between 100 and 200 °C, noncombustible products such as carbon dioxide, traces of organic compounds and water vapor are produced. Above 200 °C celluloses break down, produce flammable volatiles. If volatile compounds are mixed with air and heated to the ignition temperature, combustion reactions occur. The energy from these reactions radiates to the solid, thus propagates the combustion or pyrolysis reactions. If the burning mixture accumulates enough energy to emit radiation in the visible region, flaming combustion occurs. Above 450 °C, all volatile material is gone, and the residue remaining is an activated char. This char can be oxidized to carbon dioxide, carbon monoxide and water vapor; therefore oxidation of this char is called as afterglow.

Thermal reactions of the wood can vary, depending on the individual components and chemical content of the wood. Cellulose is mainly responsible for the production of flammable volatiles. Hemicellulose is less stable thermally than cellulose and it evolves more noncombustible gases. Lignin produces more residual char than the cellulose (Schiewind, 1989).

2.6. Thermal Analysis of Waste Wood

Thermal decomposition of small samples of wood causes two decomposition regimes. One of them occurs due to decomposition of cellulose, and the other

one occurs due to decomposition of hemicellulose. The peak in the decomposition regime at lower temperatures and the shoulder might be related with the decomposition of the hemicellulose. The higher temperatures may be related with the cellulose degradation. A peak due to the lignin degradation might not be observed.

Wood is commonly used because of its higher energy content per volume, lower ash yield and lower nitrogen content. Other advantage of wood is the low sulfur content in comparison to most of fossil fuels (Nassar, 1999). Owing to these advantages, wood is widely used for energy production. In principle, there are two ways to release heat and energy from wood. These methods are direct combustion or thermochemical conversion into gases and liquids for the gas turbines and engines. Thus, knowledge of the kinetics of the woods is essential (Hagedorn et al., 2003) because designing technologies based on the pyrolysis and combustion of renewable lignocellulosic raw materials requires good knowledge of the kinetic information on these process (Ella et al., 2005).

Three factors control the design of a gas-solid reactor; the reaction kinetics for single particles, the size distribution of solids being treated, and the flow patterns of solids and gas in the reactor. Where the kinetics are complex and not well known, and the products of reaction from a blanketing fluid phase, and temperature within the system varies greatly from position to position, analysis of the situation becomes very difficult. Therefore, in the designing the gas-solid reactors knowledge of the kinetics and shape of the particles during the reaction with surrounding gas, to know the controlling mechanism will supply important data. For example, fraction of the solid which will be converted to end product and the reaction time can be determined by using different equations. These equations are mainly based on the different mechanisms (e.i. diffusion, chemical reaction). Therefore, responsible mechanisms and characteristics of the particles must be determined in advanced for the correct design.

The temperatures at which decomposition reactions of wood start and the changes in sample weight with the reactions can be found by thermogravimetric analysis curves. Quantitative methods can be applied to thermogravimetric analysis curves to obtain kinetic parameters. The kinetic parameters usually include the activation energy, the pre-exponential factor and the order of the reaction (Schiewind, 1989).

Modern thermal analyses suggest that activation energy is the predominant factor in the reactivity equation. Activation energy essentially affects the temperature sensitivity of the reaction rate, although the pre-exponential factor is related more with material structure. Accordingly, reactivity of the wood is characterized by its activation energy alone (Ella et al., 2005).

However, these kinetic parameters are highly dependent on experimental conditions such as heating rates, sample size, moisture of the sample and the heating medium. A wide range of values have been reported for both the activation energy and the pre-exponential factor due to different methods used under different conditions and different heating rates; therefore, they are not directly comparable (Schiewind, 1989).

Activation energies for wood pyrolyzed in nitrogen range from 63 to 139 kJ/mole for pyrolysis temperature less than 300 °C and from 109 and 227 kJ/mole for temperatures greater than 300 °C. For pyrolysis in air, the values range from 96 to 147 kJ/mole. The pyrolysis proceeds faster in air than in an inert atmosphere, and this difference gradually diminishes around 310 °C (Schiewind, 1989).

Zakrzewski (2003), examined thermal kinetics of the air dried pine and beech particles (0.5-1.5 mm), in helium atmosphere under the non isothermal conditions at 5°C/min heating rate. In this study, activation energies were calculated by using solid state equations. Activation energies and pre-exponential

constant values were found for pine between 91.8-175.8 kJ/mole and 4.9×10^4 - $7.1 \times 10^{11} \text{ min}^{-1}$, respectively. It was found that diffusion models D3 and D4 approximated the experimental data better than first order reaction model F1 (Zakrzewski, 2003).

Gao (2004), investigated thermal degradation of wood treated with basic nitrogen compounds and phosphoric compounds in air and nitrogen atmosphere with 100 ml/min flow rate by differential thermal analysis and TGA from ambient temperature to 650 °C. In the study, air dried and 50 mesh size samples were used, and heating rate was chosen as a 10 °C/min. In the study, activation energies of the samples for different stages of thermal degradation were calculated by using Broido method. Activation energies of the untreated sample were found higher than the treated samples. The values were found to decrease from 126 kJ/mole to 74 kJ/mole. The char yield was found to increase from 18.5 to 40 %, and LOI (limiting oxygen index) increased from 18.5 to 40, therefore the flame retardancy of wood picked up. For the degradation of wood which was treated with MFP (melamine, formaldehyde and phosphoric acid) and UDFP (urea, dicyandiamide, formaldehyde and phosphoric acid), lower temperatures were observed (<300 °C) in the second stages of the samples, therefore; fewer flammable products and more chars were occurred from these samples. However, wood which was treated for MF (melamine formaldehyde), second stage was found at higher temperatures like untreated wood sample, this showed that wood treated with MF has poor flame retardancy (Gao, 2004).

Reine et al. (1998), studied thermogravimetric properties of the 3 types of waste wood (forest wood, old furniture and used pallets) in TGA equipment using dynamic and isothermal techniques. All experiments were performed under the nitrogen atmosphere with a flow rate of 50 ml/min. Mass of the samples was taken as a 25 mg and samples were sieved between 0.7-0.7 mm. For dynamic experiments, five different heating rates were used: 2, 20, 35, 50 and 100 °C/min. For 2 °C/min heating rate for furniture, forest and pallets activation energies

were found as a 129.6, 136.18, 127.6 kJ/mol, respectively. The pre-exponential factors were 1.91×10^7 , 3.38×10^7 , $1.23 \times 10^7 \text{ s}^{-1}$, respectively (Reina et al., 1998).

Deka et al. (2002), studied chemically treated hard wood. Three types of resins were used (urea formaldehyde, melamine formaldehyde and phenol formaldehyde) for the chemical treatment. The thermal degradation of the treated and untreated samples were studied using thermogravimetric (TGA) and differential thermogravimetric techniques at heating rates of 20 and 30 °C/min in a temperature range of 30-650 °C in static atmosphere. Weight of the samples was taken in the range of 8.10-14.75 mg. Coats and Redfern methods were used for the calculation of kinetic constants. For untreated sample at 20 and 30 °C/min heating rates, activation energies were found as 112.4 and 119.2 kJ/mol, and pre-exponential constants were found as a 46.2 and 45.2 min^{-1} , respectively. For treated samples, higher activation energy and pre-exponential constants were found. For treated samples, activation energies were found in the range of 132.6-138.5 kJ/mol, pre-exponential constants were found in the range of 49.1-52.9 min^{-1} (Deka et al., 2002).

Thermal decomposition of a solid is a very complex process which occurs in a hetero-phase system in several stages. These stages can be related with heat transport as well as a discharge of vapor-gas products of decomposition or development of a new solid phase (Zakrzewski, 2003).

In TGA, the weight of the wood samples is determined as a function of time and temperature. TGA experiments are usually performed in two ways:

1. Isothermal,
2. Non-isothermal conditions.

In isothermal conditions, sample is heated at a constant temperature. In non-isothermal conditions, sample is heated at a constant rate. For both methods,

there are some advantages and disadvantages. In the literature there are different studies performed by two methods.

Isothermal TGA is not attractive because of the excessive time. In addition, multiple experiments are required, and at least three experiments are necessary for assessment of reactivity parameters (Ella et al., 2005). In isothermal investigations, the non-isothermal stage of sample for heating to the measurement temperature is also unavoidable and, hence, it was suggested to apply a more accurate term for these methods, i.e. quasi-isothermal (Zakrzewski, 2003). However, isothermal studies are more straightforward as compared to non-isothermal studies, therefore thermal kinetics can be calculate more easily than the non-isothermal studies.

For the non-isothermal studies, one single experimental run is enough for the calculation of thermal kinetics. Shorter period of time is also needed, as compared to the isothermal conditions. Still, there are some disadvantages of this method too. The mathematical equations for linear heating are not easily analyzed. Linear heating rate, instrument sensitivity and sample size can change the thermal kinetic results. To overcome this problem, usually 8-12 °C heating rate are chosen (Ella et al., 2005).

2.7. General Information about IR Spectroscopy

An invaluable tool in organic structure determination and verification involves the class of electromagnetic (EM) radiation with wavenumbers between 4000 and 400 cm^{-1} . This category of EM radiation is termed infrared (IR) radiation and its application in chemical analysis known as IR spectroscopy.

Radiation in this region can be utilized in organic structure determination by making use of the fact that it is absorbed by interatomic bonds. Chemical bonds

in different environments will absorb varying intensities and at varying frequencies. Thus IR spectroscopy involves collecting absorption information and analyzing it in the form of a spectrum. The frequencies at which there are absorptions of IR radiation ("peaks" or "signals") can be correlated directly to bonds within the compound (Introduction to IR Spectra, 2006).

A summary of the IR absorption spectrum with respect to wavenumbers is given in Figure 2.5. There are different regions in this spectrum, like Functional Group Region and Fingerprint Region as shown in the Figure 2.4.

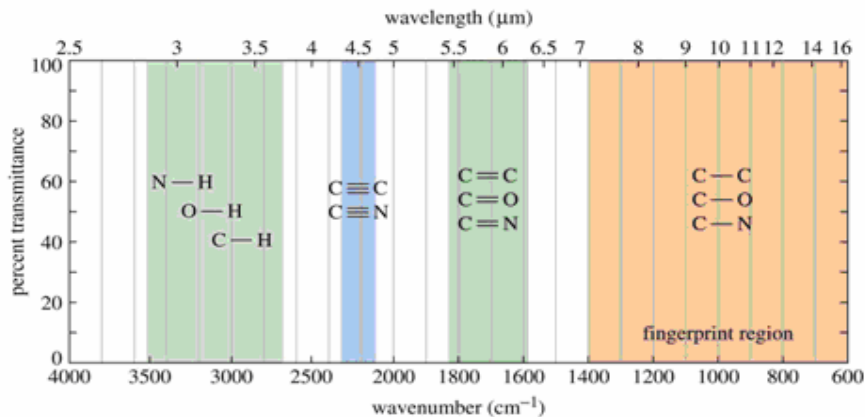


Figure 2.4. Summary of the IR absorptions (Blackburn, 2003)

The Functional Group Region is for the wavenumber of, 4000 to 1300 cm^{-1} . The appearance of strong absorption bands in the region of 4000 to 2500 cm^{-1} wavenumber usually comes from stretching vibrations between hydrogen and some other atoms, O-H, C-H and N-H stretching frequencies fall within the 3700 to 2500 cm^{-1} region with various intensities. Hydrogen bonding has a significant influence on the peak shape and intensity, generally causing peak broadening and shifts in absorption to lower frequencies (Introduction to IR Spectra, 2006).

It is not possible to acquire IR spectra of hydroxyl containing compounds without seeing this broad signal. By creating a very dilute solution of the same sample, or acquiring the IR spectra in the gas phase, hydrogen bonding is prevented through lack of molecular contact. In these situations, the broad O-H peak is replaced by a sharp signal around 3600 cm^{-1} (Introduction to IR Spectra, 2006).

The C-H stretch region centered around the wavenumber of 3000 cm^{-1} where all hydrocarbons show spectral features generating an overlap of peaks giving rise to a spectral envelope where the single contributions are not easily resolvable. The assignment of individual peaks is difficult due to this overlap. Usually C-H stretching bands occur in the wavenumber region of 3300 to 2800 cm^{-1} . The acetylenic C-H exhibits strong absorption at about 3300 cm^{-1} wavenumber. Alkenes and aromatic C-H stretch vibrations absorb at 3100 to 3000 cm^{-1} . Most aliphatic (saturated) C-H stretching bands occur at wavenumber of 3000 to 2850 cm^{-1} , with generally prominent intensities that are proportional to the number of C-H bonds (Arrigone et al., 2005).

Aldehydes often show two sharp aldehydic C-H stretching absorption bands at 2900 to 2700 cm^{-1} . The absorption bands at the 2700 to 1850 cm^{-1} region only from triple bonds and other limited types of functional groups, such as C=C wavenumber at 2260 to 2100 cm^{-1} , C=N at 2260 to 2220 cm^{-1} , diazonium salts – N⁺-N at approximately 2260 cm^{-1} , allenes C=C=C at 2000 to 1900 cm^{-1} , S-H at 2600 to 2550 cm^{-1} , P-H at 2440 to 2275 cm^{-1} , Si-H at 2250 to 2100 cm^{-1} (Introduction to IR Spectra, 2006).

The 1950 to 1450 cm^{-1} wavenumber region exhibits IR absorption from a wide variety of double bonded functional groups. Almost all the carbonyl C=O stretching bands are strong and occur at 1870 to 1550 cm^{-1} . Acid chlorides and acid anhydrides give rise to IR bands at 1850 to 1750 cm^{-1} . Whereas ketones, aldehydes, carboxylic acids, amides, and esters generally show IR absorption at

1750 to 1650 cm^{-1} wavenumber, carboxylate ions usually display stretching bands at 1610 to 1550 and 1420 to 1300 cm^{-1} wavenumber. Conjugation, ring size, hydrogen bonding, and steric and electronic effects often result in significant shifts in absorption frequencies. Nonconjugated aliphatic C=C and C=N groups have absorption bands at 1690 to 1620 cm^{-1} , with variable intensities. Aromatic compounds contain delocalized $\pi(\pi)$ electrons from the resonance stabilized double bonds, showing skeletal vibrations (including C-C stretchings within the ring) in the 1650 to 1400 cm^{-1} region and weak combination and overtone bands in the 2000 to 1650 cm^{-1} wavenumber region. Molecules containing NO_2 groups, such as nitro compounds, nitrates, and nitramines, commonly exhibit asymmetric and symmetric stretching vibrations of the NO_2 group at 1660 to 1500 and 1390 to 1260 cm^{-1} wavenumber region (Introduction to IR Spectra, 2006).

The Fingerprint Region: The region between 600 and 1400 cm^{-1} wavenumber is called Fingerprint region where complex vibrations occur. Absorptions in this region include the contributions from complex interacting vibrations, giving rise to the generally unique fingerprint for each compound. A good match between the IR spectra of two compounds in all frequency ranges particularly in the fingerprint region strongly indicates that they have the same molecular structure. Carbonyl C=O stretch at a wavenumber of 1750 to 1735 cm^{-1} , but also exhibit their characteristic absorption at 1300 to 1000 cm^{-1} wavenumber from the couplings of C-O and C-C stretches (Blackburn, 2003).

The Aromatic Region (between 910-650 cm^{-1} wavenumber): The IR bands in this region do not necessarily come from the aromatic compounds, but the absence of strong absorption in the 910 to 650 cm^{-1} wavenumber region usually indicates the lack of aromatic characters. The out-of-plane bending of ring C-H bonds of aromatic and heteroaromatic compounds gives rise to strong IR bands in the range between wavenumber of 910 and 650 cm^{-1} . Certain nonaromatic

molecules such as amines and amides can also contribute absorption in this region (Hsu, 2006).

2.8. Functional Groups of Wood with FTIR

Pandey, (1999), studied the hard wood and soft wood constituent polymers (cellulose and lignin) using FTIR spectroscopy. He estimated the holocellulose to lignin ratio for some timber species obtained from soft and hard wood species. In this study IR spectrum of wood showed O-H stretching absorptions around the wavenumber of 2900 cm^{-1} and in the fingerprint region, between wavenumber of $1800\text{-}900\text{ cm}^{-1}$. Many sharp and discrete absorption bands are observed in this region due to the various functional groups present in wood constituents. At around wavenumber of 2900 cm^{-1} C-H, at around 1740 cm^{-1} wavenumber C=O, and at around wavenumber of 1510 cm^{-1} C=C pure bands were found. However, other bands in the finger print region at lower wavenumbers than 1460 cm^{-1} are complex, having contributions from various vibration modes in carbohydrates and lignin (Pandey, 1999).

Drobinak and Mastalerz (2006), studied the Miocene conifer wood samples in order to discuss chemical variations in the structure of wood as a result of biochemical coalification. 40 samples were used for FTIR analysis for this study and depending on the transformation degree samples were divided into 4 groups: Group 1 least transformed to, group 4 most transformed to carbonization. For comparison of the groups with FTIR peak areas were measured. Peak areas represented the following groups in the various wavenumber regions were measured:

- The hydroxyl group region $3100\text{-}3600\text{ cm}^{-1}$ wavenumber,
- Aromatic stretching region $3000\text{-}3100\text{ cm}^{-1}$,
- Aliphatic stretching region $3000\text{-}2800\text{ cm}^{-1}$,

- Carboxyl/carbonyl group region 1700-1800 cm^{-1} ,
- Aromatic carbon peak a 1604 cm^{-1} and aliphatic bending region ~1350-1470 cm^{-1} ,
- Cellulose and lignin region 1300-1000 cm^{-1} , and the aromatic out-of-plane region 700-900 cm^{-1} .

The aliphatic stretching region (wavenumber of 3000-2800 cm^{-1}) was deconvoluted into individual bands to calculate CH_2/CH_3 ratios. FTIR band assignments used in this study are given in Table 2.10 (Drobniak et al., 2006).

According to FTIR results, during the transformation of wood samples from group 1 to group 4; they found an overall increase in lignin/cellulose ratio, an increase in oxygen functionalities, an increase in aliphatic stretching and bending functionalities from groups 1 to 3, followed by decrease in the wood of group 4, the appearance of aliphatic out of plane bands in group 3 and their increase in group 4, a relative increase in CH_2/CH_3 in group 4, and a relative decrease in O-H groups in group 4 compared to other groups (Drobniak et al., 2006).

Bilba et al. (2006), studied four fibers from banana and coconut trees before their incorporation in cementitious matrices. Thermal degradation of these fibers was studied between 200 and 700 °C under nitrogen atmosphere. Fourier transform infra red spectroscopy (FTIR) was used in addition to the other methods. In this study, FTIR spectra of the raw fibers were compared with the previous studies and spectra of commercial cellulose and lignin. In the FTIR spectra of raw samples a strong band at a wavenumber of 1036 cm^{-1} was seen due to C-O-C symmetric stretching dialkyl ether linkages, due to C-O stretching vibrations in cellulose, hemicellulose and minor lignin contributions. A large characteristic band at 3600-3100 cm^{-1} wavenumber was assigned to hydroxyl groups, O-H stretching vibration in carbohydrates (cellulose and hemicellulose) and lignin.

Table 2.10. FTIR band assignments (Drobniak et al., 2006)

Wavenumber	Group
3400 cm^{-1}	OH stretching vibrations of hydrogen bonded hydroxyl groups in polymeric association,
2960 and 2880 cm^{-1}	aliphatic C-H stretch, vibrations methyl (CH_3), 2920 and 2850 cm^{-1} were assigned to aliphatic C-H stretch, vibrations methylene (CH_2),
1750 cm^{-1}	C=O stretching of vibrations-carbonyl groups,
1710 cm^{-1}	C=O stretching of vibrations-carbonyl groups,
1610 cm^{-1}	aromatic ring C=C in plane methoxyl substituted benzene or phenol,
1511 cm^{-1}	C=O stretching vibrations
1445-1454 and 1420-1426 cm^{-1}	asymmetric aliphatic C-H deformation of methylene and methoxyl,
1370 cm^{-1}	symmetric aliphatic C-H bending of methyl groups,
1265-1275 cm^{-1} and 1210-1226 cm^{-1}	C-O stretch vibration in lignin guaciyl ring with C-O stretch,
1158-1161 cm^{-1} , 1105-1111 cm^{-1}	C-O stretch in cellulose,
1139-1141 cm^{-1}	aromatic C-H in plane in lignin (guaciyl),
1054-1070 cm^{-1} and 1029-1033 cm^{-1}	C-C-H deformation in cellulose, and C-C-O deformation in cellulose,

A large region of absorption involving overlapping bands in the range of 1700-1100 cm^{-1} wavenumber due to C-C, C=C, OH, CO, CH_n , C-O-C, CH aromatic linkages; bands at 2910, 2850, 1416, 700-900 cm^{-1} wavenumbers due to vibrations of CH_n aliphatic and aromatic present in carbohydrates and lignin were observed.

After pyrolysis the main differences appeared at 300 °C. At this temperature a decrease of intensities of OH, C-O, C=O, C-C, C-O-C groups, an increase for C=C groups and between 1100 and 1700 cm^{-1} wavenumbers were seen for all samples. When the temperature increased to 600 °C, intensities decreased and for CF (fabric from the bottom leaves of coconut) at 1038 cm^{-1} wavenumber the

highest peak was found. When spectra of the banana and coconut samples are compared, banana trees were found to decompose more rapidly than the coconut samples. When banana species (BL-Banana leaves, BC-The pseudo-stem core) samples pyrolyzed at 300 °C about 1600 cm⁻¹ band (aromatic skeletal modes of lignin and C=C stretching vibration of benzene) was found strongest peak not 1036 cm⁻¹. In addition to these peaks at 1314 cm⁻¹ (OH groups of carbohydrates) and at 778 cm⁻¹ (CH aromatic of carbohydrates and lignin) for BL sample, at 1550 cm⁻¹ (CO and aromatic skeletal modes of carbohydrates and lignin) and at 778 cm⁻¹ peaks were observed mainly for BC sample at 300 °C. At 400 °C the amount of C=O groups were found lower. At this temperature 1414 cm⁻¹ band was found strongest, 1600 and 1314 cm⁻¹ bands were found same intensity, the band 878 cm⁻¹ due to more intense of vibrations of CH species and inorganic compounds showed that pyrolysis led to decarbonylation and decarboxylation reactions and more inorganic compounds. Degradation of banana samples started by a decreasing of C=O bands and this caused to increasing of aromatic skeletal modes of lignin, OH, CO groups of carbohydrates at low temperature, at high temperature C-H bendings were observed. For banana and coconut samples same bands with different intensities of groups were observed due to different compositions. For BC samples approximately 1608, 1560, 1318 and 775 cm⁻¹ bands were observed, however for CF fibers approximately 1021, 1420, 1460 and 1391 cm⁻¹ bands were mainly observed. For CF, the broad signal from widening of the peaks confirmed the important degradation of the structure (Bilba et al., 2006).

Sharma et al. (2004), studied the characterization of lignin char and its reactivity for the formation of polycyclic aromatic hydrocarbons (PAHs). Char was prepared by pyrolyzing lignin under both pyrolytic and oxidative (5% O₂ in He) atmospheres at the atmospheric pressure. Temperature range was taken from 150 to 550 °C. In this study the chemical composition of char was characterized by FTIR and other techniques. In this study lignin and its chars were studied in the 4000-600 cm⁻¹ IR band by the infrared spectroscopy. A variety of bands were

observed for the lignin spectrum. At 3419 cm^{-1} OH, at 2844 cm^{-1} methoxyl, at $3000\text{-}2860\text{ cm}^{-1}$ aliphatic CH, at 3064 cm^{-1} aromatic groups, at 1513 and 1597 cm^{-1} aromatic ring modes were observed. In addition the these peaks at 855 cm^{-1} lone aryl CH wag, at 817 aryl CH wag, at 2843 cm^{-1} symmetric CH_3 stretch of the methoxyl group at 1033 cm^{-1} due to the C-O stretch for O- CH_3 and C-OH bands were observed.

The width and intensity of the bands between 1000 and 1100 cm^{-1} is dependent on presence of any sugars in the sample, while the bands for the hydroxyl group above 3000 cm^{-1} are due to alcoholic or phenolic components. The bands of the carbonyl groups appeared in the range between 1660 and 1725 cm^{-1} . The exact position of the bands was dependent on whether the C=O groups were in conjunction with the aromatic ring (position below 1700 cm^{-1}) or not (position above 1700 cm^{-1}). The most characteristic bands of lignin were at 1513 and 1597 cm^{-1} (aromatic ring vibrations) and between $1470\text{-}1460\text{ cm}^{-1}$ (CH deformation and aromatic ring vibrations). A higher intensity of the band at 1513 cm^{-1} compared to 1597 cm^{-1} showed that the lignin sample was probably obtained from softwood.

In the study the broad band for the OH in-plane bend decreased with increasing temperature. However, a band above 3600 cm^{-1} (free OH stretching) grew slowly with the pyrolysis temperature. This could be due to increased carbonization of the sample. The symmetric CH_3 stretch of the C- CH_3 group appeared at $2842\text{-}2839\text{ cm}^{-1}$ in chars and its intensity decreased rapidly when the temperature increased from 250 to $400\text{ }^\circ\text{C}$. The band was completely absent above $400\text{ }^\circ\text{C}$, shows that CH_3 groups were removed the substituted aromatic rings at high temperatures. Similar observations were made for the OC stretching at 1033 cm^{-1} and CH stretching for the aliphatics due to intensities of the these groups decreased as temperature of pyrolysis decreased. In this study the relative proportions of a functional group in different chars may be compared in terms of the corresponding peak areas. However, due to differences in the intensities of

the FTIR signals and the amount of sample in different analysis, the concentrations and path lengths were also different in various analyses. As a result, only the ratios of the peak areas with respect to a reference peak were compared in this study and the band at 1597 cm^{-1} (aromatic ring mode) was taken as the reference band and ratios of the peak areas of various functional groups relative to the reference were calculated and compared among the different char samples. As a result of electron donor substations, such as OH and OCH_3 were removed from the substituted ring at $400\text{ }^\circ\text{C}$. The OH group in chars at high temperatures was probably attached to aromatic group. In this study, the major steps were found as dehydration, carbonyl group formation and elimination, the decomposition of aliphatic units and the formation of aromatic units (Sharman et al., 2004).

CHAPTER 3

MATERIALS AND METHODS

In this study thermal gravimetric analysis was used to determine the combustion kinetics of several waste wood samples under air atmosphere. The selected waste wood samples were; pine, MDF, plywood and particleboard. For the determination of the thermal kinetics, Thermogravimetric Analyses (TGA) was used. In addition to the TG analyzer, FTIR (Fourier Transform Infrared Spectroscopy) analyzer was used in order to determine the emissions which were emitted from the samples because of thermal treatment under air at different temperatures. Emissions were determined on-line by FTIR instrument because FTIR was directly connected to TGA.

3.1. Physical and Chemical Characteristics of Waste Wood Samples

In the present study, four waste wood samples were used to investigate the thermal kinetics under air atmosphere. The list of samples is given in Table 3.1.

Table 3.1. List of waste wood samples

Sample Name	Treated	d _p ,mm
Pine	No	0.3-0.85
MDF	Yes	0.3-0.85
Plywood	Yes	0.3-0.85
Particleboard	Yes	0.3-0.85

Pine sample is an untreated sample; it does not contain any additional chemical. MDF, plywood and particle board samples were treated samples that contain different additives and chemicals.

Pine, MDF and plywood samples were obtained from a carpenter as a waste wood; particle board sample was obtained from furniture industry.

Ultimate and proximate analysis

The ultimate analyses of the all samples were performed by the Elemental Analyses Laboratory of the Central Analyses Laboratory of METU. The proximate analyses of all samples were performed by the Fuel Analyses Laboratory of the Chemical Engineering Department of METU. Ultimate elemental composition and proximate analysis results of all samples are given in Table 3.2. and Table 3.3, respectively. All samples were air dried because not to lose the very volatile chemicals in the treated samples. All samples were milled and sieved to 0.3-0.85 μm and conditioned in an oven at room temperature (25 $^{\circ}\text{C}$) for 30 min before the experiments.

Nitrogen and sulfur contents of treated samples are higher than the untreated pine sample because of the additional chemicals used during treatment.

Table 3.2. Elemental composition of all samples (on dry, ash free basis)

Sample	C (% by wt)	H (% by wt)	N (% by wt)	O (% by wt)	S (% by wt)
Pine	53.28	6.35	0.16	40.21	-
MDF	49.57	6.33	4.44	39.66	-
Particleboard	46.26	5.83	2.36	45.51	0.04
Plywood	47.12	5.92	1.19	45.72	0.05

Table 3.3. Proximate analysis and calorific values of all samples (on dry basis)

Sample	Volatile matter (% by wt)	Ash (% by wt)	Fixed carbon (% by wt)	Calorific value (MJ/kg)
Pine	88.02	0.62	11.29	19.72
MDF	86.68	2.29	11.06	19.31
Particleboard	83.82	1.22	14.38	17.51
Plywood	85.79	0.80	13.40	18.64

Calorific value and volatile matter content of untreated pine sample are higher than treated samples such as MDF, particleboard and plywood. However, treated samples have higher ash content as compared to the pine sample.

3.2. Thermal Analysis

The thermal analyses of the waste wood samples were carried out by using a Thermal Gravimetric Analyzer (TGA) located in the Central Analyses Laboratory of METU. The TGA in the laboratory was a Perkin Elmer-Pyris-1 model and it was coupled with a Perkin Elmer Spectrum-1 Fourier Transform Infrared (FTIR) Spectrometer for the analysis of evolved gases from the samples. In TGA, the weight loss of a waste wood sample was monitored in air atmosphere by using TG technique as a function of temperature. When wood sample was heated, the evolving volatile products were carried out of the furnace directly into a gas cell of the FTIR where the gases were analyzed by FTIR spectroscopy. A photograph of the TG-FTIR analyzer is shown in Figure 3.1, and a schematic diagram of the TGA-FTIR system is given in Figure 3.2.



Figure 3.1. Photograph of the TG-FTIR instrument

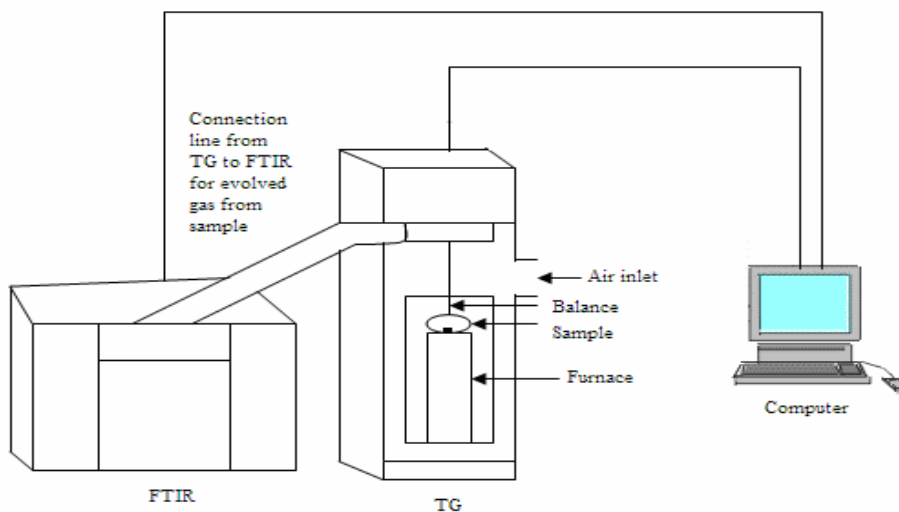


Figure 3.2. Schematic diagram of the TG-FTIR system

3.2.1. Thermogravimetric Analysis of Waste Wood Samples

About 5 mg sample was used for each experiment. Experiments were performed at 20 ml/min air flow rate and in a temperature range of 30-900 °C. For each waste wood sample, 3 heating rates, namely 10°C/min, 20°C/min and 30°C/min, were used for the experiments to understand the effect of heating rate on thermal kinetics, and emissions of the waste wood samples. For each experiment, weight loss of the waste wood samples was determined as a function of temperature.

The output of the instrument gives the TG curves as well as the derivative curves (DTG) of the sample. Properties of the TG (Perkin Elmer- Pyris-1 TGA) instrument are given in Table 3.4.

Table 3.4. Properties of the Perkin Elmer TG Analyzer (Model Pyris-1)

Sample atmosphere	Nitrogen, air, oxygen (Normal pressure)
Temperature range	Ambient-1000 °C
Scanning ranges	0.1-200 °C/min
Temperature precision	±2 °C
Balance sensitivity	0.1µg
Sample size	About 15 mg
Sample pans	Ceramic with 60µl
Calibration materials	Ni and Fe

The TG equipment was calibrated for temperature reading using nickel and iron as reference material before the commencement of the experiment.

3.2.2. FTIR Analysis of Evolved Gases

During the thermal decomposition process in the TGA, combustion gases are released from waste wood samples in air atmosphere and these gases are analyzed by FTIR analyzer simultaneously. All spectras were recorded every two seconds within a wave number interval of 4000-700 cm^{-1} with 2 cm^{-1} resolution. Nitrogen gas was used to correct the baseline of the FTIR spectrum before each experiment. Properties of the FTIR (Perkin Elmer Spectrum-1 FTIR Spectrometer) analyzer are given in Table 3.5.

After spectrums were recorded, they were searched by using Perkin Elmer Euclidean Polymer Library, and groups and chemicals were determined qualitatively in the evolved gases from the samples.

Table 3.5. Properties of the Perkin Elmer Spectrum-1 FTIR Spectrometer analyzer

Beam splitter	Multi-layer potassium bromide
Detector	Mid-infrared detector
Wavelength range	7800-350 cm ⁻¹ with KBr beam splitter
Resolution	0.5-64 cm ⁻¹
Wavelength accuracy	0.1-1600 cm ⁻¹
Signal to noise ratio For KBr optics	7,500/1 rms, 1,500/1 p-p for a 5 second measurement and 26,000/1 rms, 5,000/1 p-p for a 1 minute measurement
Available OPD Velocities	0.1, 0.2, 0.5, 1 and 2 cms-1
Atmospheric compensation	Minimizes effect of atmospheric water and CO ₂ on the sample spectra without the need for reference or calibration spectra.
Processing	1st - 4th derivative with a variable filter, smooth (Savitsky-Golay, moving average and triangular), difference, normalization, A, %T, %R, KM, LOG (1/R), ordinate modes, cm-1, nm and micron abscissa modes, +, -, *, /, difference, baseline correction, smooth, deconvolution, normalize, abex, interpolate, blank, Kramers-Kronig, ATR correction, peak table, peak height and peak area.
Materials testing	Patented COMPARE™ spectral comparison algorithm and Euclidean searching available. Spectral searching against commercially available or customer developed libraries.

3.3. Methods Used for the Calculation of Thermal Kinetics

All kinetic information can be extracted from the results of the dynamic experiments by means of various methods. All kinetic studies assume that the isothermal rate of conversion, da/dt , is a linear function of a temperature-dependent rate constant, k , and a temperature-independent function of the conversion, α , that is:

$$\frac{d\alpha}{dt} = kf(\alpha) \quad (3.1)$$

which expresses the rate of conversion, da/dt , as a function of the reactant concentration and the rate constant at a constant temperature (T).

$$\alpha = (m_0 - m_t)/(m_0 - m_\infty) \quad (3.2)$$

where:

m_0 – initial weight of the reactant,

m_t – weight at time t ,

m_∞ – final weight.

According to the Arrhenius Equation

$$k = Ae^{-E_a/RT} \quad (3.3)$$

Where A , the pre-exponential factor, is assumed to be independent of temperature, E_a is the activation energy, T is the temperature, and R is the gas constant.

Combination of Eqs. (3.1) and (3.3) gives;

$$\frac{d\alpha}{dt} = Af(\alpha) \exp(-E_a/RT) \quad (3.4)$$

In the thermal decomposition process, it is assumed that the rate of conversion is proportional to the concentration of material that has to react,

$$f(\alpha) = (1-\alpha)^n \quad (3.5)$$

$$\frac{d\alpha}{dt} = A(1-\alpha)^n \exp(-E_a/RT) \quad (3.6)$$

If the sample temperature is changed by a controlled and constant heating rate; $\beta = dT/dt$, the variation in the degree of conversion can be analyzed as a function

of temperature. This temperature is dependent on the time of heating.

$$\frac{d\alpha}{(1-\alpha)^n} = \frac{A}{\beta} \exp\left(-\frac{E_a}{RT}\right) dT \quad (3.7)$$

This is the fundamental expression of analytical methods to calculate kinetic parameters on the basis of TG data. These methods can be distinguished based on the degree of conversion measurement (α) and based on the heating rate, β .

The variation in the degree of conversion can be analyzed as a function of temperature, this temperature being dependent on the time of heating. Therefore, the rate of conversion may be written as follows:

$$\frac{d\alpha}{dt} = \frac{d\alpha}{dT} \frac{dT}{dt} = \beta \frac{d\alpha}{dT} \quad (3.8)$$

A combination of Equations (3.4) and (3.8) leads to

$$\frac{d\alpha}{dT} = \frac{A}{\beta} e^{-\frac{E_a}{RT}} f(\alpha) \quad (3.9)$$

Integration of this equation from an initial temperature, gives;

$$\int_0^{\alpha} \frac{d\alpha}{f(\alpha)} = \frac{A}{\beta} \int_0^{\alpha} e^{-\frac{E_a}{RT}} dT \quad (3.10)$$

The right hand side of the Equation (3.10) has no exact analytical solution, but making some variable substitutions and applying Cauchy's rule the expression can be solved to give:

$$\frac{A}{\beta} \int_0^T \exp\left(-\frac{E}{RT}\right) dT \cong \frac{ART^2}{\beta E} \left(1 - \frac{2RT}{E}\right) \exp\left(-\frac{E}{RT}\right) \quad (3.11)$$

If the solution of the integral on the left-hand-side of Equation (3.10) is denoted with:

$$g(\alpha) = \int_0^{\alpha} \frac{d\alpha}{f(\alpha)} = \frac{A}{\beta} \int_0^{\alpha} e^{\frac{E\alpha}{RT}} dT \quad (3.12)$$

Where $g(\alpha)$ is the integral function of conversion (Minying et al., 2003). Table 3.6 shows different expressions of $g(\alpha)$ for the six different solid state mechanisms which were used for this study for the estimation of reaction mechanisms from dynamic TG curves.

Then, after division by T^2 taking logarithms, Equation (3.10) is transformed to:

$$\ln \frac{g(\alpha)}{T^2} = \ln \frac{AR}{\beta E} \left(1 - \frac{2RT}{E}\right) - \frac{E}{RT} \quad (3.13)$$

Since, $\frac{2RT}{E} \ll 1$, Equation (3.13) will be,

$$\ln \frac{g(\alpha)}{T^2} = \ln \frac{AR}{\beta E} - \frac{E}{RT} \quad (3.14)$$

Coats and Redfern (Coats et al., 1964) makes use of an asymptotic expression to find an approximate solution for Eq. (3.10) thus; Equation (3.14) is found (Barral et al., 2005). The Coats and Redfern method requires to make an assumption about the functional form of $f(\alpha)$ or $g(\alpha)$. This implies that in each case the description of the reaction process gives a value for the reaction order n (Coats et al., 1964). The TG trace gives the relationship between α and T . This method is an integral method and in the integral methods this relation is used to

integrate the Equation (3.10) for determining the proper values of A, E, and n (Nishizaki et al., 1980).

The other assumptions of the Coats Redfern method are:

- Only one reaction mechanism operates at a time.
- The calculated E value is for this one mechanism.
- Product disappearance can be expressed by the basic rate Equation (3.1) (Turk et al., 1999).

According to the Equation (3.14), a plot of $\ln[g(\alpha)/T^2]$ against reciprocal of temperature should result in a straight line with a slope equal to $-E/R$. The formal expression of the functions $f(\alpha)$ and $g(\alpha)$ depend on the conversion mechanism and its mathematical model. If the correct $g(\alpha)$ is used, the plot of $\ln[g(\alpha)/T^2]$ against $1/T$ should give a straight line with high correlation coefficient of linear regression analysis, from which the values of E and A can be derived, therefore; the slope of the linear function will give the activation energy, E and the intercept of the line will give the pre-exponential constant, A (Vlaev et al., 2003).

In this study, Coats-Redfern method was used in order to estimate 6 solid state mechanisms (Table 3.6) for the calculation of the thermal kinetics such as activation energy and pre-exponential constant.

The function $g(\alpha)$ depends on the mechanism controlling the reaction, the size and the shape of the reacting particles (Gadalla, 1984). In a diffusion controlled reaction, numerous chemical reactions or micro-structural changes in solids take place through solid state diffusion, i.e. the movement and transport of gas molecules in solid phases. The diffusion takes place because of the presence of defects in solids.

Table 3.6. Coats and Redfern Mechanisms used for the calculation of thermal kinetics in this study (Sun et al., 2006)

Mechanism	$g(\alpha)$	Symbol
Diffusion Mechanism		
One-way transport	α^2	D1
Two-way transport	$\alpha + (1 + \alpha)\ln(1 - \alpha)$	D2
Three-way transport	$((1 - \alpha)^{1/3})^2$	D3
Ginstling-Brounshtein equation	$1 - 2\alpha/3 - (1 - \alpha)^{2/3}$	D4
Limiting surface reactions both phases		
Three dimensions	$1 - (1 - \alpha)^{1/3}$	R3
Chemical reaction		
First order	$-\ln(1 - \alpha)$	F1

D1 is the function for a one-dimensional diffusion (e.g. in the x-direction) where the process is governed by a parabolic law with constant diffusion coefficient. Since, diffusion is restricted to one dimension, x, by assumption no concentration gradient can occur in any other dimension, and concentration must therefore has the same value everywhere in the system for the same value of x. D1 mechanism describes well a process where the interface area is constant and the diminution of reaction rate is a consequence of increasing thickness of the diffusion barrier (Kim et al., 2005).

For the diffusion in cylinders and in spheres, it is necessary to retain all three dimensions, but the coordinates may advantageously be changed from rectangular to cylindrical and the spherical systems, respectively (Jacobs, 1967). D2 is for a two-dimensional diffusion controlled process into a cylinder. When the distribution of the material is such that concentration is a function of r alone, i.e., when there is no diffusion in the direction measured by z and when the distribution of material about z axis is symmetrical at all times, two-dimensional diffusion is accepted as a controlled process for cylinders.

D3 is Jander's equation. This model is used for diffusion-controlled solid-state reaction kinetics in a sphere. For spheres three-dimensional diffusion is applied. In this case, diffusion in all three directions is important. D4 is a function for a diffusion controlled reaction starting on the exterior of a spherical particle.

In phase boundary controlled reactions, it is assumed that the reaction is controlled by movement of an interface at constant velocity and nucleation occurs virtually instantaneously, so that the surface of each particle is covered with a layer of the product. Nucleation of the reactant, however, may be a random process, not followed by a rapid surface growth. R3 is a function for a sphere (three dimensional phase boundary reaction) reacting from the surface inward. If the solid state reaction follows first order kinetics (F1 function), the rate determining step is nucleation process and there is an equal probability of nucleation at each active site (Alshehri et al., 2000).

Another method used for the kinetic parameters is the **Broido method**. The assumptions of the Broido method are:

- All reactions are assumed as first order reactions (Liu et al., 1998).
- Undecomposed fraction of the reactant can be expressed by the basic rate Equation (3.17).
- Two approximations:

$$1) e^{-E/RT} \cong (T_m/T)^2 e^{-E/RT}$$

2) $T_0 \leq T_m$ are done to solve integral equations (Liu et al., 1998).

In the reaction $aA \rightarrow bB + cC$ the rate of disappearance of A may be expressed by:

$$\frac{dy}{dt} = -ky^n \tag{3.15}$$

where y is the fraction of A not yet decomposed at time t , n is the order of reaction, and k the rate constant given by the expression:

$$k = Ae^{-E/RT} \quad (3.16)$$

where A is the pre-exponential constant, and E is the activation energy of the reaction. Since in the experiment temperature increases linearly with time, then

$$T = T_0 + \beta t \quad (3.17)$$

where β is the heating rate, and T_0 is the initial temperature. Equations (3.15) and (3.17) may be combined to give,

$$dy / y^n = -(A / \beta) e^{-E/RT} dT \quad (3.18)$$

The TGA curve for such a reaction represents this last equation integrated from a temperature T_0 at which $y=1$. Thus,

$$\int_y^1 dy / y^n = A / \beta \int_{T_0}^T e^{-E/RT} dT \quad (3.19)$$

In his paper, Broido quoted two approximations. One is;

$$e^{-E/RT} \cong (T_m/T)^2 e^{-E/RT} \quad (3.20)$$

where T_m is the temperature of maximum reaction rate. In view of the fact that T_0 is generally much smaller than T_m , this approximation leads to

$$\ln\left(A/\beta \int_{T_0}^T e^{-E/RT} dT\right) \cong -\frac{E}{RT} + \ln\left(\frac{RAT_m^2}{\beta E}\right) \quad (3.21)$$

Only if n=1, the integral expression of the left-hand side of Eqn (3.19) can be obtained as follows:

$$\ln\left(\int_y^1 dy/y^n\right) = \ln\left(\int_y^1 dy/y\right) = \ln[\ln(1/y)] \quad (3.22)$$

Combining Equations (3.19), (3.21) and (3.22), the following relation can be achieved:

$$\ln[\ln(1/y)] = -E/RT + \ln(RAT_{max}^2/E\beta) \quad (3.23)$$

Equation (3.23) is called Broido method. In this equation y is the mass fraction of initial sample that has not been decomposed, T_{max} is the temperature of maximum reaction velocity, β is the rate of heating ($^{\circ}\text{Kmin}^{-1}$), A is the pre-exponential constant, E is the activation energy and R is the gas constant equal to $8.314 \text{ Jmol}^{-1}\text{K}^{-1}$. From the above derivation, it can be concluded that the Broido method is in fact based on the assumption that the order of reaction is unity (Liu et al., 1998). By using the Broido method, the activation energy of the reaction can be determined from the slope of the plot $\ln(\ln 1/y)$ versus $1/T$ (Jianzhong et al., 2004).

After TG analysis were performed for each sample for three heating rates ($10^{\circ}\text{C}/\text{min}$, $20^{\circ}\text{C}/\text{min}$ and $30^{\circ}\text{C}/\text{min}$), results of the TG analysis were examined, and together with the DTG (derivative thermogravimetry) results of the waste wood samples, various regions were determined by looking at the thermograms. For each region, activation energies and pre-exponential constants of the all waste wood samples are determined by using the *Coats-Redfern Method* and the *Broido Method*.

CHAPTER 4

RESULTS AND DISCUSSION

The experimental results of this study are presented in this chapter. The effects of the heating rate on thermal kinetics, e.i. activation energy and pre-exponential constant of one untreated and four chemically treated waste wood samples, are discussed. Test runs conducted during the experiments are summarized in Table 4.1.

Table 4.1. Test runs conducted during the experiments

Waste wood type	Heating rate		
	@ 10 °C/min	@ 20 °C/min	@ 30 °C/min
Pine	P-10	P-20	P-30
MDF	M-10	M-20	M-30
Particleboard	PB-10	PB-20	PB-30
Plywood	PL-10	PL-20	PL-30

4.1. Thermogravimetric Analysis (TGA) Results

Thermogravimetric Analysis (TGA) of all samples was carried out and thermographs were obtained at 10 °C/min, 20 °C/min and 30 °C/min heating rates. The thermograph shows the weight loss vs. temperature (also time). A sample thermograph is given in Figure 4.1. The curve shown with solid line on the thermograph shows the weight loss of the sample with respect to temperature. It is clearly seen from the figure that weight of the sample continuously decreases as the temperature increases.

The dashed line in the same figure shows the Derivative Thermogravimetry (DTG) curve which is the dW/dT drawn with respect to temperature. Four regions were observed in this curve. These regions were determined according to the approximate start and end points of the Derivative Thermogravimetry (DTG) curve which shows thermal breakdown of the organic matters and volatiles in the samples (Sonibare et al., 2005). The first region on the DTG curve was due to the moisture in the sample. The second region, where elimination of the moisture finished and main oxidation did not start precisely, was due to very volatile matters. The third region where the main weight loss occurred was due to the oxidation and removal of the volatile matters of the sample. The last region was due to the oxidation of the char remaining after the volatiles were removed from the sample. Thermal kinetics of the first region which was due to moisture was not calculated because this region was not represented in the active decomposition stage of the sample. Duplicate experiments were done in order to observe reproducibility. Examples of the repeated P-10 as an untreated sample and M-10 as a treated sample are given in Appendix A.

In the study the third region was found as the main oxidation region. In this region all the volatiles and flammable materials were released from the sample and these volatiles burned with flames (flaming combustion). It is reported in the literature that many free radical reactions and transformations which include further fission, dehydration, and disproportionation of the sugar units are involved in this region (Shafizadeh, 1981). After all the volatiles are gone, residue char is formed. Therefore, the third region was assumed as the most important region for the combustion of the samples.

4.1.1. Pine Samples

Pine Sample at 10 °C/min heating rate (P-10)

TG and DTG curves of the P-10 sample are given in Figure 4.1. The heating rate for this sample was 10 °C/min. As can be seen from Figure 4.1 four regions are seen in the DTG curve. Temperature intervals belonging to the regions are given in Table 4.2.

Table 4.2. Temperature intervals belonging to the regions

Regions	Temperature interval, (°C)	ΔT , (°C)
1 st region	30-170	140
2 nd region	170-260	90
3 rd region	260-395	135
4 th region	395-553	158

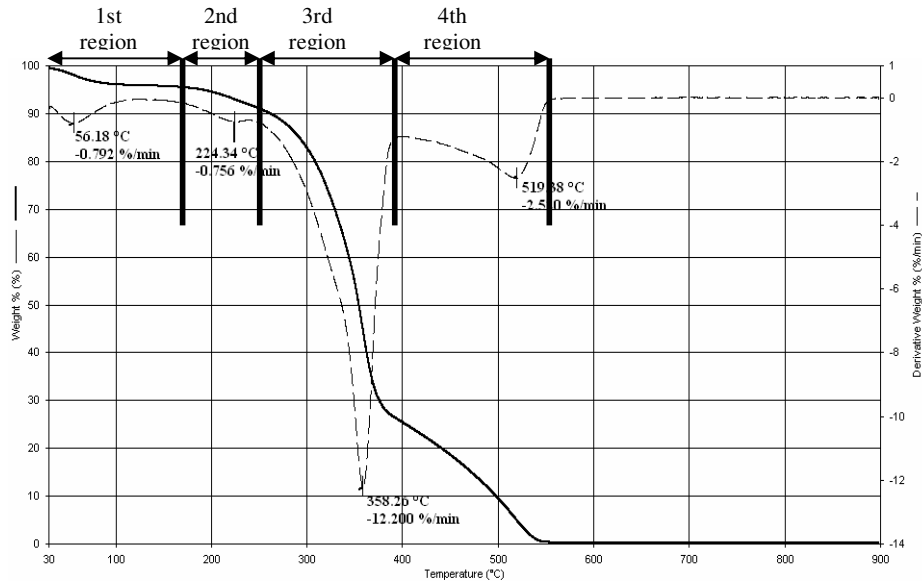


Figure 4.1. TG and DTG graph of the P-10 sample at 10 °C/min heating rate

In the first region, a small amount of weight loss of 4.7% was observed. This loss is due to moisture in the sample. In the second region, after the elimination of the moisture, a small weight loss of 4.3% was observed due to initial loss of volatiles. The third region is the region where the largest weight loss occurred. The loss in this region was 65%, and this loss was due to the escape of volatile organics from the pine structure. Finally, in the fourth region the weight loss was 26%. After volatile organics are released from the pine sample, the remaining organics (mainly fixed carbon) make a char which burns with a smaller rate than the volatile matter. For the calculation of thermal kinetics, Coats Redfern Method and Broido Method which were given in Chapter 3 were used for the second, third and the fourth regions. The first region was not included because this region belonged to the moisture removal.

According to the *Coats Redfern Method*, kinetic parameters such as activation energy (E_a) and pre-exponential constant (A) were calculated by using Equation (3.14) in Chapter 3.

In this study, for different values of α , $g(\alpha)$ functions which were given in Table 3.6 were calculated. In the study 6 solid state mechanisms were used. For example, when diffusion mechanism is assumed with two way transport in the 2nd region, $g(\alpha)$ is calculated with the following equation as given in Table 3.6:

$$g(\alpha) = \alpha + (1 + \alpha) \ln(1 - \alpha)$$

This mechanism is denoted with D2, where D represents diffusion mechanism. When $\ln g(\alpha)/T^2$ versus $1/T$ is plotted for each α value, this will give a single straight line for the correct form of $g(\alpha)$. Namely, this will allow the choice of the kinetic model (solid state mechanism) where the straight line fits the data the best and gives the highest correlation coefficient.

When D2 mechanism is accepted and plotted as explained above, the correlation coefficient obtained is 0.9634. Since the correlation coefficient is not high for this mechanisms, other mechanisms are also tested by calculating $g(\alpha)$ values for these mechanisms. The curve is plotted and again the correlation coefficient is calculated. The mechanism which gives the best fit to the linear equation with highest correlation coefficient is accepted as the true mechanism for that region. For P-10 sample, the second region is found to be represented best by mechanism D1. Similar calculations are done for the third and the fourth regions.

Therefore in this study, for each region, 6 solid state mechanisms were used by using Coats Redfern Method and as a result of this, 6 curves were obtained. According to the correlation coefficients of these curves, the solid state mechanism in each region was determined. The curve which gives the highest correlation (the best fits the data) was assumed as an effective mechanism in the region. The results of thermal kinetics by using Coats Redfern Method for P-10 sample are given in Table 4.3 together with correlation coefficients.

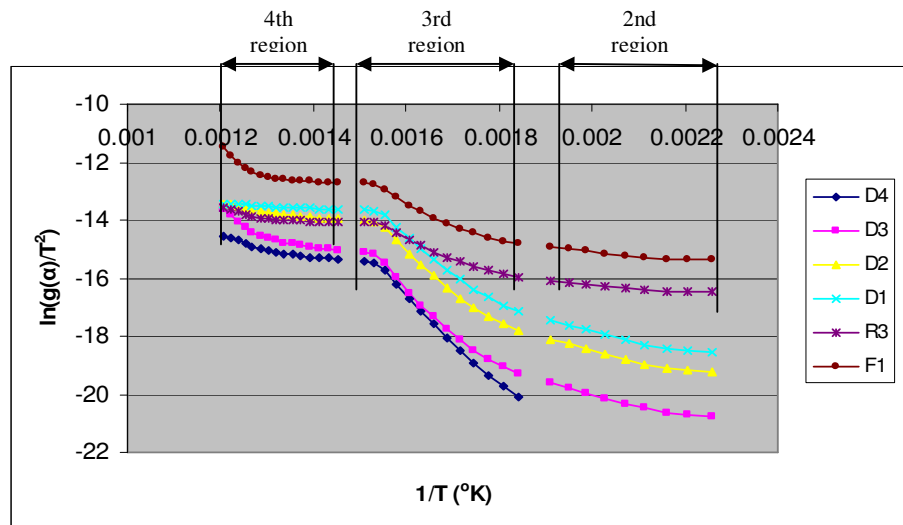


Figure 4.2. Curves showing the solid state mechanisms for Coats Redfern method for three regions of P-10 sample

Table 4.3. Activation energies and pre-exponential constants of P -10 sample for three regions

Mech.	Second region			Third region			Fourth region		
	E*	r ²	A**	E	r ²	A	E	r ²	A
D4	-	-	-	122.56	0.9922	4.39E+09	23.16	0.8946	9.44
D3	28.68	0.9632	2.00	107.97	0.9746	3.06E+08	37.35	0.8428	236.79
D2	28.31	0.9634	8.09	99.64	0.9808	2.07E+08	15.28	0.9137	7.10
D1	27.94	0.9636	14.27	92.48	0.9839	78656198	6.74	0.9135	0.83
R3	10.34	0.9358	0.39	49.05	0.9702	9411.631	13.93	0.7459	3.20
F1	10.53	0.9358	1.26	53.30	0.9634	79055.88	27.65	0.7202	323.31

* E (kJ/mole),**A (1/min), r² correlation coefficient

According to the results shown in Table 4.3, activation energies were found between 10.34-28.68 kJ/mole, for the second region in the DTG curve and the highest correlation coefficient was found with mechanism D1. However, for other diffusion mechanisms (D3 and D2) correlation coefficients were also close to that of D1. Therefore, it can be said that for this region, diffusion mechanisms are playing the main role for the oxidation of the P-10 sample. For the third region activation energies were found between 49.05-122.56 kJ/mole and highest correlation coefficient (0.9922) was found with mechanism D4. For the fourth region, activation energies were between 6.74-37.50 kJ/mole, and highest correlation coefficient were found with mechanism D1 (r²=0.9135) and mechanism D2 (r²=0.9137). Accordingly, diffusion mechanisms (D1 and D2) are responsible for the oxidation of P-10 sample in the fourth region. The highest activation energy (122.6 kJ/mole) was found in the third region where the main oxidation took place and the largest weight loss occurred. For the *Broido Method*, kinetic parameters such as activation energy (E) and pre-exponential constant (A) were calculated by using Equation (3.21) in Chapter 3:

$$\ln (\ln (1/y))=-E/RT + \ln(RAT_{max}^2/E\beta)$$

In the equation y is the mass fraction of initial sample that has not been decomposed, T is the temperature of maximum reaction velocity, β is the rate of

heating ($^{\circ}\text{Kmin}^{-1}$), A is the pre-exponential constant, and E is the activation energy. In this method for each y value the term $\ln(\ln(1/y))$ was calculated and $\ln(\ln(1/y))$ versus $1/T$ was plotted for the second, third and the fourth regions on the DTG curve. For each region one curve was obtained as shown in Figure 4.3. By using the slope and the intercept values of these curves E and A values were calculated, respectively. The results of thermal kinetics by using Broido Method for P-10 sample are given in Table 4.4 together with correlation coefficients.

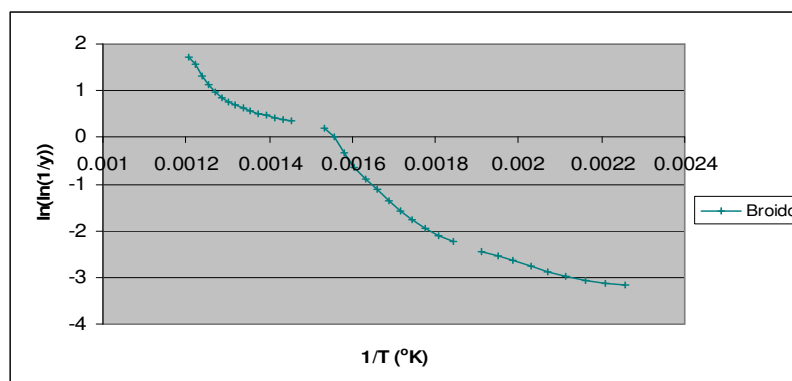


Figure 4.3. Curves showing the Broido method for three regions of P-10 sample

Table 4.4. Activation energies and pre-exponential constants of P -10 sample for three regions

Method	Second region			Third region			Fourth region		
	E*	r ²	A**	E	r ²	A	E	r ²	A
Broido	18.52	0.9755	7.77	62.28	0.9668	500988	37.50	0.8639	1864

* E (kJ/mole),**A (1/min), r² correlation coefficient

For the Broido method, activation energies were found between 19 and 62 kJ/mole. Activation energy of the third region which was calculated with the Broido Method was found about 50% lower than the Coats Redfern Method and the correlation coefficient was also low. Correlation coefficient of the third

region found with the Broido method was much lower than the Coats Redfern method. Therefore, this method did not give good results for the all regions. However for the second region with Broido method higher correlation coefficients were obtained as compared to Coats Redfern Method.

Pine Sample at 20 °C/min heating rate (P-20)

TG and DTG curves of the P-20 sample are given in Figure 4.4. The heating rate for this sample was 20 °C/min. As can be seen from Figure 4.4, four regions are detected in the DTG curves. Temperature intervals and weight losses belonging to the regions are given in Table 4.5.

Table 4.5. Temperature intervals and weight losses belonging to the regions

Regions	Temperature interval, (°C)	ΔT, (°C)	% wt loss
1 st region	30-180	150	5.9
2 nd region	180-280	100	4.7
3 rd region	280-400	120	63.0
4 th region	400-555	155	26.0

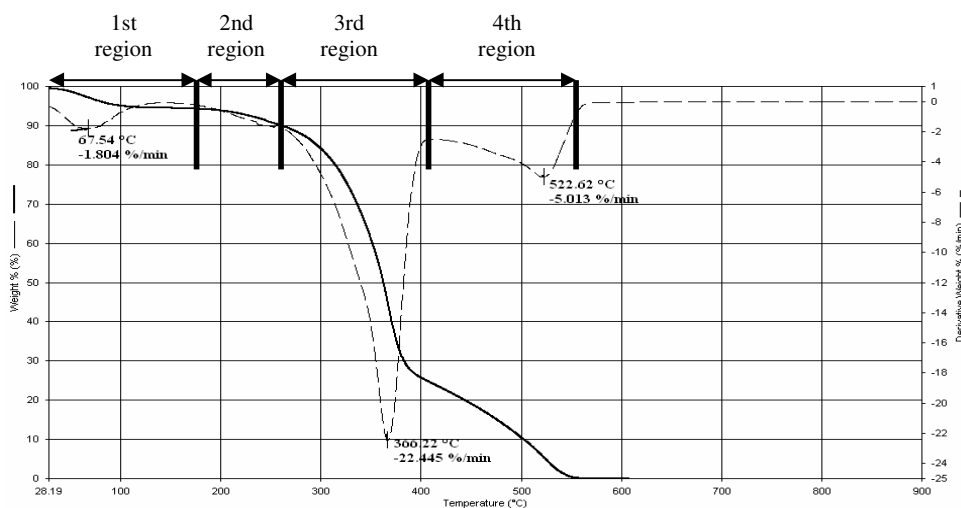


Figure 4.4. TG and DTG graph of the P-20 sample at 20 °C/min heating rate

In order to calculate thermal kinetics such as activation energy and pre-exponential constant, the procedures of these methods which were explained in P-10 sample were followed for P-20 sample, and for all the other samples. As it can be seen from Figure 4.5, different curves having different slopes were obtained for 6 different solid state mechanisms by using *Coats Redfern Method* for P-20 sample. The slope and the intercepts calculated by assuming the different mechanisms for thermal kinetics by using Coats Redfern Method are given in Table 4.6 together with correlation coefficients.

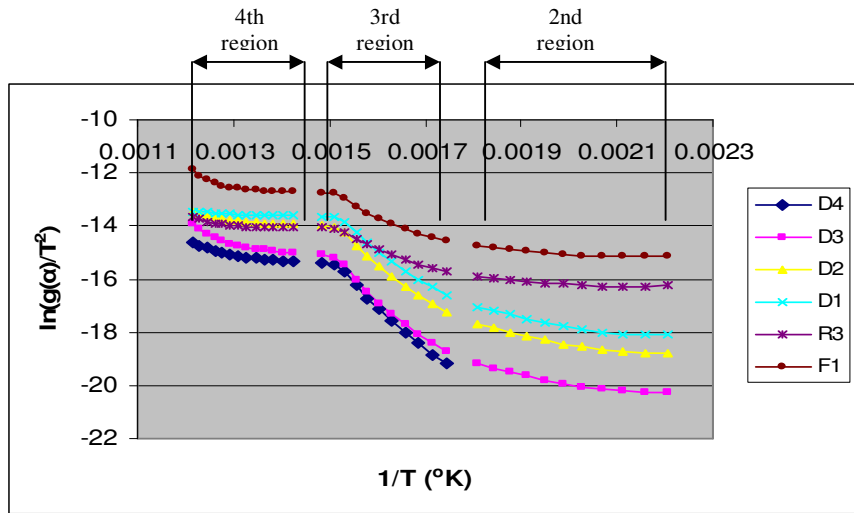


Figure 4.5. Curves showing the solid state mechanisms for Coats Redfern method for three regions of P-20 sample

Table 4.6. Activation energies and pre-exponential constants of P-20 sample for three regions

Mech.	Second region			Third region			Fourth region		
	E*	r ²	A**	E	r ²	A	E	r ²	A
D4	-	-	-	128.54	0.9934	1.04E+10	22.7	0.8963	8.33
D3	23.99	0.9304	0.64	120.21	0.9853	2.64E+09	29.34	0.8621	115.58
D2	23.56	0.9306	2.53	109.39	0.9889	1.12E+09	15.92	0.9092	7.42
D1	23.14	0.9308	4.38	100.21	0.9908	2.92E+08	6.58	0.9067	0.86
R3	7.84	0.8597	0.18	54.99	0.9829	28896.47	11.2	0.7296	2.05
F1	8.05	0.8613	0.58	60.54	0.978	311075.6	23.3	0.7468	126.21

* E (kJ/mole), **A (1/min), r² correlation coefficient

According to the results (Table 4.6), activation energies were found between 7.84-23.99 kJ/mole for the second region, and the highest correlation coefficient (0.9308) was obtained with D1 method; however, with other diffusion mechanisms such as D2, D3, good correlation coefficients were also obtained. Therefore, for this region, diffusion mechanisms seem to have the main role for the oxidation of the P-20 sample. For the third region, activation energies were found between 54.99 and 128.54 kJ/mole and the highest correlation (0.9934) was found with D4 method. As for the fourth region, activation energies were between 6.58-35.76 kJ/mole and highest correlation (0.9092) was found with D2 method; a high correlation was also found with D1 method; accordingly, diffusion mechanisms (D1 and D2) appear to be responsible for the oxidation of P-20 sample. Highest activation energy (128.54 kJ/mole) was found in the third region where the main oxidation was performed and highest weight loss occurred. Activation energy of the fourth region was found lower than the second region; therefore, the second region was found more stable than the fourth region for the sample, as it was observed in P-10 sample.

In Figure 4.6, by using the *Broido method* different curves were obtained for 3 regions of P-20 sample. To calculate thermal kinetics such as activation energy and pre-exponential constant, slope and intercept of these curves were used, respectively. Results of the calculations obtained with Broido Method are given in Table 4.7.

Activation energy of the third region which was calculated with the Broido Method was found much lower than with the Coats Redfern Method. Correlation coefficient of the second region was found good with the Broido method as compared to Coats Redfern Method, however, in the last region Broido method gave low correlation coefficient for the sample. Overall, correlation coefficients obtained with the Coats Redfern method were higher than that obtained by the Broido method.

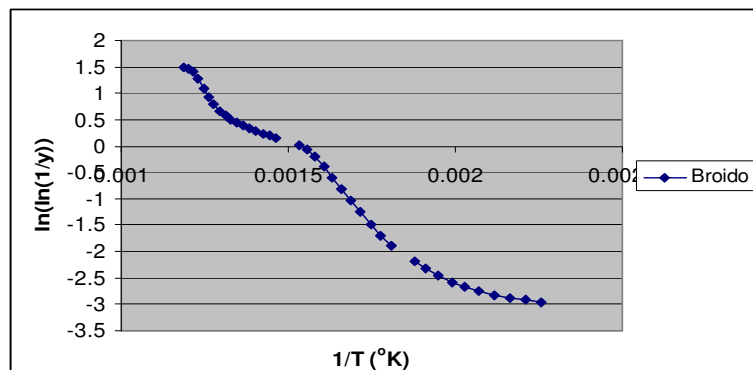


Figure 4.6. Curves obtained with the Broido method for three regions of P-20 sample

Table 4.7. Activation energies and pre-exponential constant values of P -20 sample for three regions

Method	Second region			Third region			Fourth region		
	E*	r ²	A**	E	r ²	A	E	r ²	A
Broido	16.36	0.9572	8.05	70.77	0.9831	2496855	35.76	0.8693	1274.6

* E (kJ/mole), **A (1/min), r² correlation coefficient

Pine Sample at 30 °C/min heating rate (P-30)

TG and DTG curves of the P-30 sample are given in Figure 4.7. The heating rate for this sample was 30 °C/min. As can be seen from Figure 4.7 four regions are observed in the DTG curve. Temperature intervals and weight losses belonging to the regions are given in Table 4.8.

Table 4.8. Temperature intervals and weight losses belonging to the regions

Regions	Temperature interval, (°C)	ΔT, (°C)	% wt. loss
1 st region	30-190	160	5.4
2 nd region	190-288	98	5.6
3 rd region	288-410	122	63.0
4 th region	410-575	165	26.0

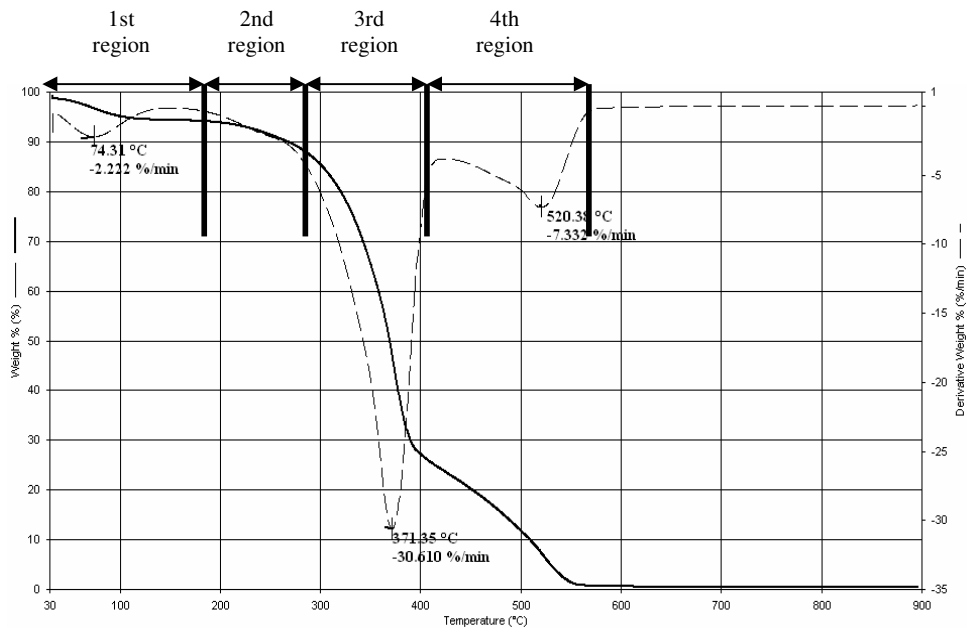


Figure 4.7. TG and DTG graph of the P-30 sample at 30 °C/min heating rate

Application of Coats Redfern Method to different regions is shown in Figure 4.8. As it can be seen from the Figure 4.8, different curves having different slopes were obtained for 6 different solid state mechanisms by using the Coats Redfern Method for P-30 sample. The slope and the intercepts calculated by assuming the different mechanisms for thermal kinetics by using Coats Redfern Method are given in Table 4.9 together with correlation coefficients.

For the first region, activation energies were found between 9.52-27.52 kJ/mole values, and highest correlation (0.9355) was found with D1 method; however, with other diffusion mechanisms, namely D2 and D3, good correlation coefficients were also obtained. Therefore, for this region, diffusion mechanisms seem to play the main role for the oxidation of the P-30 sample similar to samples P-10 and P-20. For the second region, activation energies were between 58.03-136.03 kJ/mole, and the highest correlation coefficient (0.9942) was found with D4 method. For the third region, activation energies were found between

7.23-41.26 kJ/mole and highest correlation coefficient (0.9376) was found with D2 method; D1 method also revealed the high correlations; for this reason, diffusion mechanisms (D2 and D1) are responsible for the oxidation of P-30 sample. Highest activation energy 136.03 kJ/mole was found in the second region where the main oxidation was performed and highest weight loss occurred.

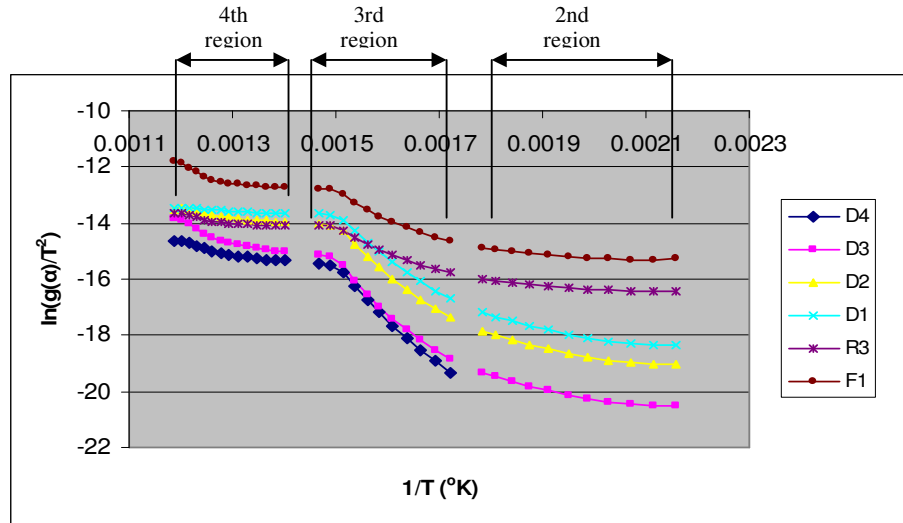


Figure 4.8. Curves indicating the solid state mechanisms by using Coats Redfern Method for three regions of P-30 sample

Table 4.9. Activation energies and pre-exponential constant values of P-30 sample with respect to the three regions

Mech.	Second region			Third region			Fourth region		
	E*	r ²	A**	E	r ²	A	E	r ²	A
D4	-	-	-	136.03	0.9942	3.25E+10	25.88	0.9257	15.53
D3	27.52	0.9349	1.27	126.41	0.9866	6.58E+09	41.26	0.8924	441.78
D2	27.08	0.9353	5.07	115.27	0.9899	2.7E+09	17.8	0.9376	11.11
D1	26.65	0.9355	8.81	105.8	0.9915	6.84E+08	7.23	0.9299	1.05
R3	9.52	0.88	0.28	58.03	0.9845	47125.66	14.28	0.8064	4.29
F1	9.74	0.8808	0.93	63.74	0.9799	514983.9	30.16	0.7977	487.41

* E (kJ/mole), **A (1/min), r² correlation coefficient

In Figure 4.9, by using the Broido method different curves were obtained for 3 regions of P-30 sample. To calculate thermal kinetics such as activation energy and pre-exponential constant, slope and intercept of these curves were used, respectively. Results of the calculations obtained with the Broido Method are given in Table 4.10.

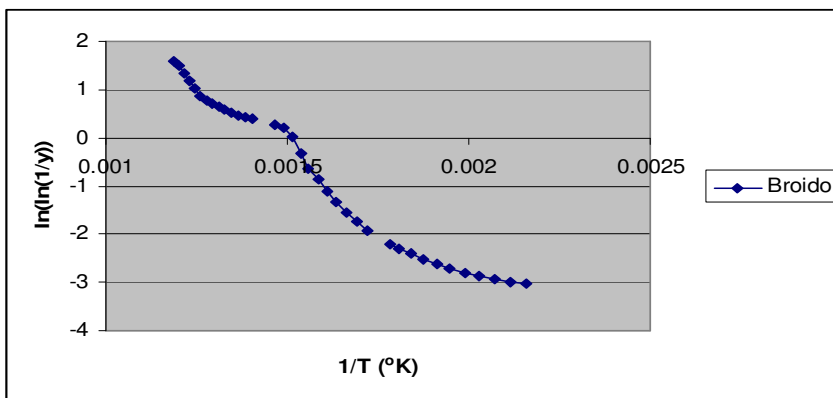


Figure 4.9. Curves showing the Broido method for three regions of P-30 sample

Table 4.10. Activation energies and pre-exponential constants of P-30 sample by using the Broido Method for three regions

Method	Second region			Third region			Fourth region		
	E*	r ²	A**	E	r ²	A	E	r ²	A
Broido	18.21	0.9581	12.19	73.99	0.9845	4037272	40.36	0.9015	2942

* E (kJ/mole), **A (1/min), r² correlation coefficient

Comparison of Results for Pine samples

When TGA and DTG results of the pine samples were examined, it can be seen that with the increasing heating rate, the derivative peak temperatures of the main thermal oxidation region, where the weight loss was also maximum,

increased and the peaks shifted to the right. Change of the peak temperatures of the pine samples in the third region with increasing heating rate is given in Figure 4.10.

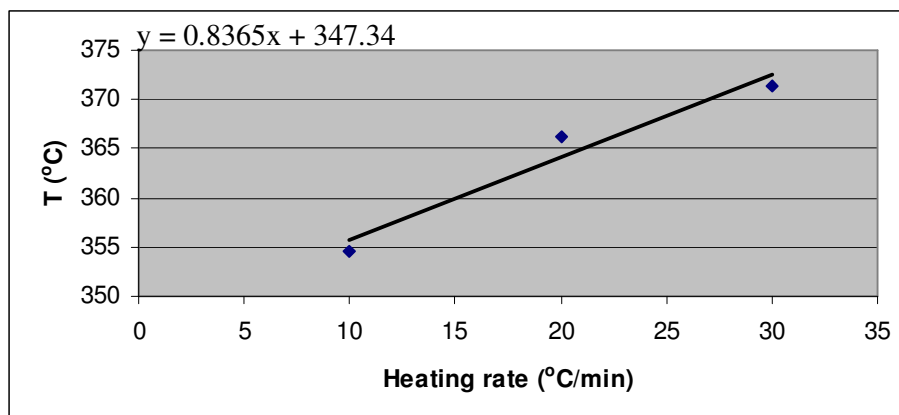


Figure 4.10. Change of maximum peak temperatures of pine sample in the third region with respect to the heating rate

As can be seen from the figure, a good linearity was observed for the first derivative peaks of the pine samples in the third region, and correlation coefficient was found as $r^2=0.9528$. When the effect of heating rate on the first derivative peak of the pine samples in the fourth region was examined, a linear correlation was not found. Change of the peak temperature of the pine samples with respect to the heating rate for the fourth region is given in Figure 4.11.

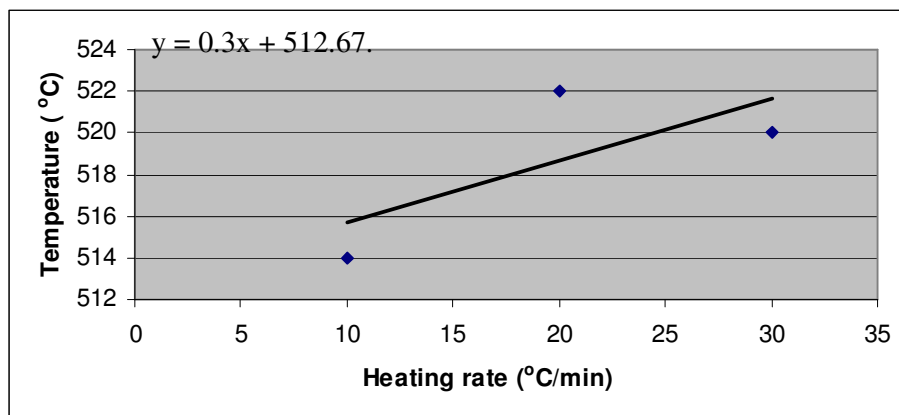


Figure 4.11. Change of maximum peak temperatures of pine samples in the fourth region according to the heating rate

As can be seen from the figure, when heating rate is increased the first derivative peak of the pine samples in the fourth region, also increased, but this increase was not so linear and correlation coefficient was found as $r^2=0.5192$. Also the heating rate was observed to have an effect on the thermal kinetic constants, i.e. activation energies and pre-exponential constants. When heating rate was increased, activation energies and pre-exponential constants of the third region where the main oxidation occurred also increased. The dominating mechanisms found in TG Analysis of pine samples with two different methods as well as the kinetic constants for the different regions are summarized in Table 4.11

Table 4.11. Activation energies and pre-exponential constants of all pine samples with respect for three regions

Regions	Methods	P -10 sample			P-20 sample			P -30 sample		
		E (kJ/mole)	r ²	A (min ⁻¹)	E (kJ/mole)	r ²	A (min ⁻¹)	E (kJ/mole)	r ²	A (min ⁻¹)
2 nd	D4									
	D3	28.686	0.9632	2.00	23.985	0.9304	0.64	27.521	0.9349	1.27
	D2	28.31	0.9634	8.09	23.556	0.9306	2.53	27.079	0.9353	5.07
	D1	27.943	0.9636	14.27	23.139	0.9308	4.38	26.65	0.9355	8.81
	R3	10.345	0.9358	0.39	7.837	0.8597	0.18	9.524	0.88	0.28
	F1	10.53	0.9358	1.26	8.048	0.8613	0.58	9.741	0.8808	0.93
	Broido	18.524	0.9755	7.77	16.36	0.9572	8.05	18.21	0.9581	12.19
3 rd	D4	122.564	0.9922	4.39E+09	128.542	0.9934	1.04E+10	136.025	0.9942	3.25E+10
	D3	107.973	0.9746	3.06E+08	120.212	0.9853	2.64E+09	126.414	0.9866	6.58E+09
	D2	99.643	0.9808	2.07E+08	109.387	0.9889	1.12E+09	115.265	0.9899	2.7E+09
	D1	92.484	0.9839	7.87E+07	100.208	0.9908	2.92E+08	105.795	0.9915	6.84E+08
	R3	49.05	0.9702	9.41E+03	54.992	0.9829	2.89E+04	58.028	0.9845	4.71E+04
	F1	53.306	0.9634	7.91E+04	60.54	0.978	3.11E+05	63.742	0.9799	5.15E+5
	Broido	62.283	0.9668	5.01E+05	70.765	0.9831	2.50E+05	73.99	0.9845	4.03E+6
4 th	D4	23.166	0.8946	9.44	22.7	0.8963	8.33	25.878	0.9257	15.53
	D3	37.35	0.8428	236.79	29.341	0.8621	115.58	41.263	0.8924	441.78
	D2	15.286	0.9137	7.10	15.923	0.9092	7.42	17.8	0.9376	11.11
	D1	6.746	0.9135	0.83	6.582	0.9067	0.86	7.23	0.9299	1.05
	R3	13.935	0.7459	3.20	11.196	0.7296	2.05	14.283	0.8064	4.29
	F1	27.651	0.7202	323.31	23.301	0.7468	126.21	30.164	0.7977	487.41
	Broido	37.501	0.8639	1.86E+03	35.756	0.8693	1274.64	40.356	0.9015	2.94E+4

In the light of these findings, it can be said by using Coats Redfern method that mechanism D1 revealed the highest correlation coefficient for the first region of the pine sample for all heating rates. As for the second and third regions, the highest correlations were obtained for mechanisms D4 and D2, respectively. Agrawal (1985) and Zakrewski (2003) examined the effective solid state mechanisms for the decomposition of the not only wood samples but also other lignocellulosic materials and they found that D3 and D4 mechanisms were effective mechanisms. Vlaev et al. (2003) studied decomposition of a lignocellulosic material, rice husk, and he found that the D4 mechanism which is Ginstling-Brounshtein equation valid for diffusion controlled reactions starting on the exterior of spherical particles with uniform radius. In the literature, F1 mechanism was also adopted for the decomposition of the lignocellulosic materials to describe experimental data (Zakrewski, 2003). In the present study, D1-D4 diffusive mechanisms were found as effective mechanisms as compared to F1 mechanism. In particular, D4 mechanism in the third region which is the main oxidation region was found as the main responsible mechanism for the combustion of the pine samples at different heating rates; therefore, in the present study, the results seem to be consistent with the literature.

In the study, when heating rate was increased, activation energies and pre-exponential constants of the pine samples in the third region also increased. However, in the second and fourth regions, this effect could not be observed on the samples; therefore, heating rate has effect on the activation energies and pre-exponential constants in the main oxidation region of the pine samples, same effect was also observed by Reina et al. (1998) and Deka et al. (2002). Because of high heating rates, material of poor heat conductivity like wood, may develop strong temperature gradients in the sample (Reina et al., 1998). Under these conditions, heating rate can produce some alterations on the thermal kinetics of the wood samples.

Significant variations can be observed in the literature about the activation energies of the decomposition of the lignocellulosic materials. Because this value can change depending on the moisture of the sample, the heating rate and the sample size (Reina et al., 1998), different values can be seen. Activation energies of the untreated wood samples in air atmosphere in the literature were found to lie between 96-147 kJ/mole (Schniwind, 1989). In the present study for main oxidation region namely third region, activation energies were found between 123-136 kJ/mole for the Coats Redfern method according as the D4 mechanism which gave the highest correlation coefficient. For the second and fourth regions lower activation energies were obtained. After the volatilization region due to char oxidation, lower activation energies were found for the lignocellulosic materials in the literature (Gao, 2004; Nassar, 1999; Vlaev et al., 2003).

As findings from the Broido method were examined for the third region, activation energies were found between 62-74 kJ/mole; therefore nearly half the values of Coats and Redfern Method were observed with the Broido method. When literature results are considered, Coats Redfern method seems to be more suitable than the Broido method for the decomposition kinetics of pine samples.

Due to high activation energy as compared to the other regions, the third region was found to be the most stable region for the decomposition, because higher amount of volatile matters are released in this region.

4.1.2. MDF Samples

MDF Sample at 10 °C/min heating rate (M-10)

TG and DTG curves of the M-10 sample are given in Figure 4.12. The heating rate for this sample was 10 °C/min. As can be seen from Figure 4.12, four

regions are seen in the DTG curve. Temperature intervals and weight losses belonging to the regions are given in Table 4.12.

Table 4.12. Temperature intervals and weight losses belonging to the regions

Regions	Temperature interval, (°C)	ΔT , (°C)	% wt. loss
1 st region	30-153	123	4.5
2 nd region	153-263	110	7.7
3 rd region	263-393	130	52.2
4 th region	393-567	174	35.6

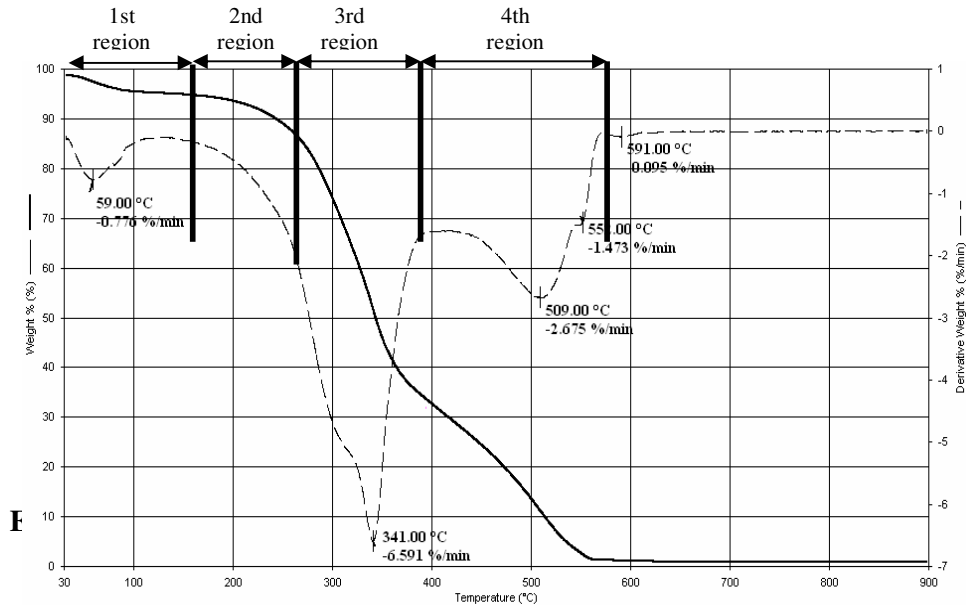


Figure 4.12. TG and DTG graph of the M-10 sample at 10 °C/min heating rate

Curves showing the solid state mechanisms for Coats Redfern Method for three regions are shown in Figure 4.13. As it can be seen from the Figure 4.13, different curves having different slopes were obtained for 6 different solid state mechanisms by using Coats Redfern Method for M-10 sample.

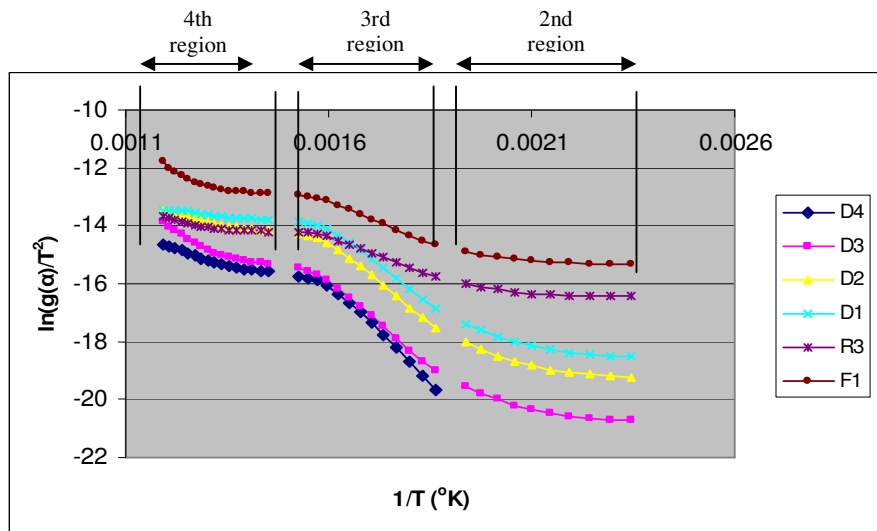


Figure 4.13. Curves showing the solid state mechanisms for Coats Redfern method for three regions of M-10 sample

In Figure 4.14, by using Broido method different curves were obtained for 3 regions of M-10 sample. To calculate thermal kinetics such as activation energy and pre-exponential constant, slope and intercept of these curves were used, respectively.

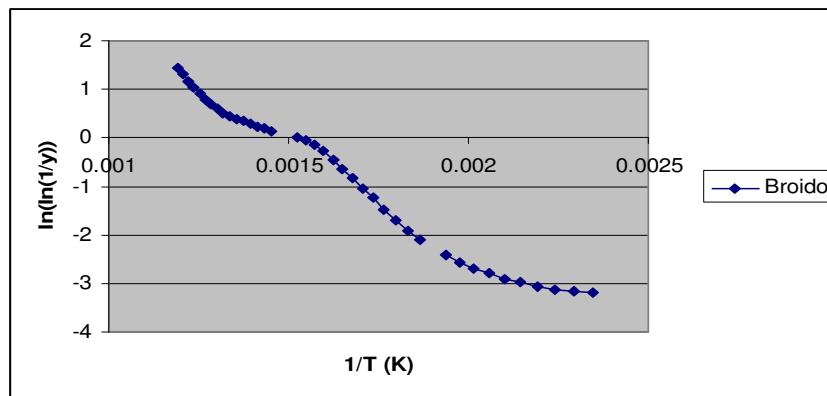


Figure 4.14. Curves obtained with the Broido method for three regions of M-10 sample

MDF Sample at 20 °C/min heating rate (M-20)

TG and DTG curves of the M-20 sample are given in Figure 4.15. The heating rate for this sample was 20 °C/min. As can be seen from Figure 4.15, again four regions are seen in the DTG curves. Temperature intervals and weight losses belonging to the regions are given in Table 4.13.

Table 4.13. Temperature intervals and weight losses belonging to the regions

Regions	Temperature interval, (°C)	ΔT, (°C)	% wt. loss
1 st region	30-170	140	4.6
2 nd region	170-270	100	9.1
3 rd region	270-400	130	52.8
4 th region	400-570	170	33.5

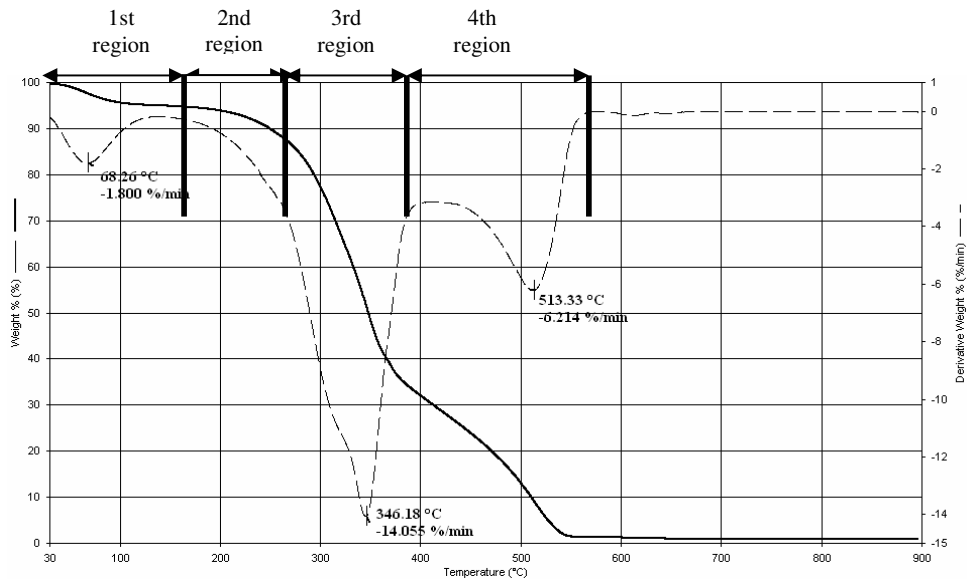


Figure 4.15. TG and DTG graph of the M-20 sample at 20 °C/min heating rate

Curves showing the solid state mechanisms for Coats Redfern Method for three regions are shown in Figure 4.16. As it can be seen from the Figure 4.16,

different curves having different slopes were obtained for 6 different solid state mechanisms by using Coats Redfern Method for M-20 sample. The kinetic constants were calculated from the slope and the intercept of different regions. In Figure 4.17, by using the Broido method different curves were obtained for 3 regions of M-20 sample. To calculate thermal kinetics such as activation energy and pre-exponential constant, slope and intercept of these curves were used, respectively.

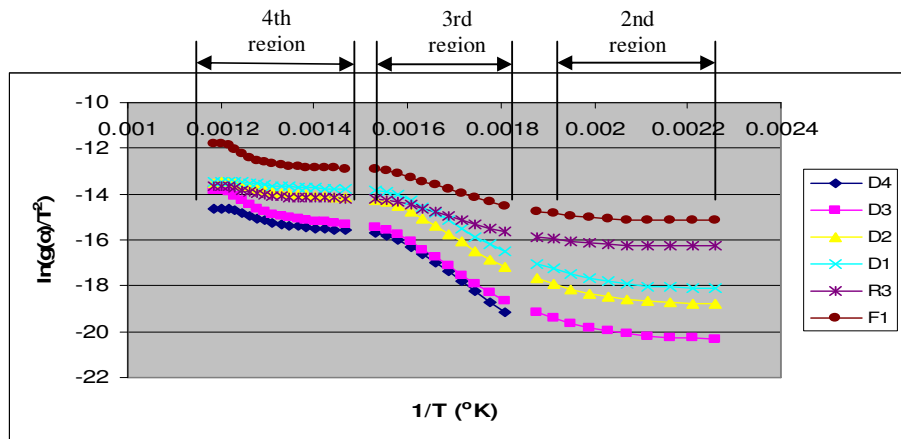


Figure 4.16. Curves showing the solid state mechanisms for Coats Redfern method for three regions of M-20 sample

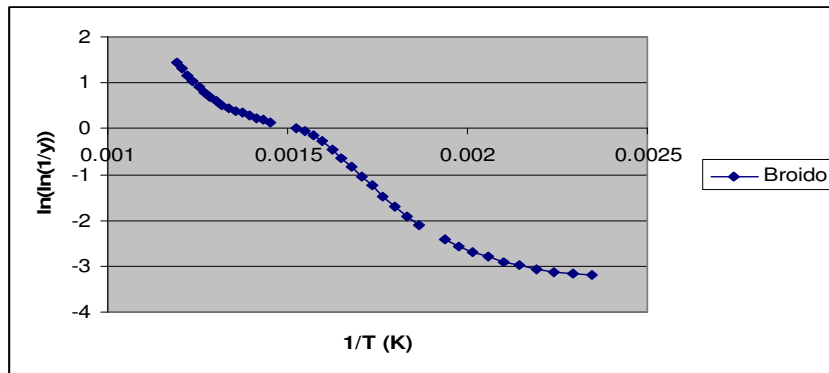


Figure 4.17. Lines showing the Broido method for three regions of M-20 sample

MDF Sample at 30 °C/min heating rate (M-30)

TG and DTG curves of the MDF-30 sample are given in Figure 4.18. The heating rate for this sample was 30 °C/min. As can be seen from the Figure 4.18, four regions are seen in the DTG curve. Temperature intervals and weight losses belonging to the regions are given in Table 4.14.

Table 4.14. Temperature intervals and weight losses belonging to the regions

Regions	Temperature interval, (°C)	ΔT , (°C)	% wt. loss
1 st region	30-170	140	5.16
2 nd region	170-285	115	7.95
3 rd region	285-413	128	53.70
4 th region	413-583	170	33.19

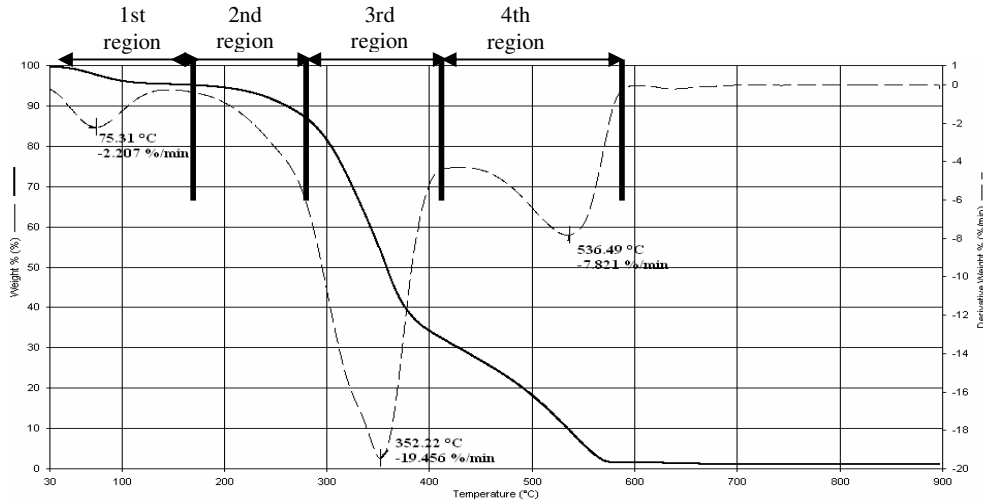


Figure 4.18. TG and DTG graph of the M-30 sample at 30 °C/min heating rate

Curves showing the solid state mechanisms for Coats Redfern Method for three regions are shown in Figure 4.19. As it can be seen from the Figure 4.19, different curves having different slopes were obtained for 6 different solid state

mechanisms by using *Coats Redfern Method* for M-30 sample. The slope and the intercepts calculated by assuming the different mechanisms for thermal kinetics by using Coats Redfern Method. The kinetic constants were calculated from the slope and the intercept of different regions. In Figure 4.20, by using the *Broido method* different curves were obtained for 3 regions of M-30 sample. To calculate thermal kinetics such as activation energy and pre-exponential constant, slope and intercept of these curves were used, respectively.

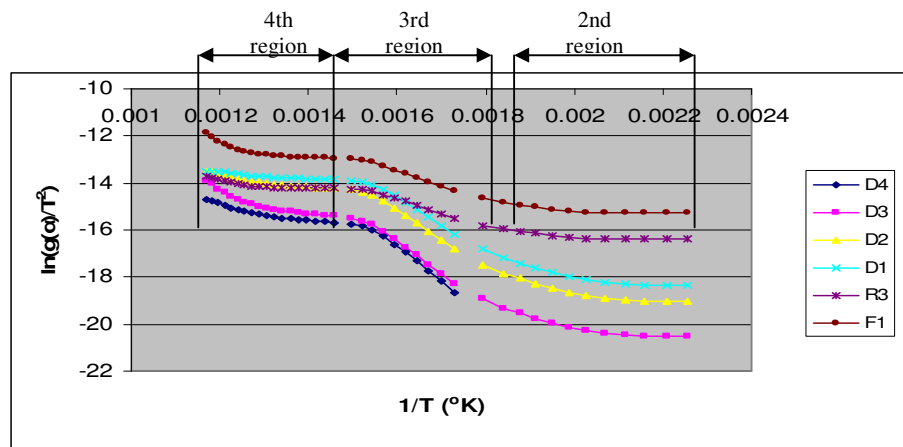


Figure 4.19. Curves indicating the solid state mechanisms for Coats Redfern method for three regions of M-30 sample

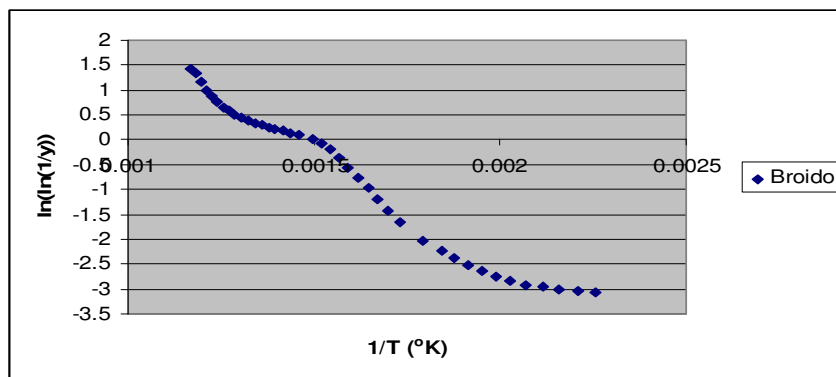


Figure 4.20. Curves showing the Broido method for three regions of M-30 sample

Comparison of Results for MDF samples

When TGA results of the MDF samples were examined, it can be inferred that with the increasing heating rate, the derivative peak temperatures of the main thermal oxidation part, where the weight loss was also maximum, increased and the peaks slipped to the right. Change of the peak temperatures (DTG) of the MDF samples in the third region with the increasing heating rate are given in Figure 4.21.

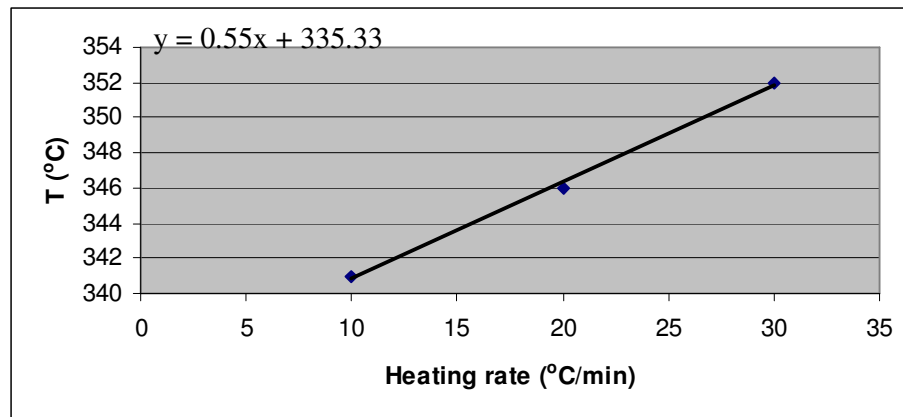


Figure 4.21. Change of maximum peak temperatures of MDF samples in the third region according to the heating rate

As can be seen from the figure, a good linearity was observed for the first derivative peaks of the pine samples in the third region, and correlation coefficient was found as $r^2=0.9973$.

When the effect of heating rate on the first derivative peak of the MDF samples in the fourth region was examined, it can be seen that there were lower correlation coefficients. Change of the peak temperature of the MDF samples with heating rate for the fourth region is given in Figure 4.22.

As can be seen in the figure, when heating rate is increased the first derivative peak of the MDF samples in the fourth region also raised, but this increase was not so good and correlation coefficient was found as $r^2=0.8768$.

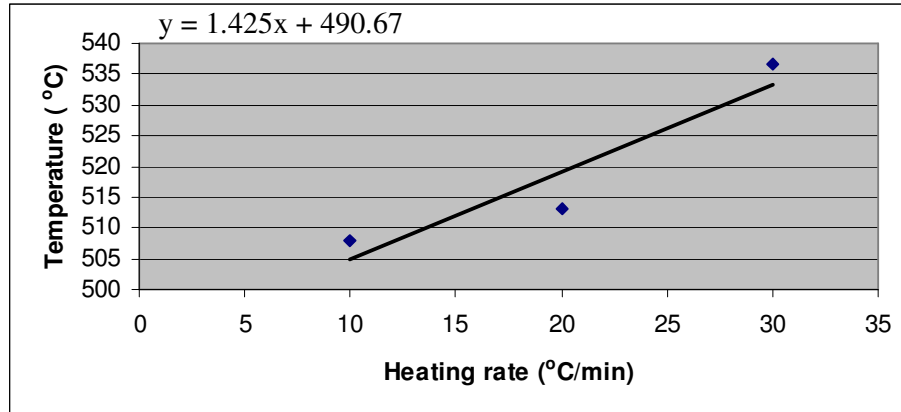


Figure 4.22. Change of maximum peak temperatures of MDF samples in the fourth region according to the heating rate

Heating rate has an effect on the thermal kinetic constants. When heating rate was increased, activation energies and pre-exponential constants of the third region where the main oxidation occurred also increased. However, there were not any significant alterations for the activation energies and pre-exponential constant of the second and the fourth regions of the MDF samples due to heating rate.

The dominating mechanisms found in TG Analysis of MDF samples with two different methods as well as the kinetic constants for the different regions are summarized in Table 4.15.

Table 4.15. Activation energies and pre-exponential constants of all MDF samples with respect of the three regions

Regions	Methods	M-10 sample			M- 20 sample			M- 30 sample		
		E (kJ/mole)	r ²	A (min ⁻¹)	E (kJ/mole)	r ²	A (min ⁻¹)	E (kJ/mole)	r ²	A (min ⁻¹)
2 nd	D4	-	-	-	-	-	-	-	-	-
	D3	26.39	0.8989	1.22	27.42	0.888	1.90	23.95	0.8644	0.52
	D2	26.03	0.8992	4.94	26.03	0.885	7.42	23.58	0.8646	2.08
	D1	25.67	0.8997	8.71	25.67	0.8889	12.67	23.22	0.8647	3.68
	R3	9.27	0.8219	0.29	9.27	0.8045	0.35	7.90	0.7447	0.16
	F1	9.45	0.8228	0.94	9.45	0.8059	1.17	8.08	0.7472	0.01
	Broido	17.31	0.9336	10.27	18.01	0.9264	14.23	16.23	0.9154	7.27
3 rd	D4	99.8	0.9817	6.52E+07	101.88	0.9796	8.54E+07	106.92	0.9795	1.45E+08
	D3	91.54	0.9906	1.52E+07	96.45	0.9872	3.63E+07	99.55	0.9874	4.31E+07
	D2	84.17	0.9865	1.23E+07	87.70	0.9824	2.22E+07	90.10	0.9829	2.85E+07
	D1	77.74	0.9818	5.30E+06	80.15	0.9769	7.69E+06	83.61	0.9777	1.05E+07
	R3	40.84	0.9876	1.91E+03	43.20	0.9835	2.97E+06	44.67	0.9839	3.24E+03
	F1	44.58	0.9913	1.46E+04	47.67	0.9879	2.64E+04	50.02	0.9888	2.75E+04
	Broido	54.27	0.9945	1.17E+05	57.54	0.9921	2.23E+05	59.03	0.9921	2.41E+05
4 th	D4	27.99	0.9427	20.51	29.00	0.9329	26.22	27.96	0.9183	14.27
	D3	40.01	0.904	304.83	43.06	0.8978	576.19	40.49	0.8797	192.96
	D2	20.93	0.9574	18.87	21.20	0.9436	20.69	20.7	0.9336	13.78
	D1	11.12	0.9746	2.66	10.77	0.9481	2.49	10.61	0.9509	2.02
	R3	13.82	0.8571	3.47	15.33	0.8243	5.09	13.88	0.7832	2.70
	F1	25.98	0.8229	193.2	29.87	0.8031	443.24	26.50	0.7676	135.80
	Broido	35.38	0.9171	1051	38.27	0.9112	1.96E+03	36.00	0.9022	780.24

According to the results (Table 4.15), for the second region, when *Coats Redfern method* was used, highest correlation (0.8647-0.8997) were found with D1 mechanism for all heating rates; however, with other diffusion mechanisms such as D2, D3, similar correlation coefficients were also obtained. Therefore, for this region, diffusion mechanisms dominate the oxidation of the MDF samples. In this region activation energies were found between 23.22 and 25.67 kJ/mole, pre-exponential constants were found 3.68 and 12.67 min⁻¹. The *Broido method* was also used for this region and activation energies were calculated between 16.23 and 18.01 kJ/mole, pre-exponential constants were found between 7.27 and 14.23 min⁻¹.

In the third region, for Coats Redfern method, the highest correlation coefficients (0.9879-0.9913) were found with F1 mechanism for all heating rates. So, F1 mechanism was found as an effective mechanism for the main oxidation region of the MDF sample. In addition to the F1 mechanism D3 mechanism also gave similar correlation coefficients. In this region activation energy values were found between 44.58 and 50.02 kJ/mole, pre-exponential constants were found between 1.46E+04 and 2.75E+04 min⁻¹. For Broido method, activation energies were calculated between 54.27 and 59.03 kJ/mole, pre-exponential constants were found between 1.17E+05 and 2.41E+05. These results were compatible in both methods.

In the fourth region, when D1 mechanism was used for Coats Redfern method, the highest correlation coefficients (0.9481-0.9747) were revealed for all heating rates. In this region, activation energies were determined between 10.61 and 11.12 kJ/mole, and pre-exponential constants were found 2.02 and 2.66 min⁻¹. For the Broido method, activation energies and pre-exponential constants were found between 35.38-38.27 kJ/mole and 780-1.96E+03 min⁻¹, respectively.

In the light of these findings, for Coats Redfern method, mechanism D1 revealed the highest correlation for the second and fourth regions of the MDF samples for

all heating rates. As for the third region, the highest correlations were obtained for the mechanism F1. In addition to the mechanism F1, good correlations were also found with D3 mechanism; therefore, for the second and the fourth regions, mechanism D1 were found as an effective mechanism for the Coats Redfern method for both pine and MDF samples; however, in the third region different mechanism was observed. In the literature, F1 mechanism was also used for the decomposition of the lignocellulosic materials (Zakrewski, 2003); therefore, in the present study, results found for MDF samples seem to be consistent with the literature.

In the study, when heating rate was increased, activation energies and pre-exponential constants of the MDF samples in the third region also increased. However, in the second and the fourth regions, this effect could not be observed on the samples for two methods; therefore, heating rate has an effect on the activation energies and pre-exponential constants in the main oxidation region of the MDF samples. The same effect was also observed by Reina et al. (1998) and Deka et al. (2002), because as heating rate increased, temperature gradients in the samples also increased (Reina et al., 1998).

Activation energies of the treated wood samples in inert atmosphere found in the literature lie between 129-140 kJ/mole (Reina et al, 1998; Deka et al. 2002). Gao (2004) examined the activation energies of the chemically treated samples. In this study for the main oxidation region, activation energies were found between 74-96 kJ/mole and pre-exponential constants were found between $2.58E+06$ - $3.84E+07 \text{ min}^{-1}$ (Gao et al., 2004; Gao et al., 2003). In this study, for treated samples lower activation energies and pre-exponential constants were found as compared to untreated sample. In the present study for MDF samples and for Coats Redfern method, with F1 mechanism activation energies were found between 45-50.02 kJ/mole.

For the second and the fourth regions lower activation energies were obtained with the Coats Redfern method. After the volatilization region lower activation energies were found due to char oxidation for the lignocellulosic materials in the literature (Gao, 2004; Nassar, 1999; Vlaev et al., 2003). As findings from the Broido method were examined for the third region, activation energies were found close to each other as compared to the pine samples.

Due to high activation energy as compared to the other regions, the third region was found to be the most stable region, because higher amount of volatile matter was released in this region; therefore the least stable region was found with the fourth region because of volatile matters were finished.

4.1.3. Particleboard Samples

Particleboard Sample at 10 °C/min heating rate (PB-10)

TG and DTG curves of the PB-10 sample are given in Figure 4.23. The heating rate for this sample was 10 °C/min. As can be seen from the Figure 4.23, four regions are seen in the DTG curve. Temperature intervals and weight losses belonging to the regions are given in Table 4.16.

Table 4.16. Temperature intervals and weight losses belong to the regions

Regions	Temperature interval, (°C)	ΔT , (°C)	% wt. loss
1 st region	30-180	150	7.00
2 nd region	180-260	80	8.00
3 rd region	260-360	100	54.00
4 th region	360-510	150	31.00

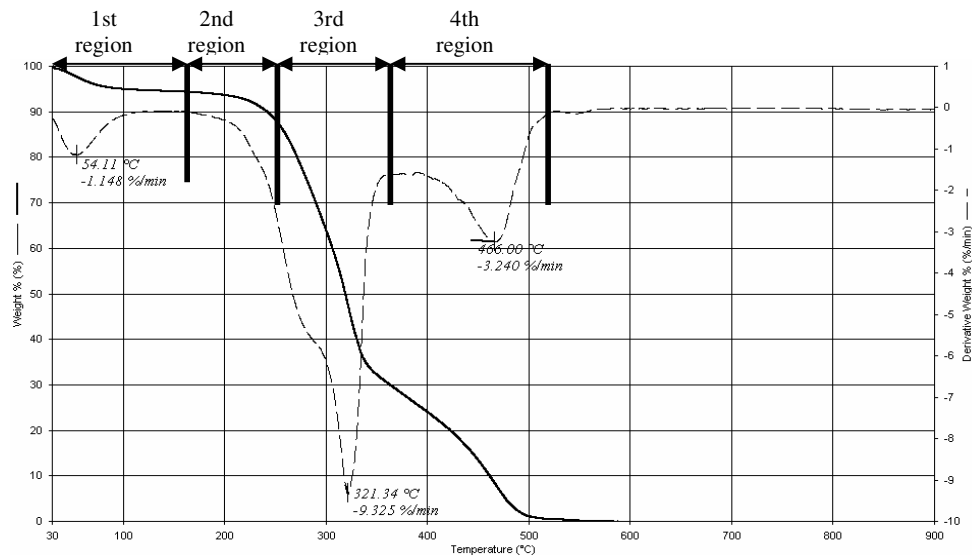


Figure 4.23. TG and DTG graph of the PB-10 sample at 10 °C/min heating rate

Curves showing the solid state mechanisms for Coats Redfern Method for three regions are shown in Figure 4.24. As it can be seen from the Figure 4.24, different curves having different slopes were obtained for 6 different solid state mechanisms by using Coats Redfern Method for PL-30 sample. The slope and the intercepts calculated by assuming the different mechanisms for thermal kinetics by using Coats Redfern Method. The kinetic constants were calculated from the slope and the intercept of different regions.

In Figure 4.25, by using Broido method different curves were obtained for 3 regions of PB-10 sample. To calculate thermal kinetics such as activation energy and pre-exponential constant, slope and intercept of these curves were used, respectively.

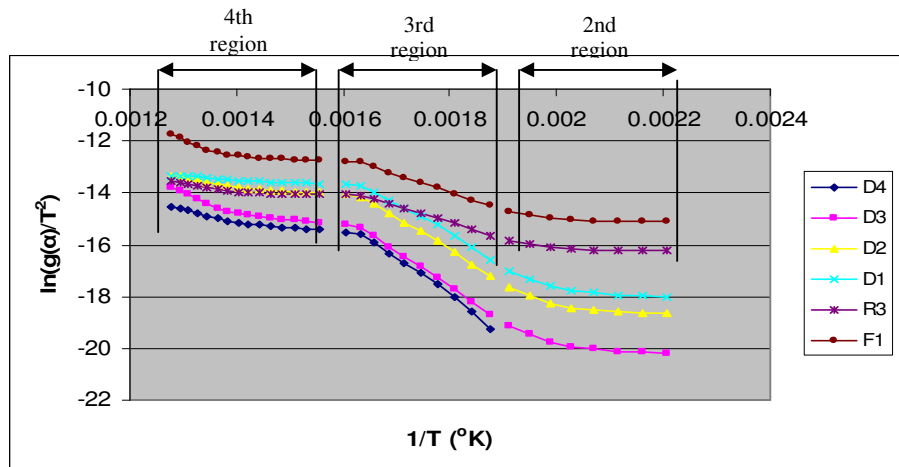


Figure 4.24. Curves showing the solid state mechanisms for Coats Redfern Method for three regions of PB-10 sample

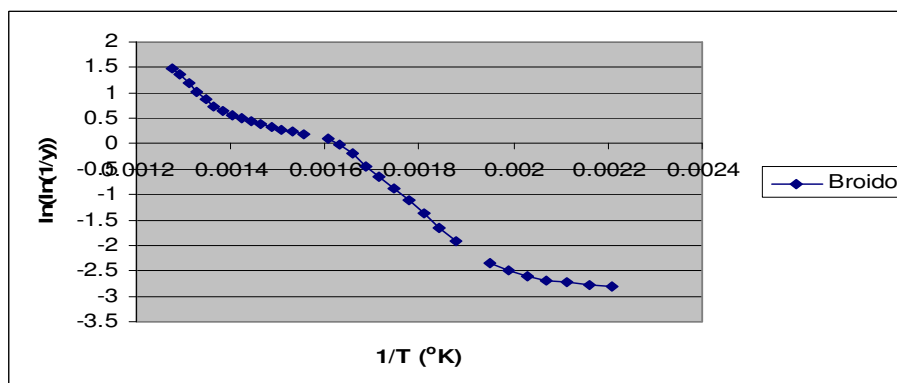


Figure 4.25. Curves showing the Broido method for three regions of PB-10 sample

Particleboard Sample -20 °C/min heating rate (PB-20)

TG and DTG curves of the PB-20 sample are given in Figure 4.26. The heating rate for this sample was 20 °C/min. As can be seen from the Figure 4.26, four regions are seen in the DTG curve. Temperature intervals and weight losses belonging to the regions are given in Table 4.17.

Table 4.17. Temperature intervals and weight losses belonging to the regions

Regions	Temperature interval, (°C)	ΔT , (°C)	% wt. loss
1 st region	30-190	160	8.50
2 nd region	190-260	70	5.50
3 rd region	260-360	100	51.60
4 th region	360-520	160	33.40

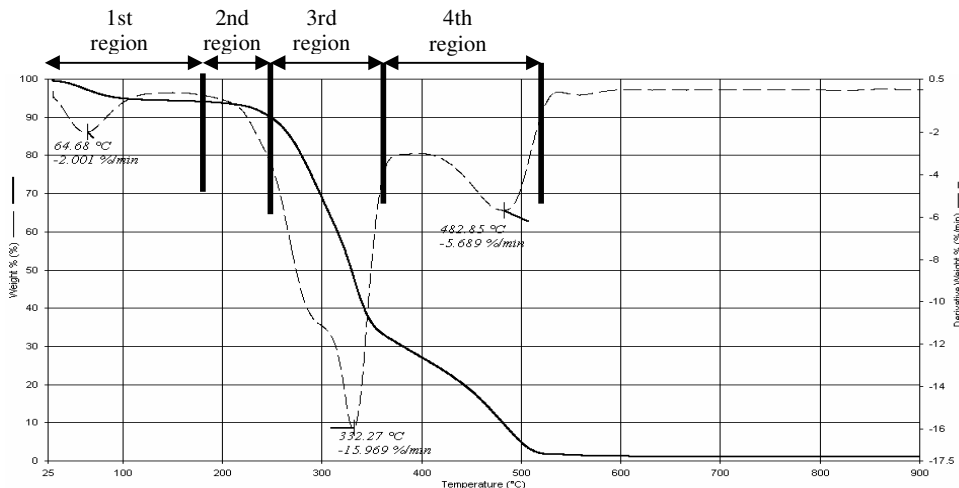


Figure 4.26. TG and DTG graph of the PB-20 sample at 20 °C/min heating rate

Curves showing the solid state mechanisms for Coats Redfern Method for three regions are shown in Figure 4.27. As it can be seen from the Figure 4.27, different curves having different slopes were obtained for 6 different solid state mechanisms by using Coats Redfern Method for PB-20 sample. The kinetic constants were calculated from the slope and the intercept of different regions.

In Figure 4.28, by using the Broido method different curves were obtained for 3 regions of PB-20 sample. To calculate thermal kinetics such as activation energy and pre-exponential constant, slope and intercept of these curves were used, respectively.

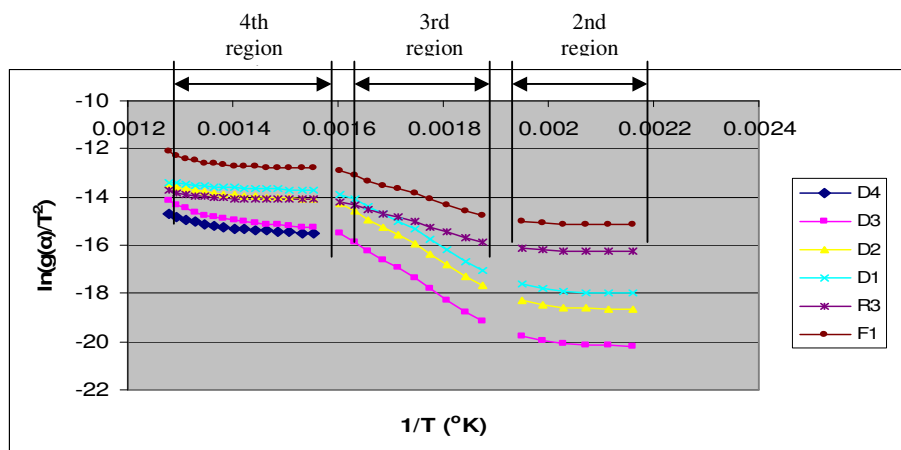


Figure 4.27. Curves indicating the solid state mechanisms for Coats Redfern method for three regions of PB-20 sample

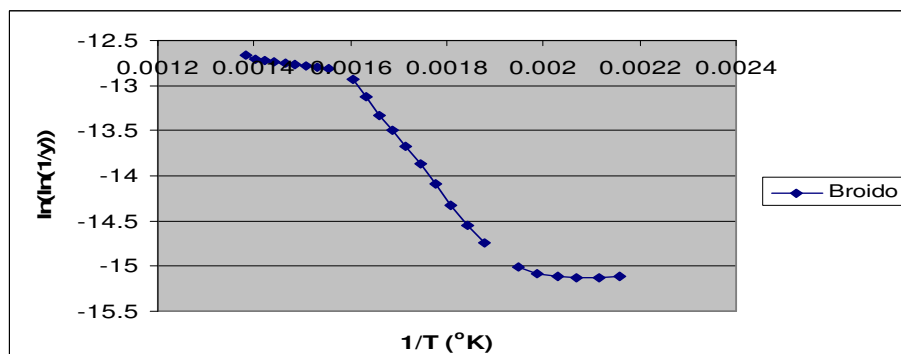


Figure 4.28. Curves showing the Broido method for three regions of PB-20 sample

Particleboard Sample at 30 °C/min heating rate (PB-30)

TG and DTG curves of the PB-30 sample are given in Figure 4.29. The heating rate for this sample was 30 °C/min. As can be seen from the Figure 4.29, four regions are seen in the DTG curve: Temperature intervals and weight losses belonging to the regions are given in Table 4.18.

Table 4.18. Temperature intervals and weight losses belonging to the regions

Regions	Temperature interval, (°C)	ΔT , (°C)	% wt. loss
1 st region	30-200	170	4.41
2 nd region	200-270	30	3.58
3 rd region	270-400	130	59.83
4 th region	400-600	200	32.18

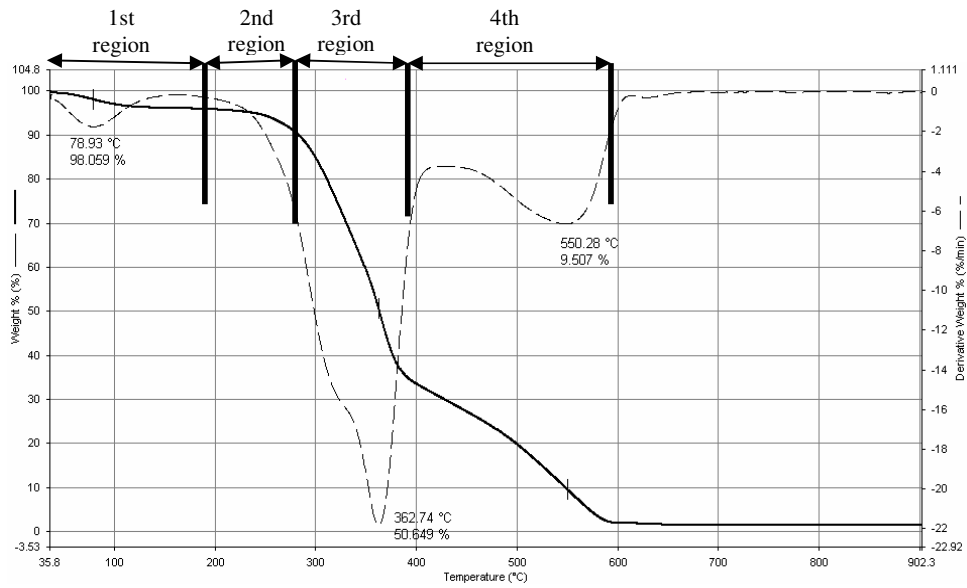


Figure 4.29. TG and DTG graph of the PB-30 sample at 30 °C/min heating rate

Curves showing the solid state mechanisms for Coats Redfern Method for three regions are shown in Figure 4.30. As it can be seen from the Figure 4.30, different curves having different slopes were obtained for 6 different solid state mechanisms by using Coats Redfern Method for PL-30 sample. The slope and the intercepts calculated by assuming the different mechanisms for thermal kinetics by using Coats Redfern Method. The kinetic constants were calculated from the slope and the intercept of different regions.

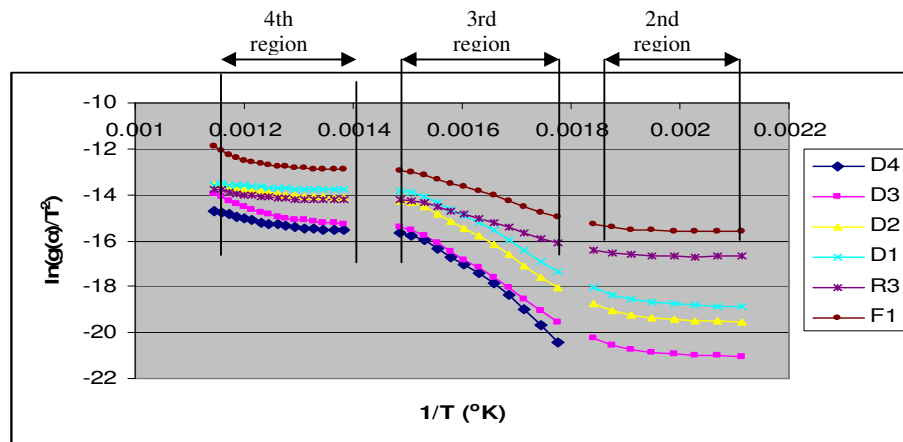


Figure 4.30. Curves which show the solid state mechanisms for three regions of PB-30 sample

In Figure 4.31, by using the Broido method different curves were obtained for 3 regions of PB-30 sample. To calculate thermal kinetics such as activation energy and pre-exponential constant, slope and intercept of these curves were used, respectively.

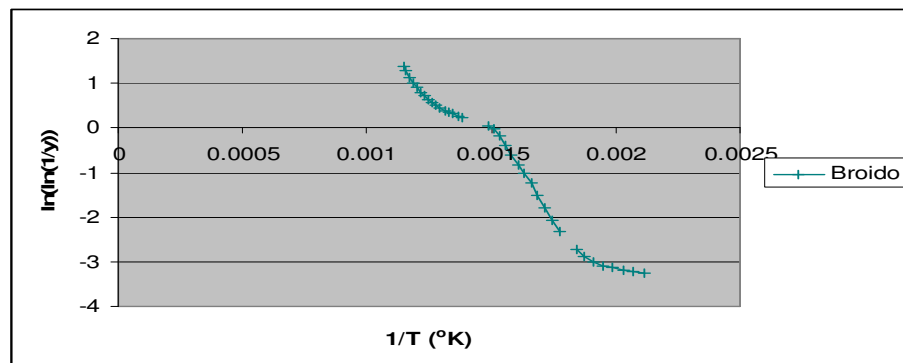


Figure 4.31. Curves showing the Broido method for three regions of PB-30 sample

Comparison of the Particleboard Results

When TGA results of the particleboard samples were examined, it can be seen that with the increasing heating rate, the derivative peak temperatures of the main thermal oxidation part, where the weight loss was also maximum, changed. Despite the changes in the place of the derivative peak temperatures, its pattern was not good linear. It is considered that the heterogen chemical content of the plywood structure lead to collapse this linearity. Change of the peak temperatures (DTG) of the particleboard samples in the third region with the increasing heating rate is given in Figure 4.32.

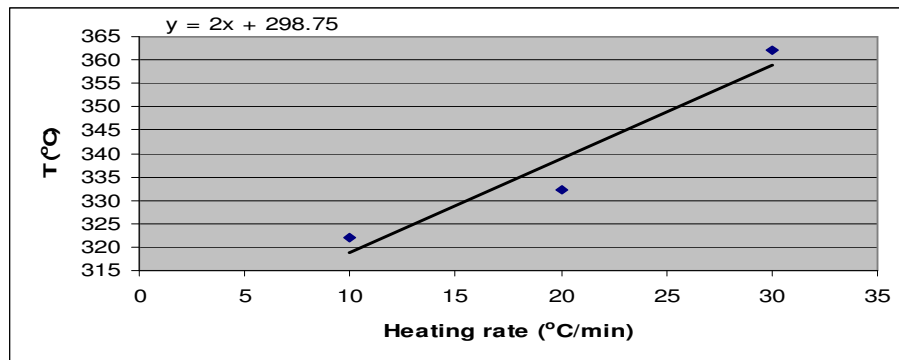


Figure 4.32. Change of maximum peak temperatures of PB samples in the third region according to the heating rate

As can be seen from the figure, there was not linear increment for the derivative pike temperatures of the particleboard samples in the third region, and correlation coefficient was found very low as $r^2=0.9266$. When the effect of heating rate on the first derivative peak of the particleboard samples in the fourth region was examined, it can be seen that there were lower correlation coefficients. As compared to third region Change of the maximum peak

temperature of the particleboard samples for the fourth region is given in Figure 4.33.

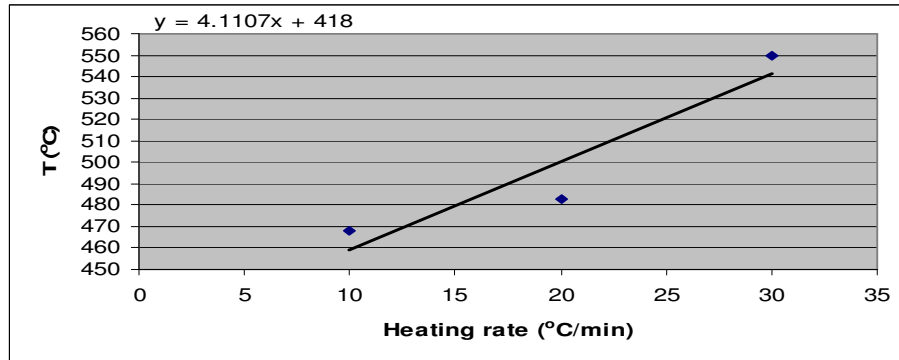


Figure 4.33. Change of maximum peak temperatures of PB samples in the fourth region according to the heating rate

When heating rate was increased, the derivative peak temperatures of the PB samples in the fourth region also increased, however this linearity ($r^2=0.9266$) was not as good as in the third region.

Heating rate has an effect on the thermal constants. When heating rate was increased, activation energies and pre-exponential constants of the third region where the main oxidation occurred also rose. However, there was not any significant alteration for the activation energies and pre-exponential constant of the second and fourth regions of the particleboard samples due to heating rate

The dominating mechanisms found in TG Analysis of particleboard samples with two different methods as well as the kinetic constants for the different regions are summarized in Table 4.19.

Table 4.19. Activation energies and pre-exponential constant values of all particleboard samples with respect of the three regions

Regions	Methods	PB-10 sample			PB- 20 sample			PB- 30 sample		
		E (kJ/mole)	r ²	A (min ⁻¹)	E (kJ/mole)	r ²	A (min ⁻¹)	E (kJ/mole)	r ²	A (min ⁻¹)
2 nd	D4	-	-	-	-	-	-	-	-	-
	D3	25.25	0.8102	1.17	21.04	0.8202	0.26	22.15	0.8202	0.14
	D2	24.79	0.8099	4.56	20.68	0.8197	1.08	21.89	0.8199	0.61
	D1	24.34	0.8096	7.81	20.33	0.819	1.91	21.64	0.8196	1.11
	R3	8.58	0.6695	0.26	6.43	0.6369	0.10	6.86	0.6438	0.08
	F1	8.81	0.6734	0.86	6.58	0.6425	0.33	6.99	0.6474	0.25
	Broido	16.89	0.878	10.39	14.78	0.8949	4.84	15.4	0.8936	3.44
3 rd	D4	113.70	0.9852	3.25E+09	127.63	0.9926	3.75E+10	153.55	0.9702	1.33E+12
	D3	107.23	0.994	1.05E+09	113.30	0.9989	2.35E+09	120.48	0.9957	2.52E+09
	D2	97.73	0.9898	5.08E+08	105.65	0.9976	1.78E+09	112.82	0.9934	2.06E+09
	D1	89.55	0.9846	1.44E+08	98.85	0.9955	7.11E+08	106.09	0.9902	8.94E+08
	R3	48.82	0.9925	1.79E+04	51.87	0.9986	2.83E+04	55.22	0.9947	2.93E+04
	F1	53.67	0.9958	1.80E+05	55.73	0.9991	2.21E+05	59.10	0.9962	2.22E+05
	Broido	62.99	0.9971	1.37E+06	65.14	0.9994	1.62E+06	68.89	0.9972	1.65E+06
4 th	D4	25.56	0.9228	25.06	21.42	0.9144	6.91	22.51	0.9045	6.20
	D3	38.00	0.8732	584.56	29.03	0.8904	49.07	32.89	0.8646	68.54
	D2	18.65	0.9419	19.53	16.38	0.9219	8.81	16.38	0.919	6.64
	D1	9.64	0.9623	2.36	8.87	0.933	1.75	7.79	0.9322	1.06
	R3	13.20	0.772	4.99	8.67	0.7552	1.10	10.08	0.7197	1.33
	F1	26.21	0.7389	484.88	16.06	0.7827	28.64	20.50	0.7289	57.49
	Broido	35.20	0.9026	1.70E+03	26.69	0.9183	247.95	29.97	0.9047	305.08

According to the results (Table 4.19), for the second region, activation energies were found between 21.04 and 25.25 kJ/mole values for the D3 mechanism which revealed the highest correlation coefficients (0.8102-0.8202) for Coats Redfern method; however, with other diffusion mechanisms such as D1, D2 similar correlation coefficients were also obtained. Therefore, for this region, diffusion mechanisms dominant on the oxidation of the PB-10 sample. In this region with D3 mechanism, pre-exponential constants were also found between 0.14 and 1.17 min⁻¹. When Broido method was used, activation energies and pre-exponential constant were found between 15.4-16.89 kJ/mole and 3.44-10.39 min⁻¹.

In the third region, for Coats Redfern method, the highest correlation coefficients (0.9958-0.9991) were found with F1 mechanisms for all heating rates. In addition to the F1 mechanism, for D3 mechanism good correlation coefficient was also found. Activation energies and pre-exponential constants were calculated between 53.67-59.10 kJ/mole and 1.80E+05-2.22E+05 min⁻¹, respectively. For Broido method, activation energies and pre-exponential constants were calculated between 62.99-68.89 kJ/mole and 1.37E+06-1.65E+06 min⁻¹, respectively.

In the fourth region, when D1 mechanism was used for Coats Redfern method, the highest correlation coefficients (0.9322-0.9623) were found for all samples. Activation energies and pre-exponential constants were found between 7.79-9.64 kJ/mole and 1.06-2.36 min⁻¹ for this mechanism. Since the Broido method was used for the calculation of activation energies and pre-exponential constants, values were found between 26.69-35.20 kJ/mole and 248-1.70E+03 min⁻¹.

In the light of these findings, for Coats Redfern method, mechanism D3 revealed the highest correlation coefficient for the second regions of the Particleboard samples for all heating rates. For the fourth region D1 mechanism revealed the highest correlation coefficients. As for the third region, the highest correlations

were obtained for the mechanism F1. In addition to the mechanism F1, close correlation coefficients were also found with D3 mechanism. In the literature, F1 and diffusion mechanisms (D4 and D3) are given as responsible mechanisms for the decomposition of the lignocellulosic materials (Zakrewski, 2003; Valaev et al., 2003); therefore, in the present study, founded results for PB samples seem to be consistent with the literature.

In the study, when heating rate was increased, activation energies and pre-exponential constants of the PB samples in the third region also increased. However, in the second and the fourth regions, this effect could not be observed for the samples, for two methods; therefore, heating rate has effect on the activation energies and pre-exponential constants in the main oxidation region of the PB samples. The same effect was also observed by Reina et al. (1998) and Deka et al. (2002) in their studies, since heating rate increased, temperature gradients in the samples also increased (Reina et al., 1998).

Gao, examined the activation energies of the chemically treated samples in different studies (Gao, 2004; Gao et al., 2003; Gao et al., 2002). In these studies for the main oxidation region, activation energies were found between 74-96 kJ/mole and pre-exponential constants were found between $2.58E+06$ - $3.84E+07$ min^{-1} (Gao et al., 2004; Gao et al., 2003). In these studies, for treated samples lower activation energies and pre-exponential constants were found as compared to untreated sample. In the present study for PB samples, for Coats Redfern method with mechanism F1 activation energies were found between 54-59 kJ/mole, pre-exponential constants were found between with $1.80E+05$ and $2.22E+05$ min^{-1} .

For the second and the fourth regions lower activation energies were obtained with the diffusion mechanisms for Coats Redfern method. After the volatilization region, lower activation energies due to char oxidation were found for the lignocellulosic materials in the literature (Gao, 2004; Nassar, 1999; Vlaev et al.,

2003). When activation energies were examined for the third region of the samples, F1 mechanism results were found close to the Broido method results as compared to the results of the pine samples. Due to high activation energy as compared to the other regions, the third region was found the most stable region, because higher amount volatile matter released in this region.

As findings from the Broido method were examined, it seems that better correlations were found for the second and the third regions. However, in the last region better correlations were found with the Coats Redfern Method as compared to the Broido Method.

4.1.4. Plywood Samples

Plywood Sample at 10 °C/min heating rate (PL-10)

TG and DTG curves of the PL-10 sample are given in Figure 4.34. The heating rate for this sample was 10 °C/min. As can be seen from the Figure 4.34, four regions are seen in the DTG curve. Temperature intervals and weight losses belonging to the regions are given in Table 4.20.

Table 4.20. Temperature intervals and weight losses belonging to the regions

Regions	Temperature interval, (°C)	ΔT, (°C)	% wt. loss
1 st region	30-190	160	6.10
2 nd region	190-250	60	5.00
3 rd region	250-350	100	55.40
4 th region	350-500	150	33.50

Curves showing the solid state mechanisms for Coats Redfern Method for three regions are shown in Figure 4.35.

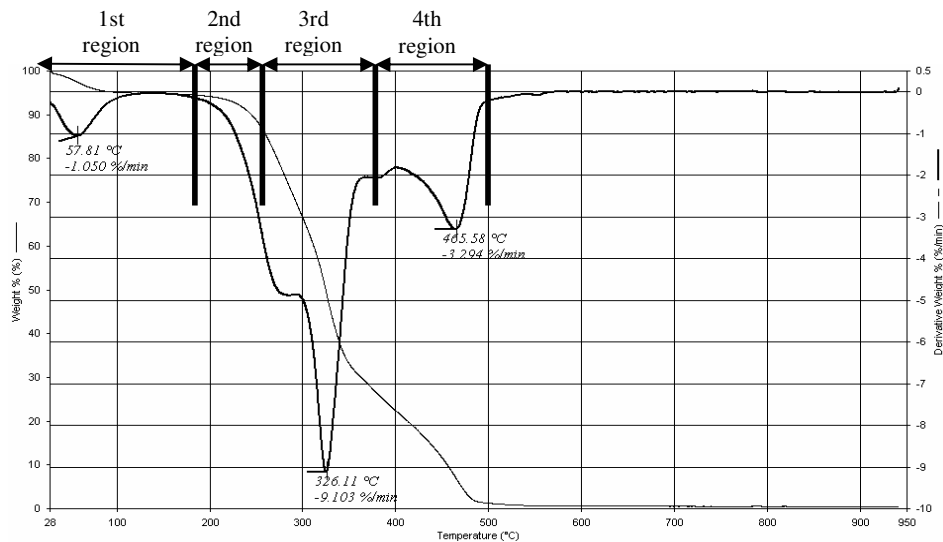


Figure 4.34. TG and DTG graph of the PL-10 sample at 10 °C/min heating rate

As it can be seen from the Figure 4.35, different curves having different slopes were obtained for 6 different solid state mechanisms by using Coats Redfern Method for PL-30 sample. The kinetic constants were calculated from the slope and the intercept of different regions.

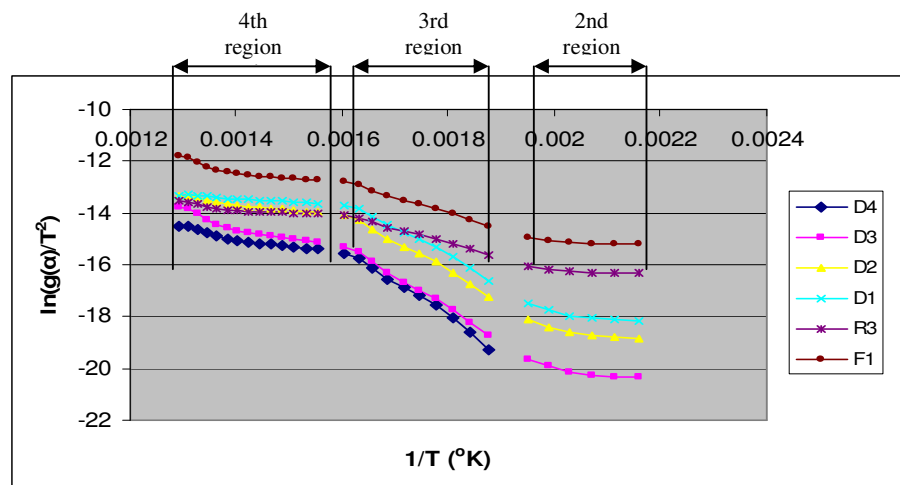


Figure 4.35. Curves indicating the solid state mechanisms for Coats Redfern method for three regions of PL-10 sample

In Figure 4.36, by using Broido method different curves were obtained for 3 regions of PL-10 sample. To calculate thermal kinetics such as activation energy and pre-exponential constant, slope and intercept of these curves were used, respectively.

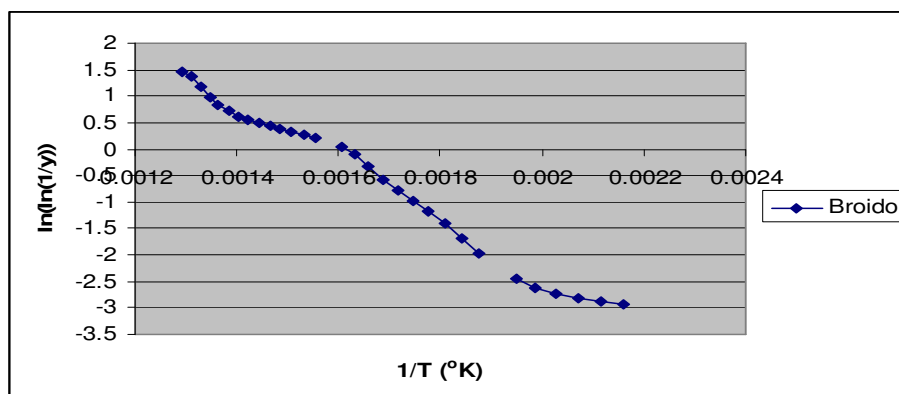


Figure 4.36. Curves showing the Broido method for three regions of PL-10 sample

Plywood Sample at 20 °C/min heating rate (PL-20)

TG and DTG curves of the PL-20 sample are given in Figure 4.37. The heating rate for this sample was 20 °C/min. As can be seen from the Figure 4.37, four regions are seen in the DTG curve. Temperature intervals and weight losses belonging to the regions are given in Table 4.21.

Table 4.21. Temperature intervals and weight losses belonging to the regions

Regions	Temperature interval, (°C)	ΔT , (°C)	% wt. loss
1 st region	30-210	180	7.80
2 nd region	210-250	40	2.13
3 rd region	250-370	120	61.00
4 th region	370-500	130	29.00

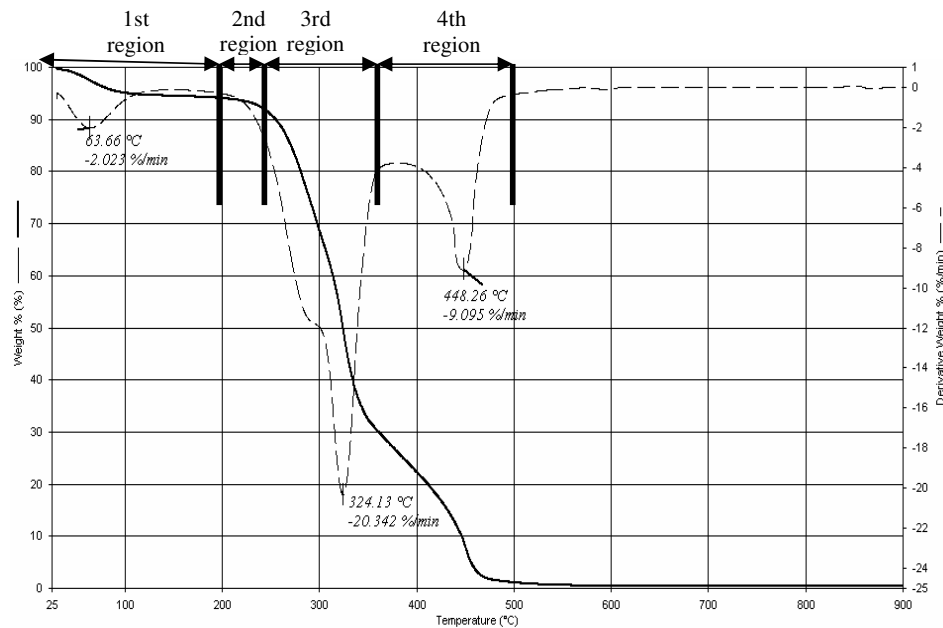


Figure 4.37. TG and DTG graph of the PL-20 sample at 20 °C/min heating rate

Curves showing the solid state mechanisms for Coats Redfern Method for three regions are shown in Figure 4.38. As it can be seen from the Figure 4.38, different curves having different slopes were obtained for 6 different solid state mechanisms by using Coats Redfern Method for PL-20 sample. The kinetic constants were calculated from the slope and the intercept of different regions.

In Figure 4.39, by using the Broido method different curves were obtained for 3 regions of PL-20 sample. To calculate thermal kinetics such as activation energy and pre-exponential constant, slope and intercept of these curves were used, respectively.

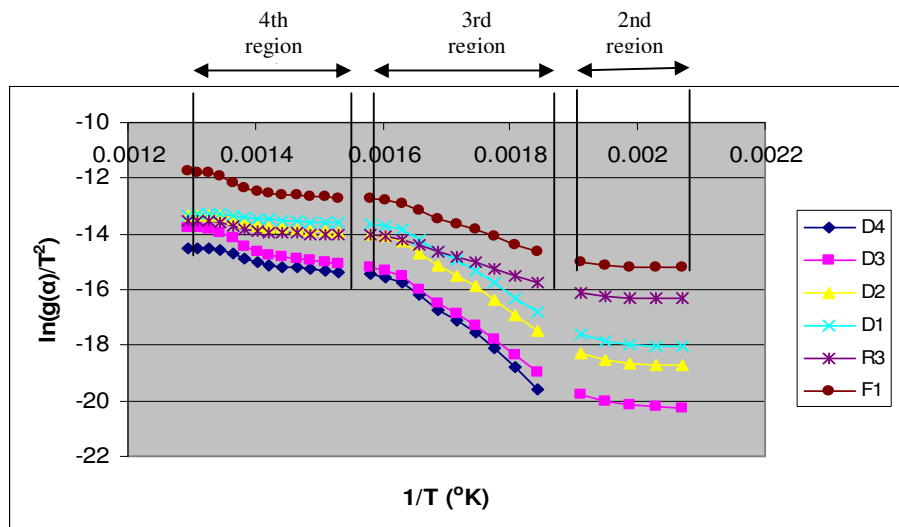


Figure 4.38. Curves showing the solid state mechanisms for Coats Redfern method for three regions of PL-20 sample

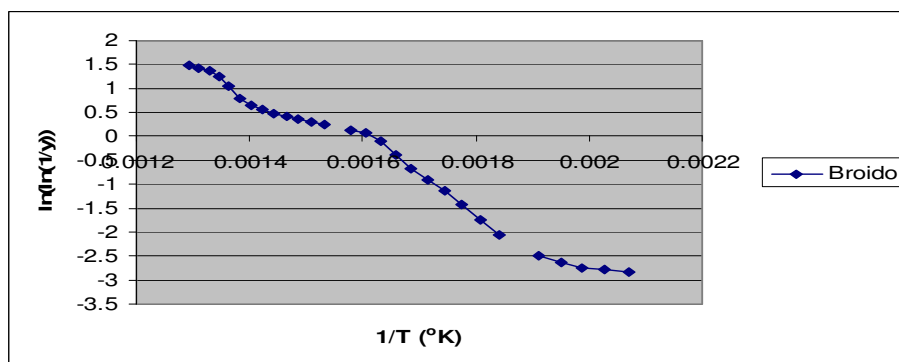


Figure 4.39. Curves indicating the Broido method for three regions of PL-20 sample

Plywood Sample at 30 °C/min heating rate (PL-30)

TG and DTG curves of the PL-30 sample are given in Figure 4.40. The heating rate for this sample was 30 °C/min. As can be seen from the Figure 4.40, four regions are seen in the DTG curve. Temperature intervals and weight losses belonging to the regions are given in Table 4.22.

Table 4.22. Temperature intervals and weight losses belonging to the regions

Regions	Temperature interval, (°C)	ΔT , (°C)	% wt. loss
1 st region	30-240	210	4.00
2 nd region	240-280	140	2.00
3 rd region	280-400	120	61.00
4 th region	400-620	220	33.00

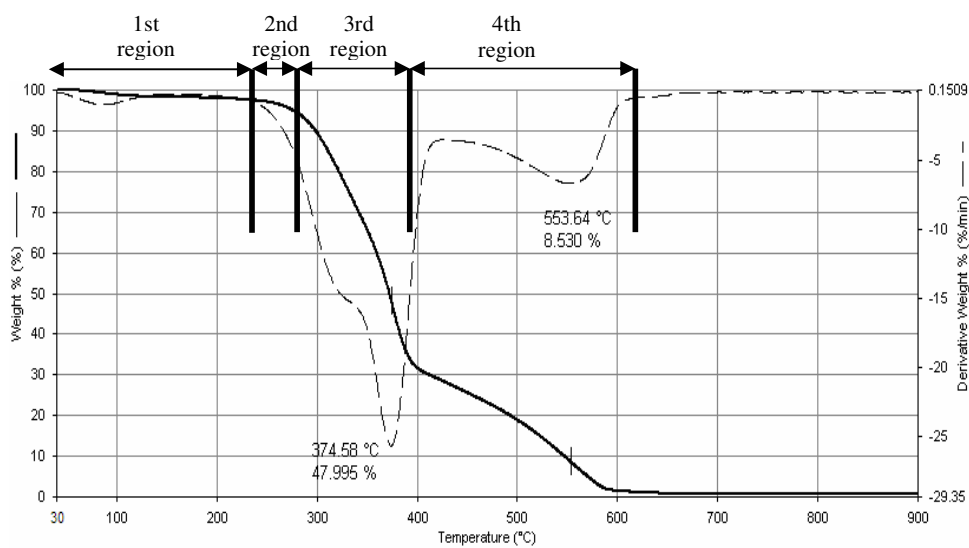


Figure 4.40. TG and DTG graph of the PL-30 sample at 30 °C/min heating rate

Curves showing the solid state mechanisms for Coats Redfern Method for three regions are shown in Figure 4.41. As it can be seen from the Figure 4.41, different curves having different slopes were obtained for 6 different solid state mechanisms by using Coats Redfern Method for PL-30 sample. The kinetic constants were calculated from the slope and the intercept of different regions.

In Figure 4.42, by using the Broido method different curves were obtained for 3 regions of PL-30 sample. To calculate thermal kinetics such as activation energy and pre-exponential constant, slope and intercept of these curves were used, respectively.

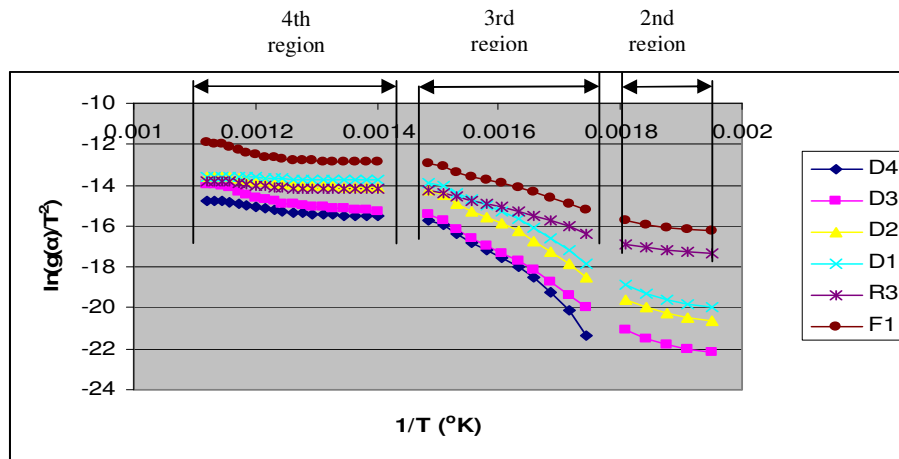


Figure 4.41. Curves which show the solid state mechanisms for three regions of PL-30 sample

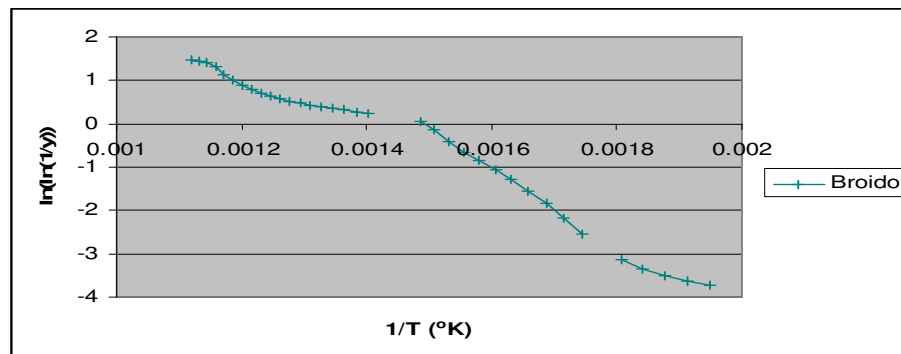


Figure 4.42. Curves showing the Broido method for three regions of PL-30 sample

Comparison of the Plywood Results

When TGA results of the plywood samples were examined, it can be inferred that with the increasing heating rate, the derivative peak temperatures of the main thermal oxidation part, where the weight loss was also maximum, changed. Despite the changes in the place of the derivative peak temperatures, its pattern was not good linear. It is considered that the heterogen chemical content of the

plywood structure lead to collapse this linearity. Change of the peak temperatures (DTG) of the plywood samples in the third region with the increasing heating rate are given in Figure 4.43.

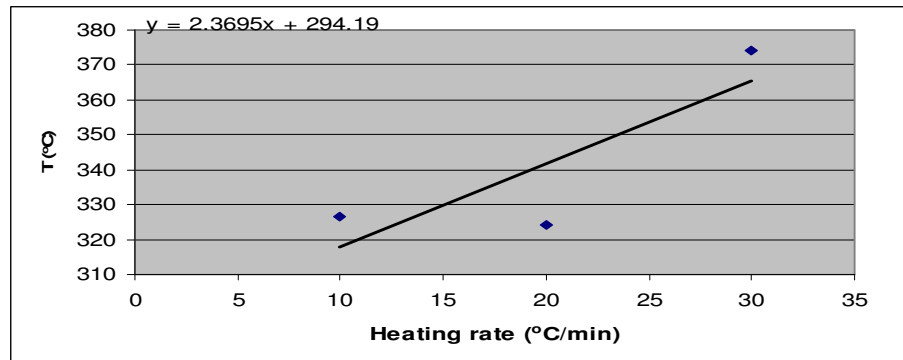


Figure 4.43. Change of maximum peak temperatures of plywood samples in the third region according to the heating rate

As can be seen from the figure, there was not linear increment for the first derivative peaks of the plywood samples in the third region, and correlation coefficient was found as $r^2=0.7109$.

When the effect of heating rate on the first derivative peak of the plywood samples in the fourth region was examined, it can be seen that there were lower correlation coefficients. As compared to third region Change of the maximum peak temperature of the plywood samples for the fourth region is given in Figure 4.44.

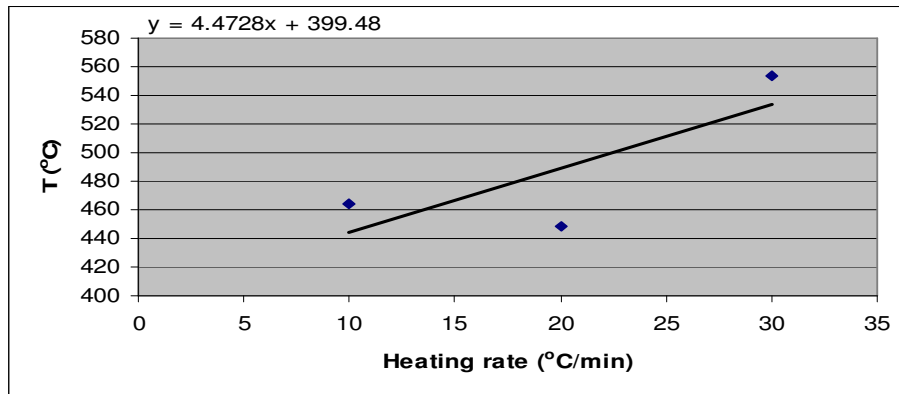


Figure 4.44. Change of maximum peak temperatures of PL samples in the fourth region according to the heating rate

As can be seen the figure, when heating rate increased for the first derivative peak of the PL samples in the fourth region, temperature also raised, but this increase was not so good, and correlation coefficient was found as $r^2=0.6172$.

Heating rate has an effect on the thermal constants. When heating rate increased, activation energies and pre-exponential constants of the third region where the main oxidation occurred, also increased. However, there were not significant alteration for the activation energies and pre-exponential constant of the second and fourth regions of the plywood samples due to heating rate.

Table 4.23. Activation energies and pre-exponential constant values of all plywood samples with respect of the three regions

Regions	Methods.	PL-10 sample			PL- 20 sample			PL- 30 sample		
		E (kJ/mole)	r ²	A (min ⁻¹)	E (kJ/mole)	r ²	A (min ⁻¹)	E (kJ/mole)	r ²	A (min ⁻¹)
2 nd	D4				-	-	-	-	-	-
	D3	27.28	0.875	1.45	24.47	0.8654	0.57	61.78	0.947	953.14
	D2	26.88	0.8749	5.83	24.08	0.865	2.31	61.37	0.9472	3.94E+3
	D1	26.49	0.8747	10.21	23.71	0.8645	4.07	60.99	0.9474	7.1E+3
	R3	9.59	0.7798	0.31	8.06	0.74	0.17	26.46	0.93	13.71
	F1	9.79	0.782	1.01	8.24	0.7436	0.56	26.65	0.93	43.9
	Broido	17.89	0.9196	11.82	16.60	0.9187	7.32	35.50	0.9583	397.61
	3 rd	D4	118.36	0.9872	7.30E+09	144.27	0.9839	1.28874E+12	169.03	0.9665
D3		106.09	0.9976	6.90E+08	123.15	0.9948	2.06E+10	147.15	0.9959	3.20131E+11
D2		98.20	0.9954	4.79E+08	114.36	0.9925	1.20E+10	139.37	0.9929	2.65973E+11
D1		91.30	0.9922	1.81E+08	106.72	0.9894	3.94E+09	132.45	10.084	1.15641E+11
R3		48.30	0.9969	1.46E+04	56.79	0.9937	8.81E+04	68.51	0.995	3.68E+5
F1		52.30	0.998	1.20E+05	61.27	0.9949	7.92E+05	72.44	0.9971	2.7E+6
Broido		61.71	0.9986	9.38E+05	70.74	0.9962	6.14E+06	82.45	0.998	2.39E+7
4 th		D4	27.63	0.951	26.68	32.93	0.9386	99.67	20.85	0.9125
	D3	38.08	0.9158	402.05	48.97	0.9231	3594.04	31.90	0.8762	58.74
	D2	19.90	0.9657	22.91	24.14	0.941	60.82	14.62	0.924	62
	D1	10.49	0.9811	3.03	14.34	0.9265	5.99	6.13	0.9134	77
	R3	13.28	0.8481	4.21	18.63	0.8777	15.62	9.53	0.7315	1.17
	F1	24.73	0.822	238.74	34.87	0.8716	2.04E+03	4.17	0.7512	12.59
	Broido	34.99	0.9147	1.74E+03	44.58	0.9267	1.28E+04	31.20	0.9025	402.81

According to the results (Table 4.23), for the second region activation energies were found between 24.47 and 60.99 kJ/mole values for the second region. D3 mechanism gave the highest correlation coefficients (0.8654-0.875) for Coats Redfern method for PL-10 and PL-20 samples, D1 mechanism gave the highest correlation coefficient (0.9474) for PL-30 sample; however, with other diffusion mechanisms such as D1, D2 similar correlation coefficients were also obtained for all heating rates. Therefore, for this region, diffusion mechanisms seem to have effect on the oxidation of the PL samples. Pre-exponential constants were calculated between $0.57\text{-}953 \text{ min}^{-1}$ for the second regions of all the samples. With Broido method activation energies and pre-exponential constants were found between 16.60-35.50 kJ/mole and $7.32\text{-}397 \text{ min}^{-1}$.

For the third region, the highest correlation coefficients (0.9949-0.998) were found with F1 mechanism for Coats Redfern method for all heating rates. Besides F1 mechanism, with D3 mechanism good correlations were also found in this region with Coats Redfern method. Activation energies and pre-exponential constants for the F1 mechanism were found between 52.30-72.44 kJ/mole and $1.20\text{E}+05\text{-}2.7\text{E}+06 \text{ min}^{-1}$. As Broido method was used for the calculation of the activation energies and pre-exponential constants values were found between 61.71-82.45 kJ/mole and $9.38\text{E}+05\text{-}2.39\text{E}+07 \text{ min}^{-1}$.

As for the fourth region, for the highest correlation coefficient (0.9811) was found with the D1 mechanism for PL-10 sample with Coats Redfern method. For PL-20 and 30 samples, the highest correlation coefficients (0.941-0.924) were found with D2 mechanisms and activation energies and pre-exponential constants were found 14.62-24.14 kJ/mole and $60.82\text{-}62 \text{ min}^{-1}$, respectively. Accordingly diffusion mechanisms (D2) appear to be responsible for the oxidation of PL-20 and 30 samples. With Broido Method, activation energies and pre-exponential constants were found between 31.20-44.58 kJ/mole and $402\text{-}1.28\text{E}+04 \text{ min}^{-1}$.

In the light of these findings, for Coats Redfern method, diffusion mechanism (D1-D3) revealed the highest correlations for the second regions of the Plywood samples for all heating rates. For the fourth region D1 and D2 mechanisms revealed the highest correlations. As for the third region, the highest correlations were obtained for the mechanism F1, in addition to the mechanism F1, very similar correlations were also found with D3 mechanism. In the literature, F1 and diffusion mechanisms (D4 and D3) are given as responsible mechanisms for the decomposition of the lignocellulosic materials (Zakrewski, 2003; Valaev et al., 2003); therefore, in the present study, founded results for PL samples seem to be consistent with the literature.

In the study, when heating rate increased, activation energies and pre-exponential constants of the PL samples in the third region also increased, however in the second and the fourth regions, this effect could not be observed for the samples, for two methods; therefore, heating rate has effect on the activation energies and pre-exponential constants in the main oxidation region of the PL samples, same effect was also observed by Reina et al. (1998) and Deka et al. (2002) in their studies, since heating rate increased, temperature gradients in the samples also increased (Reina et al., 1998).

Gao, examined the activation energies of the chemically treated samples in different studies (Gao, 2004; Gao et al., 2003; Gao et al., 2002). In these studies for the main oxidation region, activation energies were found between 74-96 kJ/mole and pre-exponential constants were found between $2.58E+06$ - $3.84E+07$ min^{-1} (Gao et al., 2004; Gao et al., 2003). In these studies, for treated samples lower activation energies and pre-exponential constants were found as compared to untreated sample. In the present study for PL samples, for Coats Redfern method with mechanism F1 activation energies were found between 52-72 kJ/mole, pre-exponential constants were found between with $1.20E+05$ and $2.7E+06$ min^{-1} ; therefore, when the results compared with literature, F1 mechanism seems more possible mechanism for this region.

For the second and fourth regions lower activation energies were obtained with the Coats Redfern method. After the volatilization region due to char oxidation, lower activation energies were found for the lignocellulosic materials in the literature (Gao, 2004; Nassar, 1999; Vlaev et al., 2003). For the third region activation energies examined, F1 mechanism results were found close to Broido method results as compared to the results of the pine samples.

Due to high activation energy as compared to the other regions, the third region was found the most stable region, because higher amount volatile matter released in this region.

As findings from Broido method were examined, it seems that better correlations were found for the second and third regions. However, in the last region better correlations were found with the Coats Redfern Method as compared to the Broido Method.

4.2. Comparison of the TGA Results of the Samples

When the results of TG analysis are compared for all samples, it is seen that thermal degradation of hemicellulose occurs first, and then cellulose decomposes. Thermal degradation occurs at lower temperatures, because of dehydration, depolymerization, oxidation, and evolution of carbon dioxide, and formation of carbonyl and carboxy groups. At higher temperatures a rapid volatilization takes place. As a result of this volatilization, volatile and flammable products are released. In contrast to cellulose and hemicellulose, decomposition of lignin takes longer time by char oxidation (Gao, 2004; Nassar, 1999). In the current study, the TG curves for waste wood samples show four regions of thermal degradation in air. Weight losses of the samples as compared to the regions are given in Table 4.24 .

Table 4.24. Weight loss of all samples for different regions

Region	Weight loss of samples, % by weight											
	P-10	P-20	P-30	M-10	M-20	M-30	PL-10	PL-20	PL-30	PB-10	PB-20	PB-30
1	4.7	5.9	5.4	4.5	4.6	5.16	6.1	7.8	4	7	8.5	4.41
2	4.3	4.7	5.6	7.7	9.1	7.95	5	2.13	2	8	5.5	3.58
3	65	63.4	63	52.2	52.8	53.7	55.4	61	61	54	51.6	59.83
4	26	26	26	35.6	33.5	33.19	33.5	29	33	31	33.4	32.18

As can be seen from Table 4.24, the largest weight loss was detected in the third region for pine samples (average 63%) among the investigated waste wood samples. For the treated samples, smaller weight losses were observed in this region. However, for the fourth regions, the largest weight losses were seen for the treated waste wood samples. Owing to chemical treatment, probably lower percentages of volatile matters were released during the main oxidation region and this increased the amount of char in the treated wood samples. This indicated the catalytic effect of adsorbed chemicals in the treated samples on the oxidation behavior of the samples (Gao, 2004; Getto et al., 1998; Nassar, 1999).

When the heating rate was increased, weight loss of the samples also increased. As heating rate was increased, higher temperatures were detected for the same weight loss for all samples, namely the highest temperatures were detected at 30 °C/min heating rates, and the lowest temperatures were observed at 10°C/min for the same weight loss. Temperatures versus weight loss for all samples at different heating rates are plotted in Figure 4.45.

As can be seen from the Figure 4.45, for the 60% weight loss, higher temperatures were observed for P-30 sample as compared to other samples, but after the 60% weight loss, the higher temperatures were observed for treated samples because of some chemicals used. Parallel weight losses were observed for other waste wood samples, especially PB and PL samples.

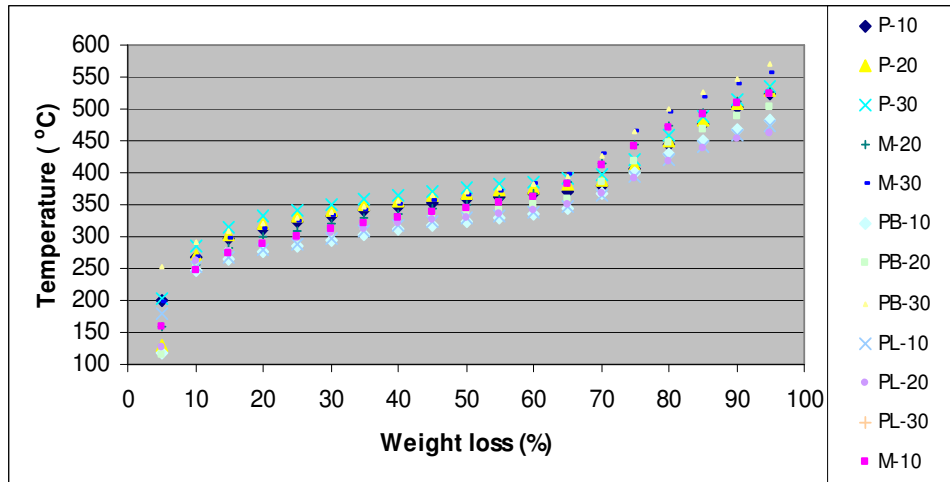


Figure 4.45. Temperature vs. weight losses of all samples at different heating rates

The temperature of the peaks in the DTG curves depends on the heating regime (Vlaev et al., 2003). Peak temperature (PT) and Burnout temperature (BT) are the main characteristic temperatures for the DTG curves. The peak temperature represents the place where the rate of weight loss is at maximum. This parameter is used mainly in the assessment of combustibility. Lower temperature shows the easily ignition. The burnout temperature shows the temperature where sample oxidation is completed (Sonibare et al., 2005). The characteristic peak and burnout temperatures of all waste wood samples for the present study are given in Table 4.25. As can be seen from the Table, generally speaking, when the heating rate was increased, peak and burnout temperatures also increased. Hence, when heating rate increased, ignitions of the samples were difficult. Among all samples, pine samples had also the highest peak temperatures; therefore, pine samples could not be ignited easily among the other samples.

Table 4.25. Peak and burnout temperatures of the samples

Sample	Peak Temperatures (°C)		Burnout Temperatures (°C)
	In 3 rd region	In 4 th region	
P-10	358	510	553
P-20	366	523	555
P-30	371	520	575
M-10	341	509	567
M-20	346	514	570
M-30	352	537	583
PL-10	326	464	500
PL-20	324	448	500
PL-30	374	554	620
PB-10	321	466	510
PB-20	332	483	520
PB-30	362	550	610

For the thermal decomposition of the waste wood samples, the third region, where the highest and rapid weight loss occurred, played important role for the combustibility of the samples. For treated samples; MDF, particleboard and plywood, the third stage of thermal decomposition was observed at lower temperatures as compared to pine sample which is an untreated sample, because chemicals in the treated samples might catalyzed the decomposition of the cellulose which makes the whole oxidative decomposition of the wood occur at lower temperatures (Gao, 2004). As a result of this, less flammable products were emitted and more char was observed from these treated samples (Gao et al., 2003). However, in the present study char yields of the treated samples were found a little lower than the char yield in the literature as 11.1-17.7% (Lee et al., 2004). This may be due to the different samples used in the literature. Low char yields of the treated flame retardancy is poor.

When, maximum weight loss rates of the samples at the peak temperature were evaluated, for the treated composite wood samples namely M, PB, and PL lower weight loss rates for the main oxidation region which is the third region were observed as compared to untreated P sample (Table 4.26). All of these data (Table 4.25 and 4.26) indicate that chemicals added to composite samples can

improve the fire retardancy of wood by lowering its weight loss rate, lowering the onset temperature for decomposition and by decreasing the formation of volatile combustibles through promotion of higher char yield as compared to the untreated sample (Lee et al., 2004). Heating rate also affect the maximum weight loss rate at the peaks. As heating rate was increased, maximum weight loss rates also increased for all samples (Table 4.26).

Table 4.26. Maximum weight loss rates for all samples

Heating rate	P		M		PB		PL	
	Max. weight loss rate (% min ⁻¹) for regions		Max. weight loss rate (% min ⁻¹) for regions		Max. weight loss rate (% min ⁻¹) for regions		Max. weight loss rate (% min ⁻¹) for regions	
	3 rd	4 th	3 rd	4 th	3 rd	4 th	3 rd	4 th
@10 °C/min	12.2	2.5	6.6	2.7	9.3	3.2	10.1	3.3
@20 °C/min	22.4	5.0	14.1	6.2	16.0	5.7	20.3	9.1
@30 °C/min	30.6	7.3	19.5	7.8	22	6.6	25.8	6.25

When thermal kinetic results of all samples were examined by using Coats Redfern Method, for all heating rates, it can be seen that in the second regions, D1 mechanism in the third regions, D4 mechanism and in the fourth regions, D1 and D2 mechanisms were found as an effective solid state mechanisms for the oxidation process for untreated pine samples. Agrawal (1985) and Zakrewski (2003) examined the effective solid state mechanisms for the decomposition of the not only wood samples but also other lignocellulosic materials and they found that D3 and D4 mechanisms were effective mechanisms. Guo et al. (2000) also studied the pyrolysis of extracted oil palm fibers, and for the low temperature regimes, he found that the three dimensional diffusion mechanisms (D3) was effective. However, for the high temperature regimes the reaction is

based on the first order reaction (F1). Vlaev et al. (2003) studied decomposition of the lignocellulosic material, rice husk, and he found that the D4 mechanism which is Ginstling Brounshtein equation valid for diffusion controlled reactions starting on the exterior of spherical particles with uniform radius. In the literature this equation refers to diffusion controlled reactions starting on the exterior of a spherical particle with radius r_0 :

$$g(\alpha) = (1 - 2\alpha/3) - (1 - \alpha)^{2/3} = 2kD\tau/r_0^2 \quad (4.1)$$

Nevertheless, in the second region, D1 mechanism for all heating rates was found to be as an effective mechanism for one of the treated sample, MDF; still, good correlation coefficients were found with other diffusion mechanisms. In the third region, F1 mechanism was yielded the highest correlation, but D3 mechanism also revealed high correlation, as compared to F1 mechanism. In the fourth region, D1 mechanism seemed effective solid state mechanism. For plywood and particleboard samples, effective solid state mechanisms were found to be D3, F1, and D1-D2 for the second, the third and the fourth regions, respectively.

For the second region of the samples, other diffusion mechanisms also gave high correlation coefficients. The general disadvantage of dynamic thermal analysis is that in many cases more than one function $g(\alpha)$ fits the experimental results. As a result of this problem, selection of the responsible mechanism and estimation of the real kinetic parameters (E, A) can become difficult (Alshehri et al., 2000). Same problem was also observed in this study; especially in the second region of the samples similar correlation coefficients for the diffusion mechanisms were observed. Therefore, generally speaking diffusion mechanism was selected as a responsible mechanism as a result of TG analyses. As a remedy to this problem, combined usage of isothermal and non isothermal methods in TGA is the proper solution to identify the correct mechanism. Therefore, in the future studies combined methods for TG analyses including dynamic and isothermal studies

will help to determine the exact mechanisms and thermal constants for the waste wood samples.

Consequently, for the treated samples such as MDF, plywood, particleboard samples, in second and fourth regions of these samples diffusion mechanisms; in the third region of the samples F1 mechanism was assumed as the main mechanism which is responsible for the oxidation of these samples. Therefore, for the thermal oxidation of the waste wood composites, in the main oxidation region F1 mechanism seems to be responsible mechanism; however for untreated samples D4 mechanism was found as an effective mechanism. *As a conclusion, treatment of the wood with different additives and glues altered the thermal oxidation process and changed the effective mechanism.*

With Broido Method, good correlation coefficients were obtained for pine samples, except the third region. In the second region, higher correlation coefficients were found as compared to Coats Redfern Method. On the other hand, when activation energies and pre-exponential constants found with Broido Method were compared with that of Coats Redfern Method, dissimilar results were obtained especially in the third regions of the pine sample. However, for the MDF, particleboard and plywood samples similar results were found (Table 4.27).

For the third regions of the treated samples such as MDF, plywood and particleboard, higher correlation coefficients were found with Broido method as compared to Coats Redfern Method. Nishizaki et al. (1980) have compared the results of application of different methods for determination of kinetic parameters for the process of polystyrene degradation measured by TGA. However, the assessment of different methods was qualitative because true values for the kinetic constants were not known. In order to remove this uncertainty, Petrovic et al. (1986) constructed a synthetic TG curve. Different methods were applied to the theoretical (synthetic) curve to back calculate the

values of E, A and n. Then, results of these different methods were compared. In this study, Coats Redfern Method was also included among the methods tested. 2% lower activation energies and pre-exponential constants were found with Coats Redfern Method. Therefore, Coats and Redfern method was found to fit the theoretical curve with the least error.

Momoh et al. (1996) investigated the thermogravimetric properties of the tropical timbers with the Broido method. In this study the activation energies of the first decomposition step were compared with other values of the cellulose decomposition. Fairly good agreements were obtained because all the analyses used the same model, i.e. the first-order equation, to describe the decomposition behaviour for the cellulose pyrolysis. From the plots of $\ln(\ln(1/y))$ vs. $(1/T)$, the correlation coefficient (r^2) values were found unsatisfactory (Liu et al.,1998).

In our study for treated samples, higher correlation coefficients were found in the main oxidation region as compared to untreated samples. It can be seen that such agreements are not surprising, because for the treated samples first order reaction was found as a responsible mechanism. Therefore, since Broido method was based on the first order reaction, good correlation coefficients were obtained. However, for the untreated samples lower correlation coefficients were found with Broido method as compared to treated samples in the main oxidation region, because for untreated samples D4 mechanism was found as a responsible mechanism and it is different than the first order models.

In conclusion, it can be said that for the calculation of the kinetic constants in the main oxidation region for the **treated samples** Broido method is satisfactory. For the **untreated samples** the Coats Redfern Method can be preferred for the calculation of kinetic constants due to good correlation coefficients obtained and also due to the agreement of the results with literature. Comparison of the activation energies found in the present study and other studies in the literature are given in Table 4.27.

For pine samples (i.e., untreated), the activation energy values and pre-exponential constant values of the samples were compared with treated samples (MDF, plywood, particleboard) higher activation energies were found for the main oxidation region. The presence of the inorganic materials influences the thermal degradation of the lignocellulosic materials and may act as a flame retardant by lowering the activation energy of the thermal reaction (Nassar, 1999). Nassar in 1999, investigated to the treated and untreated bagasse samples, and he found that the activation energies of the untreated pith was larger than the dye-treated pith, which indicated that the untreated pith is thermally more stable. Similar results were obtained by Gao. In his study, lower activation energies were obtained from the treated wood samples (Table 4.27) (Gao, 2004; Gao et al., 2003; Xu et al., 2002). However, Deka et al., found that the treated wood samples to be thermally more stable than the untreated one (Deka et al., 2002). In the present study, activation energy of the treated samples was found lower than the untreated pine sample. This also indicate that the chemicals in the waste wood samples change the mechanism of thermal decomposition in such a way as to reduce the decomposition temperatures of wood, which can lead to less flammable volatile products and more char (Gao et al., 2003). When activation energies of the treated waste wood samples (MDF, particleboard and plywood samples) were compared with each other (Table 4.27), closer values were found because of the similar production techniques and chemicals. Consequently, it must be stated that the chemical composition of each type of wood together with the chemicals added to the wood for each application, have a very important function in the kinetic behavior of the thermal decomposition of the wood (Reina et al., 1998).

Table 4.27. Comparison of the activation energies found in the present study with that of literature for the main oxidation region

Literature	Sample	Ea (kJ/mole) In nitrogen atmosphere	Ea (kJ/mole) In air atmosphere
Present study	Pine	-	123-136* (62-74)**
	MDF	-	45-50 (54-59)
	Particleboard	-	54-59 (63-69)
	Plywood	-	52-72 (62-82)
Gao (2004) (@ 10 °C/min)***	Untreated wood	-	126
	MF treated wood	-	95
	MFP treated wood	-	74
	UDFP treated wood	-	80
Gao (2003) (@ 10 °C/min)***	Untreated wood	-	184.2
	Na ₃ PO ₄ +Na ₂ CO ₃ treated wood	-	72.4
	(NH ₂) ₂ (CN) ₂ +(NH ₄) ₂ HPO ₄ treated wood	-	58.8
	NH ₂ CONH ₂ +(NH ₄) ₂ HPO ₄ treated wood	-	52.9
	NH ₄ Cl+(NH ₄) ₂ HPO ₄ treated wood	-	62.9
	NH ₄ Br+(NH ₄) ₂ HPO ₄ treated wood	-	67.6
	H ₃ BO ₃ :+Na ₂ B ₄ O ₇ treated wood	-	101.6
Antal et al.(2003)	Wood	109-138	-
Reina et al. (1998) (@ 5 °C/min)	Furniture	129.36	-
	Forest	136.18	-
	Pellet	127.61	-
Deka et al. (2002) (@ 20 °C/min)	Untreated wood	112	-
	Treated wood	132-138	-
(@ 30 °C/min)	Untreated wood	119	-
	Treated wood	130-134	-
Zakrewski (2003) (@ 5 °C/min)	Pine wood	85.6-168.3	-
Schniewind (1989)	Wood (T<300°C)	63-139	96-147

*Result of the Coats Redfern Method for the highest correlation in the third region (main oxidation region) of the sample, **Parenthesis show the results of the Broido method in the third region***Results of the main oxidation region of the samples

For all samples, activation energy and pre-exponential constant values were also affected by the heating rate because the temperature of the peaks in the DTG curves depends on the heating regime. Consequently, the kinetic parameters characterizing the different processes were anticipated to be different (Vlaev et al., 2003). Especially in the third region of the samples, this effect was observed clearly, because activation energy and pre-exponential constant values were got higher with increasing heating rate. The highest activation energies and pre-exponential constant values were found in the third regions of all samples due to high volatile released in this region (Vlaev et al., 2003). Accordingly, the third regions of all samples were found as the most stable region among the other regions. For all samples, the lowest activation energies for the Coats Redfern method were found in the last region due to lower content of the volatile matters in the samples (Table 4.28). This situation was also observed by Gao (2004), however for the second region values of the activation energies were found lower than the results of the Gao, this was probably caused different reasons, mainly due to selection of the regions, difference between the heating rate, flow rate, operational conditions, sample size and amount and the other conditions. In addition to the operational conditions, sample type mainly affects the thermal constants, in the present study composite waste wood samples which were formed wood particles were used directly; however, Gao used the wood samples for the chemical treatment; therefore, for only one chemical type was studied, but in the present study different chemical and additives could be used for the production of the waste wood samples.

Table 4.28. Comparison of the results of the present study and literature for the second and fourth regions

	Sample type	Region	Activation energy (kJ/mole)
Present study	Pine	Second region	23-28* (16-19)**
		Fourth region	15-18* (35-40)
	MDF	Second region	23-26 (16-17)
		Fourth region	10-11 (35-38)
	Particleboard	Second region	21-25 (15-17)
		Fourth region	8-10 (27-35)
	Plywood	Second region	24-61 (17-36)
		Fourth region	11-24 (31-45)
Gao (2004)	Untreated	First region	68
		Third region	18
	MF treated	First region	29
		Third region	17
	MFP treated	First region	50
		Third region	15
UDFP treated	First region	57	
	Third region	13	

*Result of the Coats Redfern Method for the highest correlation in the Second and fourth region,

**Parenthesis shows the results of the Broido method in the fourth region.

4.3. FTIR Results of the Waste Wood Samples

For the spectrums of the waste wood samples, mainly eight regions were defined for all three heating rates. These regions and peaks were identified by comparing the spectrums in the literature. These are;

- Around the wavenumber of 3600 cm^{-1} free OH stretching of alcohol and phenol groups. A band about 3600 cm^{-1} probably corresponds to free OH stretching vibrations (Sharman et al., 2004; Spectroscopy tutorial, 2005).

- Below the wavenumber of 3000 cm^{-1} , aliphatic CH stretching region ($3000\text{-}2800\text{ cm}^{-1}$) (Guo et al., 2000; Sobkowiak et al., 1992; Meldrum et al., 1991).
- CO_2 absorption band around wavenumbers of 2405-2247, 2240-2394, 2416-2247, 2405-2230, 2285, 2289, 2300 cm^{-1} (Meldrum et al., 1991; Lu et al., 1999; Marcilla et al., 2005).
- CO absorption band around wavenumbers of 2247-2016, 2240-2056, 2247-2033, 2230-2028, 2020-2190, $2000\text{-}2178\text{ cm}^{-1}$ (Lu et al., 1999).
- Carbonyl C=O absorption band (carboxylic acids, esters saturated aliphatics, aldehydes and acetyl derivatives) around wavenumbers of $1800\text{-}1700\text{ cm}^{-1}$ (Abdel-Nasser et al., 2006; Moore et al., 2001). The exact position of the band was dependent on whether the C=O groups were in conjunction with the aromatic ring (position below 1700 cm^{-1}) or not (position above 1700 cm^{-1}) (Sharman et al., 2004). Most of the carbonyl groups in wood are due to hemicellulose component, and they include mainly esters and acids. Most of the free esters and acids absorb in the wavenumber range from $1750\text{ to }1735\text{ cm}^{-1}$. The carbonyl groups that can occur in the lignin matrix include aldehydes and ketones, and these tend to absorb at a lower wave number region (between $1750\text{-}1680\text{ cm}^{-1}$ due to ketones, carboxyls, aldehydes and esters, e.g., aldehydes, $1760\text{-}1720\text{ cm}^{-1}$; ketones, $1700\text{-}1670\text{ cm}^{-1}$) (Owen et al., 1989; Koch et al., 1998). In this study absorption at wavenumber of 1744 cm^{-1} was attributed to a C=O band ('hemicellulose band' mainly originating from uronic acids of xylans) for both sample types (treated and untreated wood samples).
- Aromatic ring vibrations of lignin at wavenumbers of the 1505 and 1508 cm^{-1} . These type of bands are called C=C skeletal vibrations (around

1510 cm^{-1}) (Pandey, 1999; Moore et al., 2001). Smith in 2005 observed aromatic C-C stretching band between 1400-1600 cm^{-1} region and Marcilla in 2005 was observed lignin aromatic skeletal vibrations at 1505-1515 cm^{-1} (Smith, 2005; Marcilla, 2005). The most characteristic bands of lignin were at 1513 cm^{-1} and 1597 cm^{-1} , and between 1470-1460 cm^{-1} (CH deformations and aromatic ring vibrations were observed in the studies). A higher intensity band at 1513 cm^{-1} shows that the lignin sample was probably obtained from softwood (Sharman et al., 2004).

- Aliphatic bending region between wavenumbers of 1350 and 1500 cm^{-1} region.
- 1350-1000 cm^{-1} region. The 1350-1000 cm^{-1} band region is very complex because of many different functional groups. The complex band between 1200 and 900 cm^{-1} , mainly represents the wood polysaccharides (Faix et al., 1991). In this region C-N stretching of aromatic amines and aliphatic amines, C-O stretching of oxygenated groups, C-O-C vibrations of formates, acetates, benzoates and C-H wag of alkyl halides can be observed. In this region, this is caused by combination and overlapping of C-O stretching bands and by several deformations (Sharman et al., 2004). 1000-1400 cm^{-1} region includes cellulose and lignin band. Lignin bands are in 1200-1300 cm^{-1} region and cellulose bands are in 1000-1200 cm^{-1} region (Drobniak et al., 2006).

In addition to these peaks, some different absorption bands were also observed for M, PB and PL samples, due to chemical content of these samples. These absorptions were;

Ammonia peaks were observed for the M, PB, PL samples when spectrums were compared with the reference ammonia spectrum (Schanzer et al., 2002).

Absorption band of the ammonia was given at the 965, 930 cm^{-1} (fingerprint) band region in the reference spectrum of the ammonia.

The peak belongs to isocyanate group was also observed at 2251 cm^{-1} as a result of comparison of the spectrums with the different literature studies. In other studies, the peaks belong to isocyanate groups were defined at similar places like 2250 cm^{-1} , 2260 cm^{-1} , 2255 cm^{-1} and 2238 cm^{-1} . In the relevant literature, less intense and well-defined bands at 2155, 2157 and 2127, 2122 cm^{-1} were also observed due to the presence of cyanide groups (Bion et al., 2003; Barral et al., 2005; Tait et al., 1997; Thomsan et al., 2001; Venkov et al., 2006). The result of the Perkin-Elmer ATR of Polymers Library IR scan shows that Isophorone diisocyanate, Phenyl isocyanate, 1-naphthylisocyanate, 4-chlorophenyl isocyanates were also found with different correlations from the combustion of these samples.

When spectrums of the M, PB and PL were compared with the reference spectrum of the formaldehyde, similar band absorptions were also detected between spectrums of these samples and reference formaldehyde spectrum. Functional groups and observed wave numbers for formaldehyde and their literature values are given in Table 4.29. As a result of combustion of these samples; ammonia, formaldehyde and other emissions were released from the structure; therefore, it was assumed that for the production of these composite wood samples, urea or melamine formaldehyde were used as glue and these chemicals are released from the samples during the oxidation process, because when melamine was heated in a closed system, ammonia was evolved (Getto et al., 1998).

Phosphoric acid and nitrogen compounds are used commonly as fire retardant chemicals. Phosphorus is observed from wavenumber of 900 to 1300 cm^{-1} in only chemicals that were accepted as a P=O, P-O-C and P-O-P, but it was difficult to identify these groups because the spectra is similar to the untreated

wood spectra (Getto, 1998). Therefore, in this study, phosphorus was not identified from the spectrums of the treated samples owing to the spectrums of these samples were found similar to the untreated pine spectrums for the band between 900 and 1300 cm^{-1} .

Table 4.29. Functional groups: observed wave numbers and their literature values (Poljansek et al., 2005; Schanzer et al., 2002)

Functional group	Literature data of wavenumber, cm^{-1}	Observed wavenumber, cm^{-1}
CH stretch general	2822	2821
CH bend overtone	2724	2722
C-H bend	1390	1397
C=O stretch	1770	1772,1769
C=O stretch	1722	1715

In addition to the ammonia, formaldehyde and isocyanate group absorptions at the spectrums of the PB and PL samples as a result of the IR scan benzoylbromide and phenyl chloroformate were also found.

4.3.1. 3-D/FTIR Results of the P Samples

P-10 Sample

3-D figure of the P-10 sample is given in Figure 4.46. Main eight groups in the FTIR spectrum for P-10 sample are displayed in this figure.

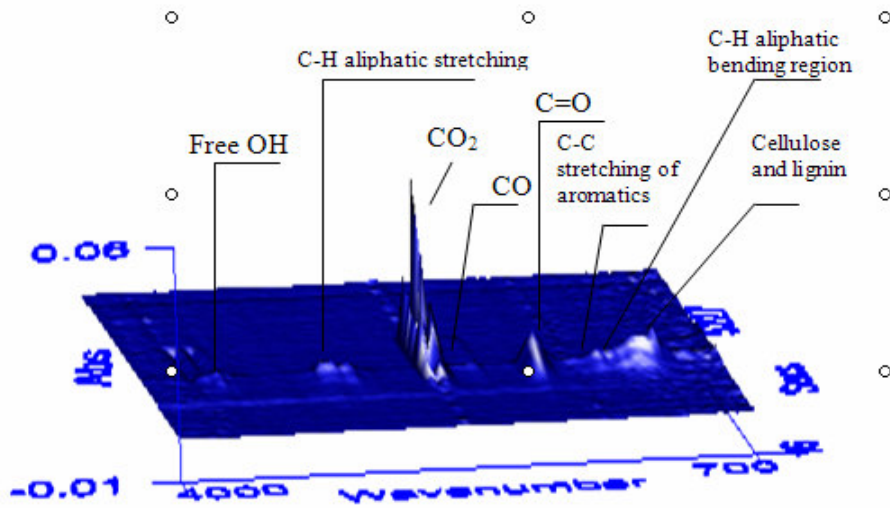


Figure 4.46. 3-D presentation of the P-10 sample

Main absorption of the groups was observed between 257 °C (1500 s) and 367 °C (2200 s), except CO₂. CO₂ emissions stopped at 534 °C (3200 s) for P-10 sample.

P-20 Sample

3D figure of P-20 sample is given in Figure 4.47.

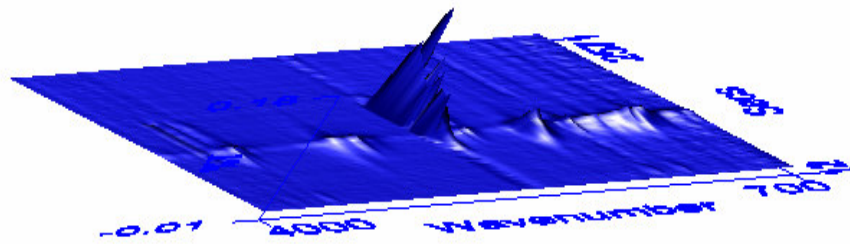


Figure 4.47. 3-D presentation of the P-20 sample

Main absorptions of the groups occurred between 267 °C (800 s) and 375 °C (1125 s) except CO₂. CO₂ emissions stopped at 580 °C (1740 s) for P-20 sample.

P-30 Sample

3-D figure of P-30 sample is given in Figure 4.48.

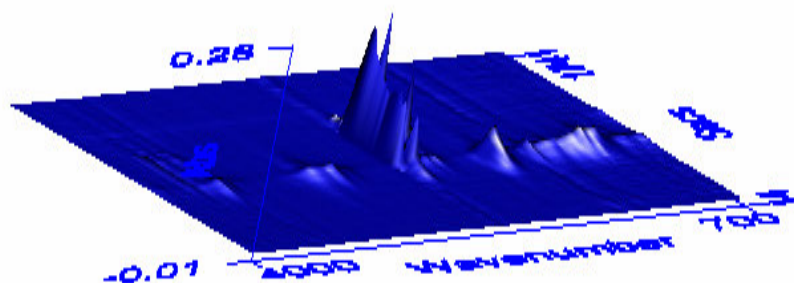


Figure 4.48. 3-D presentation of the P-30 sample

Main absorption of the groups were observed between 300 °C (600 s) and 395 °C (790 s), except CO₂. CO₂ emissions stopped at 600 °C (1200 s) for P-30 sample. With the increasing heating rate, it is observed that intensities of the groups evolved from the samples increased too. After baseline corrections were done and all spectrums were made smooth to remove noise, peak areas of the groups in the FTIR spectrum were calculated by using the computer program. For the calculation of areas, baseline corrections of the spectrums were done for all pine samples; however, due to high noise for the first region, and due to low absorption for the third region area, calculations could not performed for all pine samples.

For the calculation of the area of the carbonyl groups (C=O) (between 1700 and 1800 cm^{-1}), baseline was drawn between 1623 and 1977 cm^{-1} . For the calculation of the area of the alkanes (between 2800 and 3000 cm^{-1}), baseline was drawn nearly between 2653 and 3132 cm^{-1} . For the calculation of the area of the free OH (about 3550-3680 cm^{-1}), baseline was drawn between 3369-3718 cm^{-1} and for the calculation of the areas of the cellulose and lignin bands (between 1000 and 1300 cm^{-1}), for lignin (1200-1300 cm^{-1}), for aromatic bending region (between 1340 and 1466 cm^{-1} , and for aromatic skeletal vibrations (between 1494 and 1519 cm^{-1}), baseline was drawn between 1539 and 938 cm^{-1} , and areas were calculated for these intervals. Areas of peaks in seven regions (for different functional groups) are plotted in Figure 4.49, 4.50 and 4.51 for the P-10, P-20 and P-30 samples, respectively.

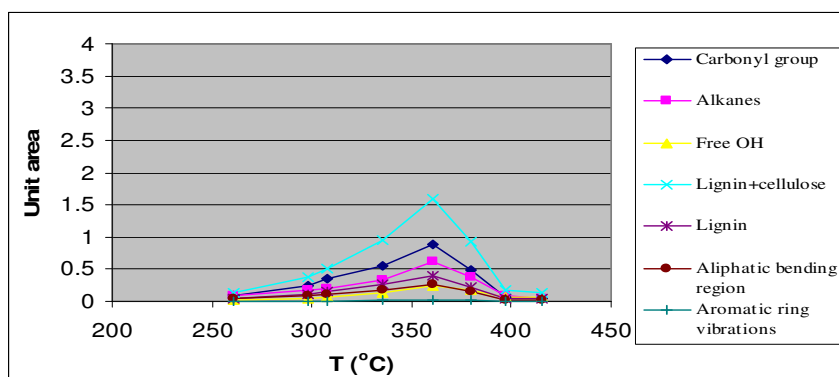


Figure 4.49. Areas of the seven regions of P-10 sample

When Figures 4.49-4.51 were examined, it can be seen that as heating is increased, areas for the groups which were released from samples are increased. After a certain temperature, areas of the groups reached a maximum value and then areas began to decrease due to decreasing of volatile matters in the samples. As can be seen from the Figures, when heating rate was increased, maximum temperatures where the highest absorptions occurred and amount of emissions

increased. Therefore; it seems that heating rate affected the amount of emissions and maximum temperatures where the highest emissions occurred.

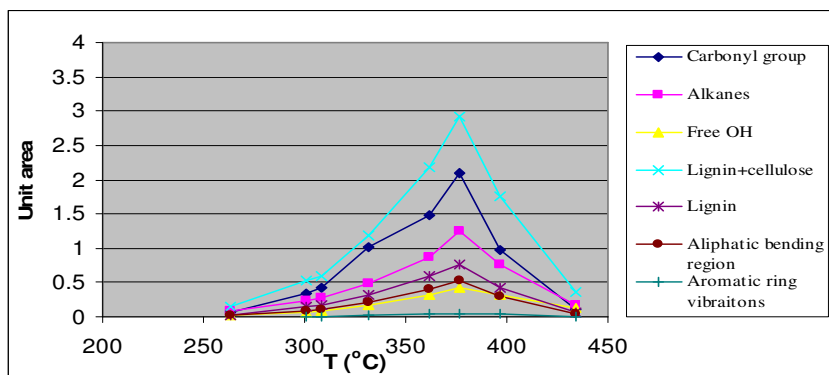


Figure 4.50. Areas of the seven regions of P-20 sample

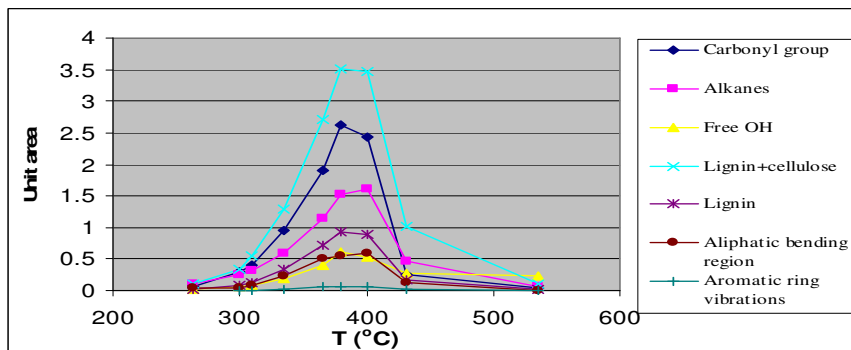


Figure 4.51. Areas of the seven regions of P-30 sample

4.3.2. 3-D/FTIR Results of the M Samples

M-10 Sample

3D figure of the M-10 sample as a result of FTIR is given in Figure 4.52. Main nine groups in the FTIR spectrum for M-10 sample are also displayed in this figure.

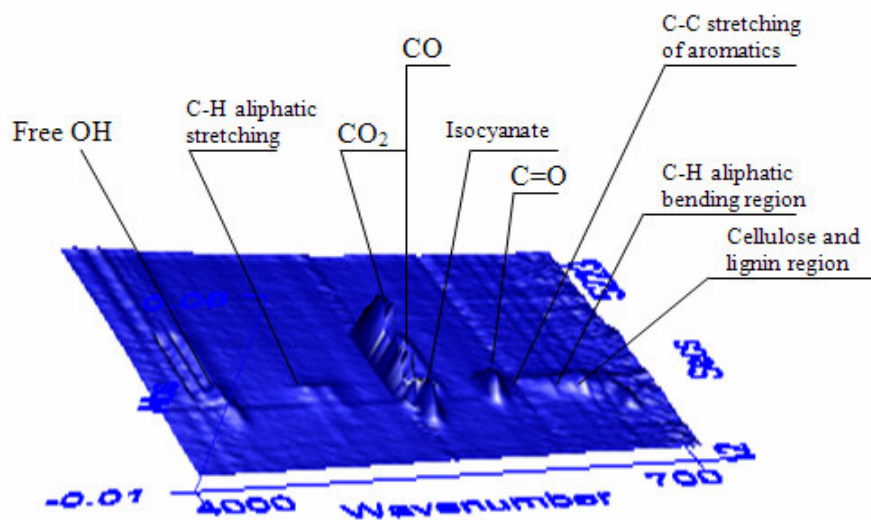


Figure 4.52. 3-D presentation of the M-10 sample

Main absorptions of the groups was observed between 263 °C (1400 s) and 372 °C (2050 s), except CO₂. CO₂ emissions stopped at 563 °C (3200 s) for M-10 sample.

M-20 Sample

3D figure of M-20 sample as a result of FTIR analysis is given in Figure 4.53

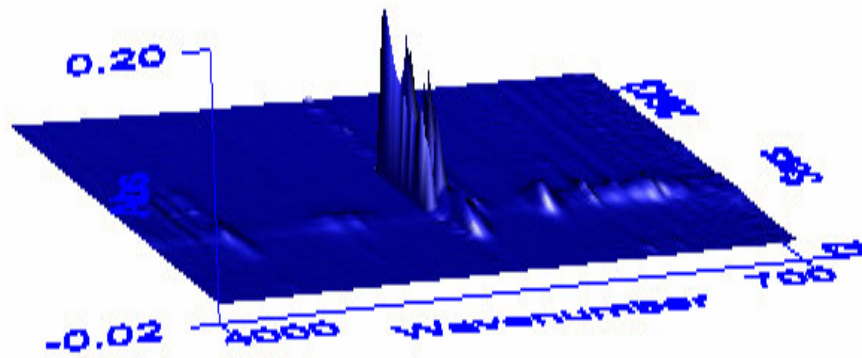


Figure 4.53. 3-D presentation of the M-20 sample

Main absorptions of the groups occurred between 272 °C (725 s) and 397 °C (1100 s), except CO₂. CO₂ emissions stopped at 563 °C (1600 s) for M-20 sample.

M-30 Sample

3-D figure of M-30 sample is given in Figure 4.54.

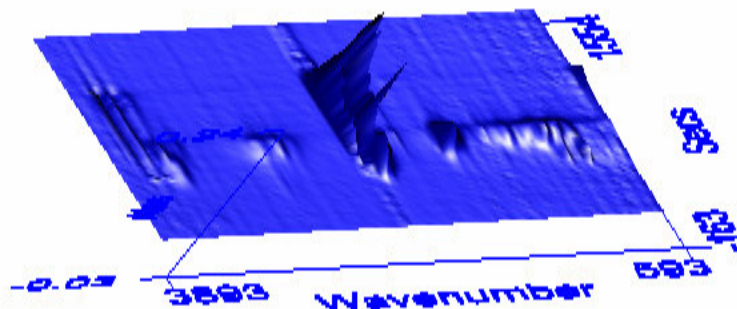


Figure 4.54. 3-D presentation of the M-30 sample

Main absorptions of the groups were observed between 292 °C (525 s) and 412 °C (780 s), except CO₂. CO₂ emissions stopped at 580 °C (1100 s) for M-30 sample.

After baseline corrections were done and all spectrums were made smooth to remove noise, peak areas of the groups in the FTIR spectrum were calculated by using the computer program. For the calculation of areas, baseline corrections of the spectrums were done for all M samples; however, due to high noise and low absorptions for the second and fourth regions, area calculations could not be performed for all samples.

For the calculation of the area of the isocyanate group peak at 2251 cm⁻¹, baseline was drawn between 2022 and 2411 cm⁻¹, for ammonia (between 896 and 986 cm⁻¹), baseline was drawn between 1561 and 896 cm⁻¹, for carbonyl groups (C=O) (between 1700 and 1800 cm⁻¹), baseline was drawn between 1573 and 1955 cm⁻¹, for alkanes (between 2800 and 3000 cm⁻¹), baseline was drawn nearly between 2664 and 3171 cm⁻¹, for free OH (about 3459-3600 cm⁻¹), baseline was drawn between 3391-3800 cm⁻¹ and for the calculation of the areas

of the cellulose and lignin bands (between 1000 and 1300 cm^{-1}), for lignin (1200-1300 cm^{-1}), for aromatic bending region (between 1340 and 1466 cm^{-1}), and for aromatic skeletal vibrations (between 1494 and 1519 cm^{-1}), baseline was drawn between 1561 and 896 cm^{-1} , and areas were calculated for these intervals.

Areas of peaks in nine regions (for different functional groups) are plotted in Figure 4.55, 4.56 and 4.57 for the M-10, M-20 and M-30 samples, respectively.

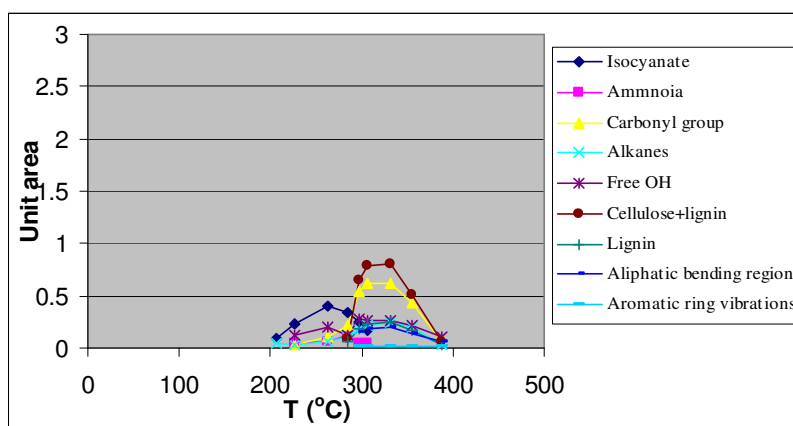


Figure 4.55. Areas of the nine regions of M-10 sample

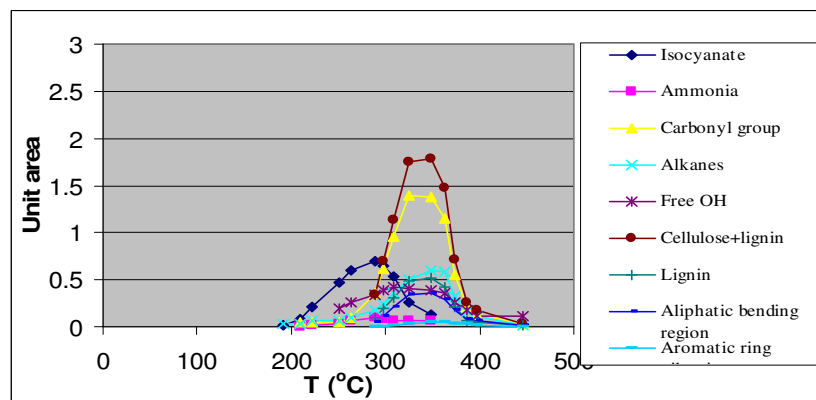


Figure 4.56. Areas of the nine regions of M-20 sample

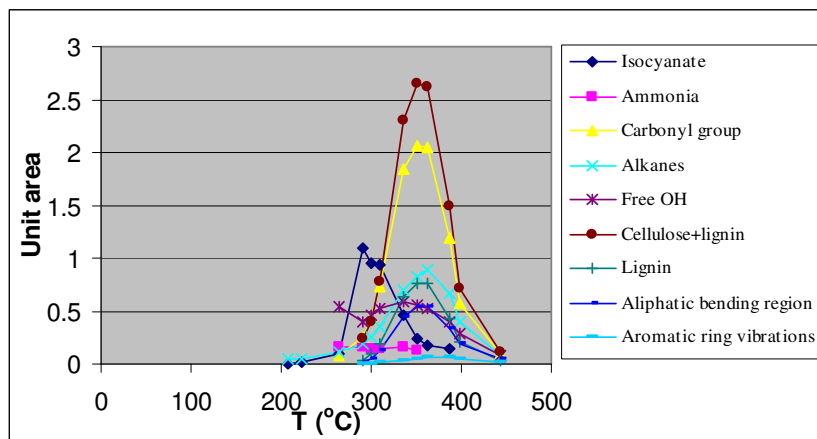


Figure 4.57. Areas of the nine regions of M-30 sample

When Figures 4.55-57 were examined, it can be seen that as heating rate increased, emissions which were released by samples increased because samples burned at faster rate and these caused the higher emissions from the structure. After a certain temperature, emissions reached the highest value and then decreased due to decreasing of volatile matters in the samples.

However, isocyanate group and ammonia showed different trends than the other emissions, because they reached their maximum points early as compared to other groups such as carbonyl, alkanes, and aromatics due to highest volatilization characteristics of these chemicals.

4.3.3. 3-D/FTIR Results of the PB-30 Sample

3D figure of the PB-30 sample as a result of the FTIR analysis is given in Figure 4.58.

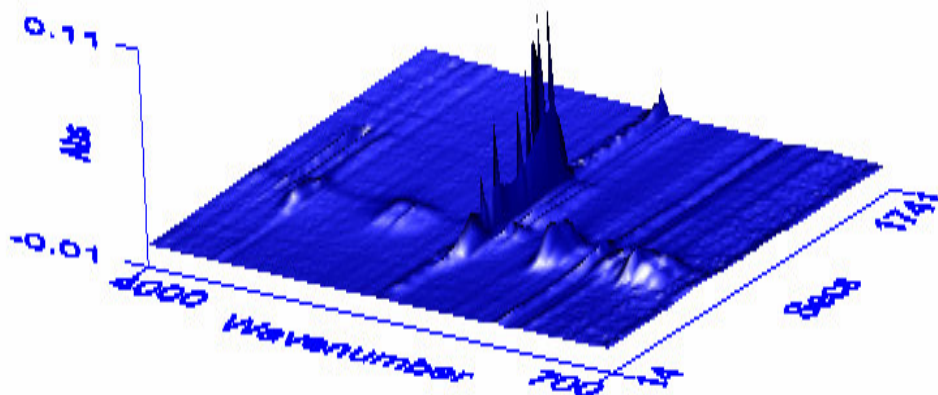


Figure 4.58. 3-D presentation of the PB-30 sample

Main absorptions of the groups were observed between 280 °C (480 s) and 390 °C (700 s), except CO₂. CO₂ emissions stopped at 610 °C (1140 s) for PB-30 sample. For the calculation of areas, baseline corrections of the spectrums were done for the all PB samples and for the calculation of the peak area of the isocyanate group peak at 2251 cm⁻¹, baseline was drawn between 2157 and 2433 cm⁻¹, for ammonia (for peaks at 963 and 930 cm⁻¹), baseline was drawn between 1550 and 899 cm⁻¹, for carbonyl groups (C=O) (between 1700 and 1800 cm⁻¹), baseline was drawn between 1567 and 2467 cm⁻¹, for alkanes (between 2800 and 3000 cm⁻¹), baseline was drawn nearly between 2416 and 3143 cm⁻¹, for free OH (about 3450-3800 cm⁻¹), baseline was drawn between 3250-3938 cm⁻¹ and for the calculation of the areas of the cellulose and lignin bands (between 1000 and 1300 cm⁻¹), for lignin (1200-1300 cm⁻¹), for aromatic bending region (between 1340 and 1466 cm⁻¹, and for aromatic skeletal vibrations (between 1494 and 1519 cm⁻¹), baseline was drawn between 1550 and 899 cm⁻¹, and areas were calculated for these intervals (Figure 4.59).

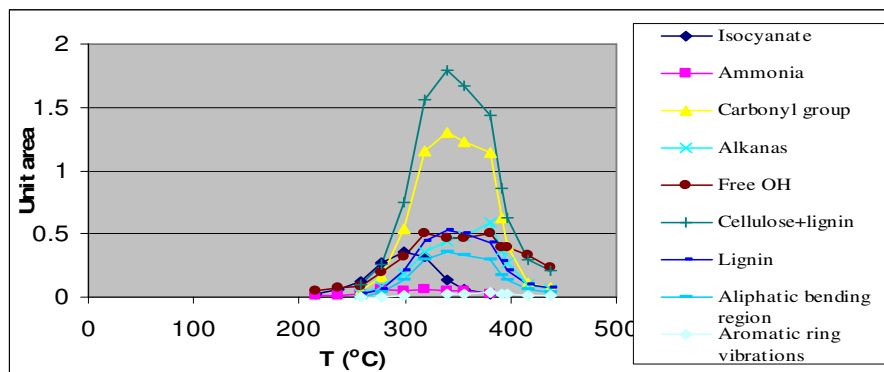


Figure 4.59. Areas of the nine regions of PB-30 sample

After a certain temperature, emissions reached the highest value and then decreased due to decreasing of volatile matters in the sample. However, isocyanate group and ammonia showed different trends than the other emissions due to higher volatilization characteristics.

4.3.4. 3-D/FTIR Results of the PL-30 Sample

3D figure of the PL-30 sample as a result of FTIR analysis is given in Figure 4.60.

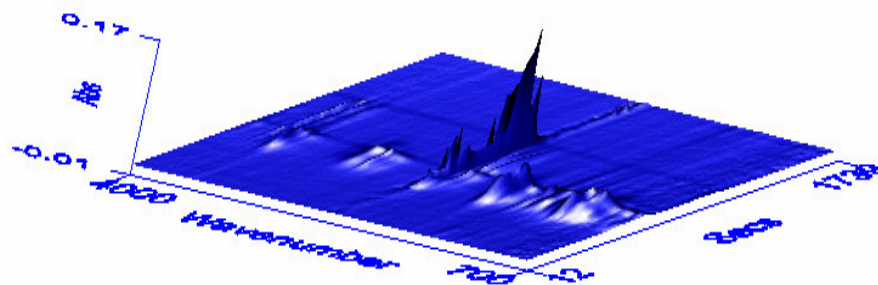


Figure 4.60. 3-D presentation of the PL-30 sample

Main absorptions of the groups was observed between 280 °C (480 s) and 390 °C (700 s), except CO₂. CO₂ emissions stopped at 610 °C (1140 s) for PL-30 sample.

For the calculation of areas, baseline corrections of the spectrums were done for the all PL samples and for the calculation of the peak area of the isocyanate group peak at 2251 cm⁻¹, baseline was drawn between 2157 and 2433 cm⁻¹, for ammonia (for peaks at 963 and 930 cm⁻¹), baseline was drawn between 1550 and 899 cm⁻¹, for carbonyl groups (C=O) (between 1700 and 1800 cm⁻¹), baseline was drawn between 1567 and 2467 cm⁻¹, for alkanes (between 2800 and 3000 cm⁻¹), baseline was drawn nearly between 2416 and 3143 cm⁻¹, for free OH (about 3450-3800 cm⁻¹), baseline was drawn between 3250-3938 cm⁻¹ and for the calculation of the areas of the cellulose and lignin bands (between 1000 and 1300 cm⁻¹), for lignin (1200-1300 cm⁻¹), for aromatic bending region (between 1340 and 1466 cm⁻¹, and for aromatic skeletal vibrations (between 1494 and 1519 cm⁻¹), baseline was drawn between 1550 and 899 cm⁻¹, and areas were calculated for these intervals (Figure 4.61).

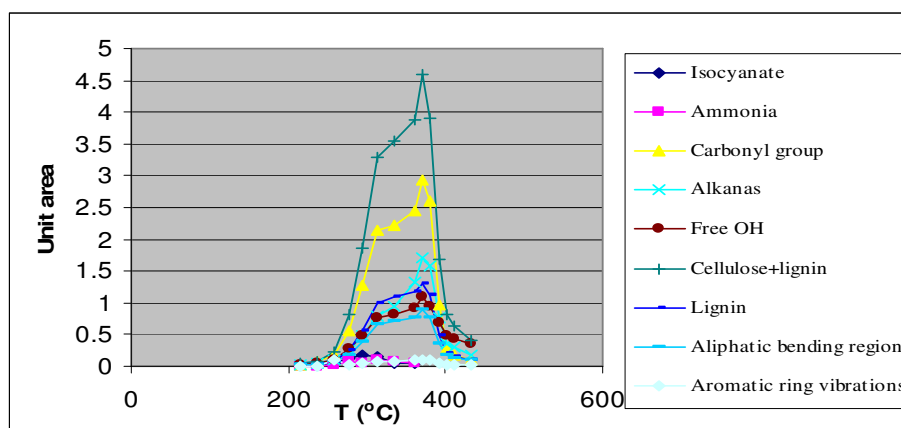


Figure 4.61. Areas of the nine regions of PL-30 sample

After a certain temperature, emissions reached the highest value and then decreased due to decreasing of volatile matters in the sample. However, isocyanate group and ammonia showed different trends because of higher volatilization characteristics of these chemicals were assumed as a reason of this situation.

4.3.5. Comparison of the FTIR Results for all Samples

When all of the 3D/FTIR results of the P and M samples were taken into consideration, it can be stated that main absorption interval of the groups and emissions increased to higher temperatures with increasing heating rate (Table 4.30).

Table 4.30. Releasing temperatures of the main groups of P and M samples in the FTIR spectrums as a result of heating rate

Samples	Temperature at which CO ₂ release started significantly (°C)	Temperature at which all emissions release started significantly (°C)	Temperature at which all emissions release stopped significantly except CO ₂ (°C)	Temperature at which CO ₂ release stopped significantly (°C)
P-10	280 (1500 s)	280 (1500 s)	397 (2200 s)	563 (3200 s)
P-20	280 (750 s)	280 (800 s)	405 (1125 s)	571 (1625 s)
P-30	305 (550 s)	305 (550 s)	425 (790 s)	580 (1100 s)
M-10	218 (1125 s)	263 (1400 s)	372 (2050 s)	563 (3200 s)
M-20	230 (600 s)	272 (725 s)	397 (1100 s)	563 (1600 s)
M-30	230 (400 s)	292 (525 s)	412 (780 s)	580 (1100 s)

For all P and M samples, due to increasing heating rate, emissions and groups were released early; for example, emissions started to be released at 2200 s for P-10 sample, at 218 s for M-10 sample; however, emissions started to be released at 600 s significantly for P-30 sample, 650 s for M-30 sample.

When FTIR spectrum results of all the samples at the 30 °C/min heating rate were compared, Table 4.31 was obtained.

Table 4.31. Releasing temperatures of the main groups of all samples in the FTIR spectrums at 30 °C/min heating rate

Samples	Temperature at which CO ₂ emissions release started significantly (°C)	Temperature at which all emissions release started significantly (°C)	Temperature at which all emissions release stopped significantly except CO ₂ (°C)	Temperature at which CO ₂ release stopped significantly (°C)
P-30	305	305	425	580
M-30	255	292	412	580
PB-30	252	280	390	610.
PL-30	252	280	390	610

When the temperature intervals of the main absorption groups (Table 4.30 and 4.31) were examined for all samples, these intervals seem to be very similar to the regions defined in the TGA results of the all samples, therefore, the third region where highest weight loss were performed and main oxidation was occurred, was seen in the FTIR results as a main absorption region. Accordingly, TGA and FTIR results of the all samples seem to be consistent with each other. Temperatures of the emissions release started for the treated samples were found lower than the untreated pine sample and the temperature of the emissions stopped for the treated sample were found lower than the untreated pine sample. Therefore, treated samples started to thermal decomposition early due to catalytic effect of the chemicals. As temperatures which were the highest amount emissions released for each sample were compared, the highest temperatures were found with the P-30 sample (Table 4.32); therefore, the lowest temperatures which was the highest amount emissions were released, were found for the treated samples as a conclude treatment of the wood with the chemicals

accelerated the thermal decomposition and this decreased the temperature which was the highest amount emissions were released.

Table 4.32. Temperatures which was the highest amount emissions were released as compared to sample type

Sample	Temperature which was the highest amount emissions were released (°C)
P-10	361
P-20	377
P-30	391
M-10	330
M-20	338
M-30	356
PB-30	340
PL-30	370

In the study, it was not found noteworthy amount of ammonia which was produced from the untreated pine sample, because pine contains a little amount 0.016wt% of nitrogen. However, due to glue, M sample contains 4.40wt% nitrogen, PB sample contains 2,36wt% nitrogen, PL sample contains 1.19wt% nitrogen and this glue release nitrogen in the form of NH₃, HCN and HNCO (Prins et al., 2006). Therefore, in the study owing to the oxidation of the treated samples; M, PB, PL in air atmosphere, ammonia, formaldehyde, isocyanate group, phenyl group and benzoylbromide emissions released. Therefore, toxic emissions released to environment from the treated samples as compared to pine sample during the oxidation process depending on the chemicals used during production of the sample. For example Isophorone diisocyanate and Phenyl isocyanate which were found as a result of oxidation of M samples with IR searched, are called as toxic and dangerous for environment by EPA EU, and UN (Isophorone-diisocyanate,1999).

CHAPTER 5

CONCLUSIONS

- The TG curves for waste wood samples investigated in this study show four regions of thermal degradation in air. The first region on the DTG curve was due to the moisture in the sample. The second region was due to very volatile matters. The third region where the main weight loss occurred was due to the oxidation and removal of the volatile matters of the sample. The last region was due to the oxidation of the char remaining after the volatiles were removed from the sample.
- Addition of the chemicals to the wood improved the fire retardancy of wood by lowering its weight loss rate, lowering peak temperatures for decomposition and by decreasing the formation of volatile combustibles through promotion of higher char yield as compared to the untreated sample.
- When thermal kinetic results of pine samples were examined by using Coats Redfern Method, diffusion mechanisms were found to be an effective mechanism for all regions. For the main oxidation region, D4 mechanism (Ginstling-Brounshtein equation) was found as the main diffusion mechanism for pine sample.
- For the treated samples such as MDF, plywood and particleboard, diffusion mechanisms in the second and the fourth regions of these samples were found to be effective mechanisms. However, for the main oxidation region of these samples F1 mechanism (First order reaction)

was assumed as main mechanism. Accordingly, treatment of the wood with different additives and glues seemed to alter the thermal oxidation process and change the effective mechanisms.

- When activation energies and pre-exponential constants are compared by using the Broido Method and the Coats Redfern Method, dissimilar results were obtained especially in the third region of the pine samples, but for the MDF, particleboard and plywood samples more similar results were found.
- For treated samples (MDF, plywood and particleboard), lower activation energies were found for the main oxidation region because of the chemicals which may act as catalysts by lowering the activation energy of the thermal reaction. Consequently, chemicals added to wood for different purposes, have a very important role in the kinetic behavior of the thermal decomposition of the wood.
- When all of the FTIR results of the pine as an untreated sample and MDF as a treated sample were taken into consideration, it can be stated that as the heating rate is increased, the amount of emissions also increased.
- When FTIR results of the pine (as an untreated sample) and MDF, plywood and particleboard (as treated samples) were compared, for all spectrums of the wavenumbers; around 3600 cm^{-1} free OH stretching of alcohol and phenol groups were observed. At the wavenumber below 3000 cm^{-1} aliphatic C-H stretching region, absorption of the CO_2 and CO, absorption of the carbonyl groups (carboxylic acids, esters saturated aliphatics, aldehydes and acetyl derivatives) in the range from 1800 to 1700 cm^{-1} , aromatic ring vibrations of lignin at 1505 cm^{-1} for pine samples and 1508 cm^{-1} for treated samples, aliphatic bending region

between 1350 and 1500 cm^{-1} and at 1000-1300 cm^{-1} region that includes cellulose and lignin band were observed. However, in addition to these groups and gases, there were some toxic and carcinogenic gases like formaldehyde, isocyanate group, ammonia, phenyl group and benzoylbromide observed as a result of the combustion of treated samples.

REFERENCES

Agrawal R. K., 1985. On the use of the Arrhenius equation to describe cellulose and wood pyrolysis, *Thermochim. Acta*, 91, 343-349.

Alshehri S.M., Monshi M.A.S., Abd El-Salam N.M., Mahfouz R.M., 2000. Kinetics of the thermal decomposition of γ -irradiated cobaltous acetate, *Thermochimica Acta*, 363, 61-70.

Anderson L.L., Tillman D.A., 1977. *Fuels from waste*, Academic press Inc., London

Arrigone G.M., Hilton M., 2005. Theory and practice in using Fourier transform infrared spectroscopy to detect hydrocarbons in emissions from gas turbine engines, *Fuel*, 84, 1052-1058.

Balat M., 2005. Use of biomass sources for energy in Turkey and a view to biomass potential, *Biomass and Bioenergy*, 29, 32-41.

Ballı R., 2005. Forest products markets and marketing, Capacity building in sharing forest and market information, Workshop, Czech Republic, www.fao.org/regional/SEUR/events/Krtiny/docs/TurM_en.pdf, accessed on August 2006.

Barral L., Diez F.J., Gabal G., Lopez J., Montero B., Montes R., Ramirez C., Rico M., 2005. Thermodegradation kinetics of a hybrid inorganic-organic epoxy system, *European Polymer Journal*, 41, 1662-1666.

Bilba K., Arsene M.A., Ouensanga A., Study of banana and coconut fibers Botanical composition, thermal degradation and textural observations, *Bioresource Technology*, In press, Corrected Proof.

Bion N., Saussey J., Haneda M., Daturi M., 2003. Study by in situ FTIR spectroscopy of the SCR of NO_x by ethanol on Ag/Al₂O₃—Evidence of the role of isocyanate species, *Journal of Catalysis*, 217, 47-58.

Blackburn J., 2003. *Organic chemistry*, Prentice Hall, 5th edition, NY.

Barral F., Feldman A., Bunel C., 2005. Hydrogenated hydroxy-functionalized polyisoprene (H-HTPI) and isocyanurate of isophorone diisocyanates (I-IPDI): reaction kinetics study using FTIR spectroscopy, *Polymer*, 46, 15–25.

Cheremisinoff P.N., Morresi A.C., 1976. Energy from solid wastes, Marcel Dekker Inc., New York.

Coats A.W., Redfern J.P., 1964. Kinetic parameters from thermogravimetric data, *Nature*, 201, 68-69.

De Jong W.; Pirone A.; Wojtowicz M.A., 2003. Pyrolysis of Miscanthus Giganteus and wood pellets: TG-FTIR analysis and reaction kinetics, *Fuel*, 82, 1139-1147.

Deka M., Saikia C.N., Baruah K.K., 2002. Studies on thermal degradation and termite resistant properties of chemically modified wood, *Bioresorce Technology*, 84, 151-157.

Demirbaş A., 2004. Bioenergy, Global warming and environmental impacts, *Energy Sources*, 24, 225-236.

Dias F. M., Do Nascimento M. F., Martinez-Espinosa M., Lahr F. A. R., Valarelli I. D., 2005. Relation between the compaction rate and physical and mechanical properties of particleboards, *Materials Research*, 8, 5.

Drobniak A., Mastalerz M., 2006. Chemical evaluation of Miocene wood: Example from the Belchatow brown coal deposit, central Poland, *International Journal of Coal Geology*, 66, 3, 157-178.

Ediger V.Ş., Kentel E., 1999. Renewable energy potential as an alternative to fossil fuels in Turkey, *Energy Conversion and Management*, 40, 743-755.

Ella E.S., Yuan G., Mays T., 2005. A simple kinetic analysis to determine the intrinsic reactivity of coal chars, *Fuel*, 84, 14–15, 1920–1925.

Energy and Natural Sources Panel, 2003. Energy and natural sources panel, Vision 2023, Preliminary report, The Scientific and Technical Research Council of Turkey (TUBITAK), Ankara.

Energy sector in Turkey, 2006. http://www.turkeynow.org/db%5Cdocs%5C%5C05_Energy.pdf, accessed on March 2006.

Enters T., 2001. Logging and mill residues in Asia and Pacific, Asia-Pacific Commission Forestry Commission, Trash or treasure? FAO-Rap publication.

Exploitation of agricultural residues in Turkey- Life Training Course Technical Notes, 2005. Ankara, Turkey.

Esin T., Cosgun N., A study conducted to reduce construction waste generation in Turkey, *Building and Environment*, In press, Corrected Proof.

Faix O., Bremer J., Schmidt O., Stevznovic T., 1991. Monitoring of chemical changes in white-rot degraded beech wood by Pyrolysis-gas chromatography and Fourier-transform infrared spectroscopy, J., *Journal of Analytical and Applied Pyrolysis*, 21, 147-162.

FAO (Food and agriculture organization of the United Nations), Forestry items, <http://faostat.fao.org/site/512/default.aspx>, 2006, Accessed on August 2006.

FAO Corporate Document Repository, 2006. The potential use of wood residues for energy generation, www.fao.org/docrep/T0269E/t0269e08.htm - 68k, accessed on August 2006.

Forestry Special Impression Commission Report, 2001. State Planning Organization (SPO), Eight Five Year Development Plan, Ankara.

Fung P.Y.H., Krischbaum M.U.F., Raison R. J., Stucley C., 2002. The potential for Bioenergy production from Australian forests, its contribution to national greenhouse targets and recent developments in conversion processes, *Biomass and Bioenergy*, 22, 223-236.

Gao M., 2004. Thermal degradation of wood in air and nitrogen treated with basic nitrogen compounds and phosphoric acid, *Combustion Science and Technology*, 176, 2057-2070.

Gao M., Pan D.X., 2003. Study on the thermal degradation of wood treated with amino resin and amino resin modified with phosphoric acid, *Journal of Fire Sciences*, 21, 189-201.

GDF (General Directorate of Forestry), 2006. Industrial and fuelwood production amounts in 2005, <http://www.ogm.gov.tr/ip1/uretlim.htm>, accessed on August 2006.

Getto H., Ishihara S., 1998. The functional gradient of fire resistance laminated board, *Fire and Materials*, 22, 89-94.

Guo J., Lua A.C., 2000. Effect of heating temperature on the properties of chars and activated carbons prepared from oil palm stones, *Journal of Thermal Analysis and Calorimetry*, 60, 417-425.

Hagedorn M. M., Bockhorn H., Krebs L., Muller U., 2003. A comparative kinetic study on the pyrolysis of three different wood species, *J. Anal. Appl. Pyrolysis*, 68, 69, 231-249.

Hepbaşlı A., Utlu Z., 2004. Evaluating the energy utilization efficiency of Turkey's renewable energy sources during 2001, *Renewable and Sustainable Energy Reviews*, 8, 237-255.

Hsu C.P.S., 2006. Edited by Frank Settle, Handbook of Instrumental Techniques for Analytical Chemistry, Chapter 15, Infrared Spectroscopy, Prentice-Hall, Inc., <http://www.prenhall.com/settle/chapters/ch15.pdf>, accessed on January 2006.

Ibach.R.E., 1999. Chapter 14, Wood Preservatives, Wood handbook-Wood as an engineering material, Forest Products Laboratory., Gen. Tech. Rep. FPL-GTR-113. Madison.

IEA (International Energy Agency), 2006. Key world energy statistics, <http://resourcescommittee.house.gov/Press/reports/energy/ieaegystat03.pdf>, accessed on August 2006.

Introduction to IR Spectra, 2006. <http://www.chem.ucla.edu/~webspectra/index.html>, Accessed on January 2006, accessed on August 2006.

IPCC (Intergovernmental Panel on Climate Change), 1996. Greenhouse Gas Inventory Reference Manual: Revised 1996 IPCC Guidelines for National Greenhouse Gas Inventories, Vol. 3, 3-28, Paris.

Isophorone diisocyanate, <http://www.inchem.org/documents/icsc/icsc/eics0499.htm>, accessed on August 2006.

- Jacobs M.H., 1967. Diffusion Processes, Springer Verlag, New York.
- Jianzhong X., Xiaolong Z., Hongqiang Q., 2004. Study on the thermal stability of flame retardant wools, *CJI*, 6, 10, 74.
- Kaya D., 2006. Renewable energy policies in Turkey, *Renewable and Sustainable Energy Policies Reviews*, 10, 2, 152-163.
- Kaygusuz K., Kaygusuz A., 2002. Renewable energy and sustainable development in Turkey, *Renewable Energy*, 25, 431-453.
- Kim S., Kim W.K., Kaczynski R.M., Acher R.D., Yoon S., Anderson T.J., Crisallea O.D., Payzant E.A., Li S.S., 2005. Reaction kinetics of CuInSe₂ thin films grown from bilayer InSe/CuSe precursors, *J. Vac. Sci. Technol. A*, 23, 2, 310-315.
- Klass D. L., 1998. Biomass for renewable energy, fuels and chemicals, Academic Press, California.
- Koch A., Krzton A., Finqueneisel G., Heintz O., Weber J.B., Zimny T., 1998. A study of carbonaceous char oxidation in air by semi-quantitative FTIR spectroscopy, *Fuel*, 77, 6, 563-569.
- Kumar S., Gaikwad S. A., Shekdar A. V., Kshirsagar P.S., Singl R.N., 2004. Estimation method for national methane emission from solid waste landfills, *Atmospheric Environment*, 38, 3481-3487.
- Lee H.L., Chen G.C., Rowell R.M., 2004. Thermal properties of wood reacted with a phosphate pentoxide amine system, *Journal of Applied Polymer Science*, 91, 2465-2481.
- Levenspiel O., 1972. Chemical reaction engineering, Wiley international edition, 2nd edition, John Wiley and Sons. Inc., New York.
- Liu N.A., Fan W.C., 1998. The Kinetic Methods for which No Assumption about the Order of Reaction is Needed, *Fire and Materials*, 22, 219-220.
- Lu R., Purushothamma S., Yang X., Hyatt J., Pan W., John T., Lloyd W.G., 1999. TG/FTIR/MS study of organic compounds evolved during the co-firing of coal and refuse-derived fuels, *Fuel Processing Technology*, 59, 35-50.

Marcilla A., Gomez A., Menargues S., 2005. TGA/FTIR study of the catalytic pyrolysis of ethylene-vinyl acetate copolymers in the presence of MCM-41, *Polymer Degradation and Stability*, 89, 145-152.

McKendry P., 2002. Energy production from biomass (part 1): Overview of biomass, *Bioresource Technology*, 83, 37-46.

Meldrum B.J., Rochester C.H., 1991. Infrared spectra of carbonaceous chars under carbonization and oxidation conditions, *Fuel*, 70, 57-63.

Minying L., Lijun G., Qingxiang Z., Yudong W., Xiaojuan Y., Shaokui C., 2003. Thermal degradation process and kinetics of poly (dodecamethylene-isophthalamide), *CJI*, 5, 6, 43.

Momoh M., Eboatu A.Z., Kolewole A.G., Horrocks A.G., 1996. Thermogravimetric Studies of the Pyrolytic Behaviour in Air of Selected Tropical Timbers, *Fire and Materials*, 20, 173-181.

Moore A.K., Owen N.L., 2001. Infrared Spectroscopic studies of solid wood, *Applied Spectroscopy Reviews*, 30, 1, 65-86.

Nassar M.M, 1999. Thermal Analysis kinetics of baggasse and rice straw, *Energy Sourcse*, 21, 131-137.

Nishizaki H., Yoshida K., Wang J. H., 1980. Comparative study of various methods for thermogravimetric analysis of polystyrene degradation, *Journal of Polymer Applied Science*, 25, 12, 2869-2877.

Ocak M., Ocak Z., Bilgen S., Keleş S., Kaygusuz K., 2004. Energy utilization, environmental pollution and renewable energy sources in Turkey, *Energy Conversion and Management*, 45, 845-864.

Owen N.L., Thomas D.W., 1989. Infrared studies of hard and soft woods, *Applied Spectroscopy*, 43, 3, 451-455.

Öztürk M. 2006. Management of construction debris, Ministry of Environment and Forestry, Ankara, www.cevreorman.gov.tr/belgeler/molozson.doc, accessed on August 2006.

Pandey K.K., 1999. A study of chemical structure of soft and hardwood and wood polymers by FTIR spectroscopy, *Journal of Applied Polymer Science*, 71, 1969-1975.

Peek R., 2004. Wood waste management in Germany - material reuse versus energy production. COST E 37, Reinbek.

Petrovic Z. S., Zavargo Z. Z., 1986. Reliability of methods for determination of kinetic parameters from thermogravimetry and DSC measurements, *Journal of Polymer Applied Science*, 32, 4, 4353-4367.

Phyllis, 2006. Database for biomass and waste, Energy Research Center of Netherlands, <http://www.ecn.nl/phyllis/>, accessed on August 2006.

Poljansek I., Krajnc M., 2005. Characterization of phenol formaldehyde prepolymer resins by in line FTIR spectroscopy, *Acta Chim. Slov.*, 52, 238-244.

Prins M.J, Bastiaans R., Oijen V.J., Goey L.P.H., 2006. Ammonia Formation Rates in Biomass Pyrolysis, AIChE 06, San Francisco, California.

Pulp and paper sludge to energy, 2006. Preliminary assessment of technologies, CANMET energy technology center, Report No: 34, www.cifq.qc.ca/imports/_uploaded/PPsludge.pdf, accessed on August 2006.

Reina J., Velo E., Puigjaner L, 1998. Thermogravimetric study of the pyrolysis of waste wood, *Thermochimica Acta*, 320, 161-167.

Schanzer C., Bühner H. G., 2002. Investigating the curing of amino resins with TGA-MS and TGA-FT-IR, FH, *Spectroscopy Europe*, 14, 6, 21-23.

Schniewind A.P., 1989. Concise Encyclopedia of Wood and Wood Based Materials, 1st edition, Pergamon Press, Elmsford, 271-273.

Scotland R., 2003, The Recycling of waste wood by thermal conversion, A Report to identify the feasibility of utilizing waste wood as a feedstock for use in Bioenergy Technologies, Glasgow.

Sharman R.K., Wooten J.B., Baliga V.L., Lin X., Chan W.G., Hajaligol M.R., 2004. Characterization of chars from the pyrolysis of lignin, *Fuel*, 83, 1469-1482.

Shafizadeh F., 1981. Basic Principles of Direct Combustion, in Biomass Conversion Processes for Energy and Fuels, Sofer S.S, Zaborsky O.R, (Eds), Plenum Publishing Corporation, New York: 103-124.

Shimada E., Yamashita H., Matsumoto S., Ikuma Y., Ichimura H., 1999. The oxidation kinetics of spherically shaped palladium powder, *Journal of Materials Science*, 34, 4011-4015.

Sims R.E.H., 2002. The brilliance of Bioenergy: In business and practice, James and James Ltd, London.

SIS (State Institute of statistics), 2006. Waste inventory for the manufactured goods in 2004, http://www.die.gov.tr/TURKISH/SONIST/CEVRE/t04_271205.xls, accessed on August 2006.

Skodras, G., Grammelis, P., Samaras, P., Vourliotis, P., Kakaras, E., Sakellariopoulos, G.P., 2002. Emissions Monitoring During Coal Waste Wood Co-Combustion in an Industrial Steam Boiler, *Fuel*, 81, 5, 547-554.

Smith E., 2005. Characterization of waste materials using FTIR spectroscopy: Process monitoring and quality assessment, *Spectroscopy Letters*, 38, 247-270.

Sobkowiak M., Painter P., 1992. Determination of the aliphatic and aromatic CH contents of coals by FT-i.r.: studies of coal extracts, *Fuel*, 71, 1105-1125.

Sonibare O.O., Ehinola O.A., Egashira R., KeanGiap L, 2005. An investigation into the thermal decomposition of Nigerian Coal, *J. Appl. Sci.*, 5, 104-107.

Spectroscopy Tutorial: Reference, <http://orgchem.colorado.edu/hndbksupport/specttutor/irchart.html>, accessed on January 2005.

Sun J.T., Huang Y.D., Gong G.F., Cao H.L., 2006. Thermal degradation kinetics of poly (methylphenylsiloxane) containing methacryloyl groups, *Polymer Degradation and Stability*, 91, 339-346.

Tait J.K.F., Davies G., McIntyre R., Yarwood J., 1997. FTIR-ATR studies of interfacial interactions in epoxy resin/polymer laminate structures, *Vibrational Spectroscopy*, 15, 79-89.

Thomsan M.A., Melling P.J., Slepski A.M., 2001. Real time monitoring of isocyanate chemistry using a fiber optic FTIR probe, *Polymer Preprints*, 42, 1, 310-311.

Tillman D.A., Rossi A.J., Kitto W.D., 1981. Wood combustion, Principles, processes and economics, Academic press INC., USA.

Todd J. J., 2003. Wood smoke handbook: Wood heaters, Firewood and Operator Practice, Eco Energy Options, Environment Australia, NSW Environment Protection Authority.

Tsai W.T., 2007. Bioenergy from landfill gas (LFG) in Taiwan, *Renewable and sustainable energy reviews*, 11, 2, 331-344.

Turk M.J., Ansari A.S., Alston W.B., Gahn G.S., Frimer A.A., Scheiman D.A., 1999. Evaluation of the thermal oxidative stability of polyimides via TGA technique, *Journal of Polymer Science, Part A: Polymer Chemistry*, 37, 3943-3956.

Venkov T., Dimitrov M., Hadjiivanov K., 2006. FTIR spectroscopic study of the nature and reactivity of NO_x compounds formed on Cu/Al₂O₃ after co-adsorption of NO and O₂, *Journal of Molecular Catalysis A: Chemical* 243, 8–16.

Vlaev L.T., Markovska I.G., Lyubchev L.A., 2003. Non isothermal kinetics of pyrolysis of rice husk, *Thermochemica Acta*, 406, 1-7.

WEC/TNC (World Energy Council-Turkish National Committee), 1996. Turkey Energy Report-1995, Ankara.

WEC/TNC (World Energy Council-Turkish National Committee), 2006. General energy balances in 2003 for Turkey, <http://www.dektmk.org.tr/turkish/Rapor/2003istatistik/2003istindex.htm>, accessed on April, 2006.

Wereko-Broby C.Y., Hagan E.B., 1996. Biomass conversion technologies, John Wiley & Sons Ltd, New York.

Wickens G.E., 2001. Economic botany, principles and practices, Kluwer Academic Publishers, Dordrecht.

Xu J.Z., Gao M., Guo H.Z., Liu X.L., Li Z., Wang H., Tian C., 2002. Study on the thermal degradation of cellulosic fibers treated with flame retardants, *Journal of Fire Sciences*, 20, 227-235.

Youngquist J.A., 1999. Chapter 10, Wood-Based Composites and Panel Products, Wood handbook—Wood as an engineering material, Forest Products Laboratory, Gen. Tech. Rep. FPL–GTR–113. Madison.

Zakrzewski R., 2003. Pyrolysis kinetics of wood comparison of iso and polythermal thermogravimetric methods, *Electronic Journal of Polish Agricultural Universities*, 6, 2.

APPENDIX A

REPEATED TG ANALYSIS OF P-10 AND M-10 SAMPLES

Repeated Pine Sample at 10 °C/min heating rate (RP-10)

TG and DTG curves of the RP-10 sample are given in Figure A.1. The heating rate for this sample was 10 °C/min. As can be seen from the Figure A.1, four regions are seen in the DTG curve. Temperature intervals and weight losses belonging to the regions are given in Table A.1.

Table A.1. Temperature intervals and weight losses belonging to the regions

Regions	Temperature interval, (°C)	ΔT , (°C)	% wt. loss
1 st region	30-170	140	5.90
2 nd region	170-260	90	4.10
3 rd region	260-395	135	64.00
4 th region	395-553	158	26.00

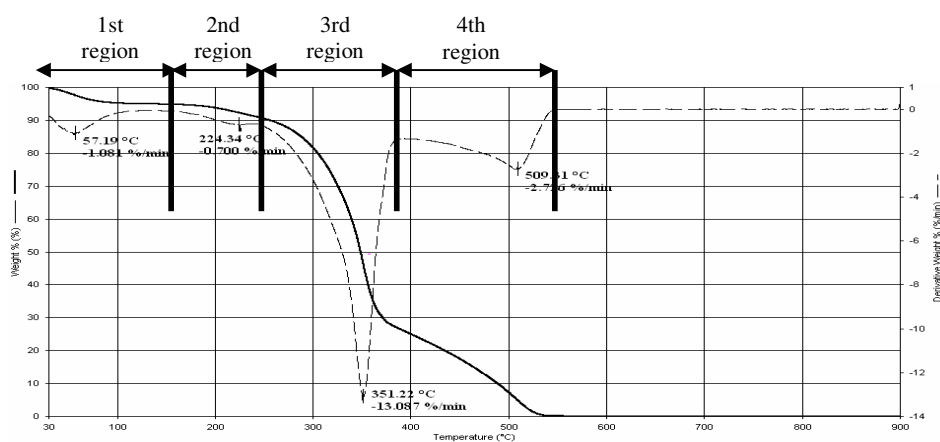


Figure A.1. TG and DTG graph of the RP-10 sample at 10 °C/min heating rate

Curves showing the solid state mechanisms for Coats Redfern Method for three regions are shown in Figure A.2. As it can be seen from the Figure A.2, different curves having different slopes were obtained for 6 different solid state mechanisms by using Coats Redfern Method for RP-10 sample. The slope and the intercepts were calculated by assuming the different mechanisms for thermal kinetics by using Coats Redfern Method. The kinetic constants were calculated from the slope and the intercept of different regions.

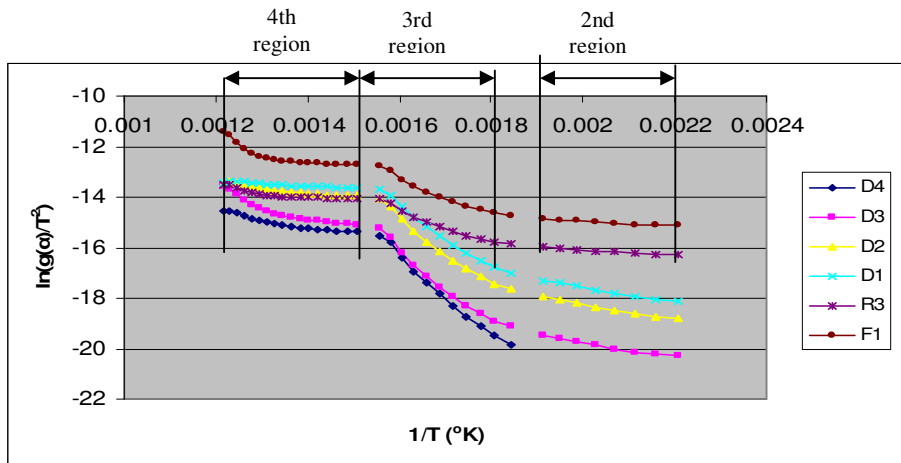


Figure A.2. Curves indicating the solid state mechanisms for Coats Redfern method for three regions of RP-10 sample

In Figure A.3, by using the Broido method different curves were obtained for 3 regions of RP-10 sample. To calculate thermal kinetics such as activation energy and pre-exponential constant, slope and intercept of these curves were used, respectively.

Results of the Coats Redfern and Broido Methods are given in Table A.2.

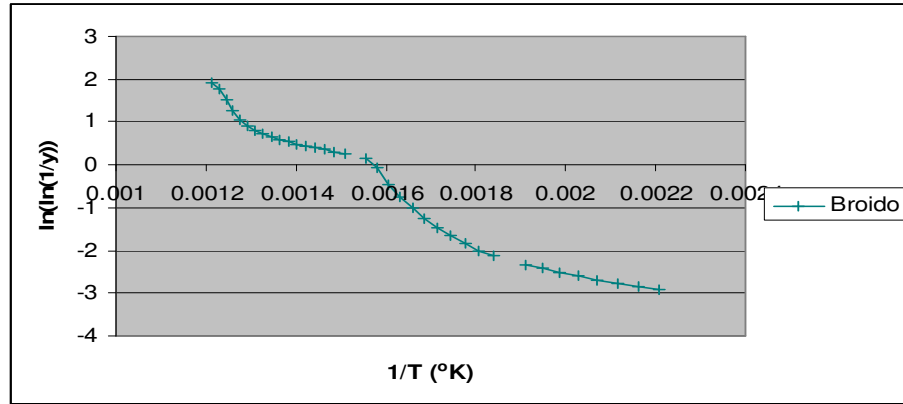


Figure A.3. Curves showing the Broido method for three regions of RP-10 sample

Table A.2. Activation energies and pre-exponential constant values of RP -10 sample with respect to the three regions

Mech.	Second region			Third region			Fourth region		
	E*	r ²	A**	E	r ²	A	E	r ²	A
D4			-	122.70	0.9882	5.75E+09	24.98	0.9143	14.5
D3	24.47	0.9788	0.80	107.97	0.9694	4.92E+08	40.91	0.8626	509.9
D2	24.07	0.9789	3.19	99.64	0.9755	3.23E+08	17.03	0.9325	10.1
D1	23.68	0.979	5.58	92.48	0.9801	1.19E+08	6.96	0.9318	1.0
R3	8.19	0.9574	0.21	49.05	0.9642	1.21E+04	14.32	0.7627	4.6
F1	8.39	0.9578	0.68	53.30	0.9569	1.03E+05	31.89	0.7277	813.6
Broido	16.48	0.9867	9.47	62.28	0.9674	8.04E+05	42.704	0.848	5585.8

* E (kJ/mole), **A (1/min), r² correlation coefficient

According to the results (Table 4.4), for the second region, activation energies were found between 8.39-24.474 kJ/mole values, and highest correlation (0.979) was found with D1 method; however, with other diffusion mechanisms, good correlation coefficients were also found. Thus, for this region, diffusion mechanisms play the main role for the oxidation of the RP-10 sample. For the third region, activation energies were between 49.05-122.698 kJ/mole, and highest correlation (0.9882) was found with D4 method. For the fourth region, activation energies were between 6.96-40.912 kJ/mole and highest correlation

(0.9325) was found with D2 method; with D1 method, high correlation was also found; for this reason, diffusion mechanisms (D2 and D1) are responsible for the oxidation of RP-10 sample. Highest activation energy was found in the third region where the main oxidation was performed and highest weight loss occurred, as a 122,698 kJ/mole for the RP-10 sample. Activation energy of the fourth region was found lower than the second region; therefore, second region was found more stable than the fourth region for the sample. With Broido method for the second, the third and the fourth regions, activation energies were calculated as a 17, 62, 43 kJ/mole, respectively, therefore when Coats Redfern Method as compared to Broido method dissimilar results were found.

Repeated MDF Sample at 10 °C/min heating rate (RM-10)

TG and DTG curves of the RM-10 sample are given in Figure A.4. The heating rate for this sample was 10 °C/min. As can be seen from the Figure A.4, four regions are seen in the DTG curve. Temperature intervals and weight losses belonging to the regions are given in Table A.3.

Table A.3. Temperature intervals and weight losses belonging to the regions

Regions	Temperature interval, (°C)	ΔT, (°C)	% wt. loss
1 st region	30-153	123	5.45
2 nd region	153-253	100	6.01
3 rd region	253-383	130	54.43
4 th region	383-553	170	34.11

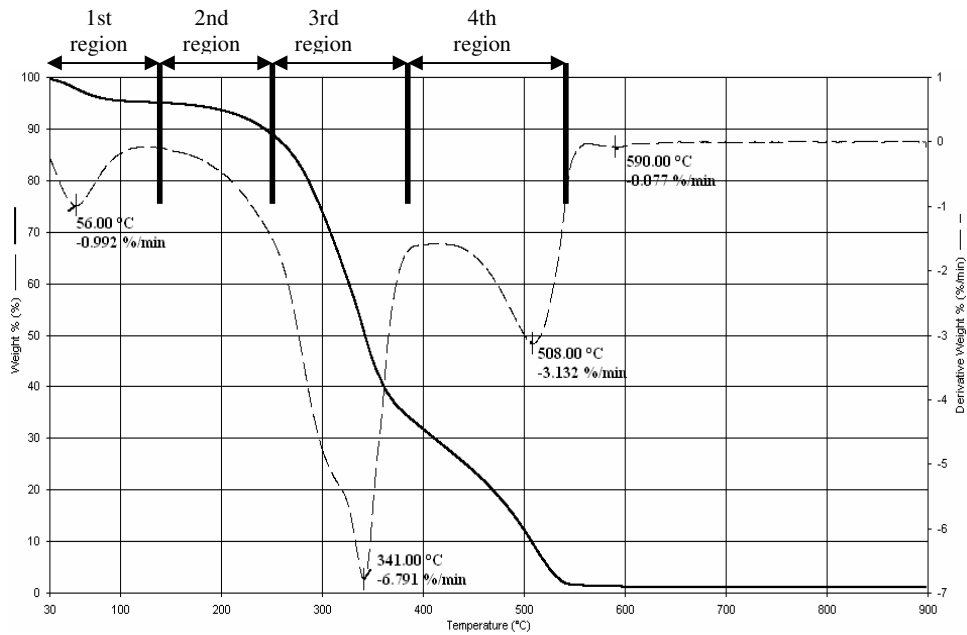


Figure A.4. TG and DTG graph of the RM-10 sample at 10 °C/min heating rate

Curves showing the solid state mechanisms for Coats Redfern Method for three regions are shown in Figure 4.16. As it can be seen from the Figure A.5, different curves having different slopes were obtained for 6 different solid state mechanisms by using Coats Redfern Method for RM-10 sample. The slope and the intercepts calculated by assuming the different mechanisms for thermal kinetics by using Coats Redfern Method. The kinetic constants were calculated from the slope and the intercept of different regions.

In Figure A.6, by using Broido method different curves were obtained for 3 regions of RM-10 sample. To calculate thermal kinetics such as activation energy and pre-exponential constant, slope and intercept of these curves were used, respectively.

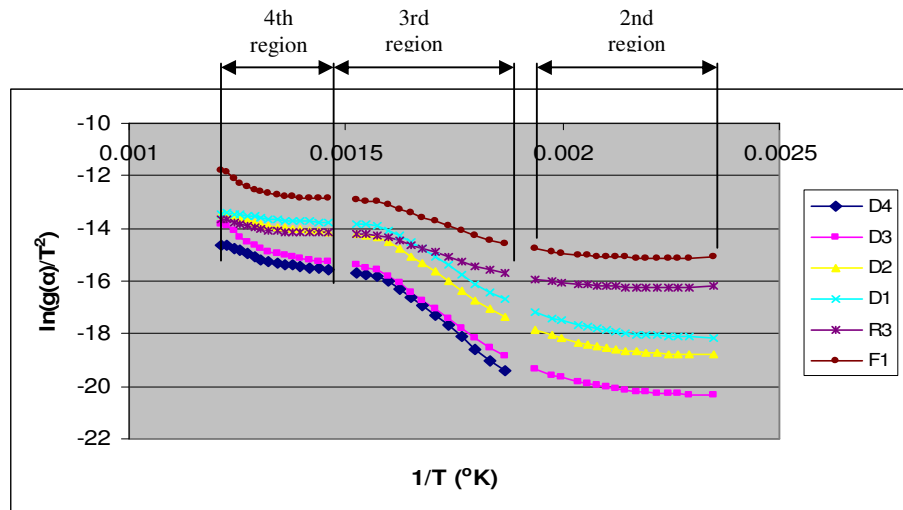


Figure A.5. Curves indicating the solid state mechanisms for Coats Redfern method for three regions of RM-10 sample

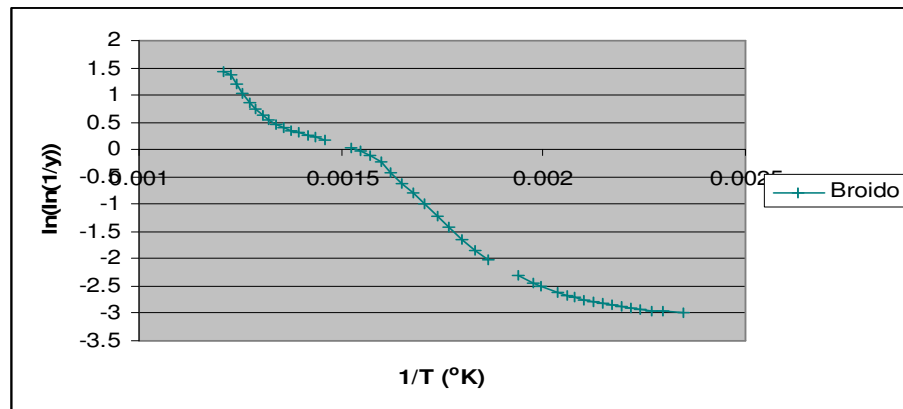


Figure A.6. Curves showing the Broido method for three regions of RM-10 sample

Results of the Coats Redfern and Broido Methods for RM-10 sample are given in Table A.4.

Table A.4. Activation energies and pre-exponential constant values of RM -10 sample with respect to the three regions

Mech.	Second region			Third region			Fourth region		
	E*	r ²	A**	E	r ²	A	E	r ²	A
D4			-	96.73	0.9842	3.75E+07	28.94	0.9161	26.40
D3	21.86	0.8649	0.41	89.87	0.9911	1.16E+07	41.79	0.8757	463.38
D2	21.49	0.8652	1.67	82.24	0.9874	8.81E+06	21.54	0.9321	22.65
D1	21.13	0.8654	2.95	75.62	0.9829	3.63E+06	11.37	0.9511	2.95
R3	7.00	0.7352	0.14	40.01	0.9884	1.65E+03	14.76	0.8201	4.51
F1	7.18	0.7382	0.46	43.89	0.9916	1.31E+04	27.81	0.7956	297.28
Broido	15.03	0.9174	5.72	53.56	0.9947	1.05E+05	36.54	0.9083	1384.28

* E (kJ/mole), **A (1/min), r² correlation coefficient

According to the results (Table A.4), for the second region, activation energies were found between 7.00-21.86 kJ/mole values and the highest correlation (0.87) was found with D1 method; however, with other diffusion mechanisms, good correlation coefficients were also found. Thus, for this region, diffusion mechanisms play the main role for the oxidation of the RM-10 sample. For the third region, activation energies were between 41.01-96.73 kJ/mole, and highest correlation (0.99) was found with F1 method. For the fourth region, activation energies were between 11.37-41.79 kJ/mole and highest correlation (0.93) was found with D1 method. Highest activation energy was found in the third region where the main oxidation was performed and highest weight loss occurred, as a 44 kJ/mole for the RM-10 sample. With Broido method for the second, the third and the fourth regions, activation energies were calculated as a 15, 53, 36 kJ/mole, respectively. With Broido Method for the third region similar results were found as compared to F1 mechanism which gave the highest correlation coefficient with Coats Redfern Method, however this similarity could not found for the other regions.